Chapter6 Shore line model

6.1 General

The prediction of the shoreline changes is crucial for a sustainable plan for coastal management. The physical features along the coast should be well understood before placing any coastal countermeasures along the coast. The numerical modeling is one of the tools which could be used to understand the mechanism of the shoreline changes under the effect of wave, different sediment properties, and variable structures. The numerical analysis is one of cost-effective options to investigate the physical mechanisms of the observed phenomena and to provide the predictions of long term shoreline evolution.

In this respect, the shoreline change model was applied to reasonably explain physical procedures of the observed shoreline changes, accounting for sediment size distributions. The calibrated model is then used for predictions of the future shoreline changes accounting for different climate scenarios. The present model accounted for the quantitative characteristics of coastal structures and river mouths. The improved numerical model simulates the wave transformation (explained in the previous chapter), regional sediment transport, sediment size, and shoreline changes. The model composed of two parts, Energy Balance Equation model and one - line model.

6.2 Literature review on shoreline and bathymetry change modeling

Modeling studies of the shoreline and bathymetry changes can be are categorized in term of spatial and temporal scales. There are three large categories for the classification of the shoreline and bathymetry modeling, Figure 6.1 (modified from Hanson and Kraus, 2011). The first category is the shoreline change models (one - line models). The main assumption of this kind of models is that erosion and accretion occurs without changing beach profiles within the depth shallower than the depth of closure, beyond which no sediment moves. Considere, (1956) developed the first formulation of the one line model by describing the shoreline change phenomenon with a diffusion equation. Several studies followed this, i.e., Hanson, (1987) developed GENESIS (GENEralize model for SImulating Shoreline changes), which is applicable under several boundaries and constraints. Danish Hydraulic Institute developed LITPACK. Dabees et al. (1998) developed ONELINE which contributes to the one line model with new features on how to deal with structures in a shoreline change model.

Saied, (2004) developed the Integrated Coastal Engineering model (ICEM) and used the one-line as a shoreline change model. Both Dabees et al. (1998), and Saied, (2004) applied their models to simulate the shoreline change along the coast of Ras El Bar resort (westward of Damietta promontory, Egypt) to evaluate the performance of constructing detached breakwaters for the protection of this area from erosion.

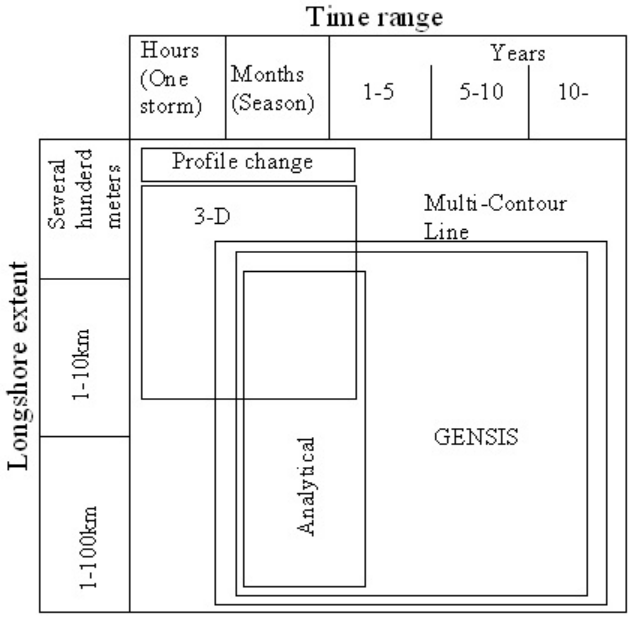

Figure 6.1. Spatial and temporal scales of the modeling approaches (modified from Hanson and Kraus 2011)

Kumada et al. (2002) considered the sorting of the sand of mixed grain size over a simple case (straight shoreline confined between two groins). Different analytical solutions were derived for the one-line concept. Barbaro et al. (2010) developed an analytical solution of the one-line model for the analysis of the shoreline change by random waves. In case of short term analysis or severe storm conditions, the beach profile could change extremely and may not return into its initial shape, which disturbs the validity of the basic assumption of the one-line model.

The second category is beach profile change models. This type of models deals with short term changes caused by cross-shore sediment movement. Bakker, (1968) extended the one-line model by introducing one more line to examine the cross shore sediment transport between the two lines; he applied his method to determined the shoreline evolution near groins.

The last third category is the 3-D models, which calculates the morphological changes in the

3-D domain. This kind of models needs a complex and detailed computations of the 3-D hydrodynamic. Perlin, and Dean (1983) extended Baker's model to a multi-line model. Uda et al. (1998) developed a contour line change model for coasts with steep slopes and to simulate the deformation of the river mouth delta. Dabees and Kamphus (2000) developed a contour line model (NLINE), which allows the local profile formation in existence of complex beach / structure configurations. Shibutani et al. (2009) developed N-line model considering the effect of beach nourishment. Uda et al. (2010) built up a new model for predicting three-dimensional beach changes by expanding Hsu and Evans' equation

The profile change models and the 3-D models are being so sophisticated respected to the one - line model. Since the length of the study site is too long (250 km) and the time interval of our study exceeds 50 years and not being so sophisticated, the one - line model is chosen for the simulation of the shoreline changes in the current study. The one-line model is one of most practical methods which can yield reasonably accurate shoreline changes with relatively less effort of model calibrations and with relatively poor availability of the input data.

6.3 Objective of present one-line model

The shoreline change model was applied to explain physical procedures of the observed shoreline changes, accounting for sediment size distributions. The calibrated model is then used for predictions of the future shoreline changes accounting for different climate scenarios. The present model accounted for the quantitative characteristics of coastal structures and river mouth. The model was applied first around Rosetta promontory then extended to cover the entire NDC.

6.4 Description of one-line model

The key parameters and the input data, which affect the predictive accuracy of the one - line model are; 1) the initial shoreline, 2) breaking wave conditions (H_b, α_b), 3) beach conditions (grain sizes, beach slopes), 4) coastal structures, and 5) the sediment transport empirical parameters.

The current shoreline change model is based on the one-line theory. No sediment supply is considered from the both branches of the Nile River as concluded from the TL analysis. The model accounted for the influence of the coastal structures. Since there are many structures placed along the coast, the sediment transport rate was calculated by Ozasa and Brampton's

(1980) formula, which accounts for the influence of the alongshore variation of the breaking wave height, which can be predominant especially around the area shaded by a coastal structure. The empirical parameters were calibrated using the shoreline data acquired from the land-sat images. Due to the high curvature of the shoreline along the study site, the one-line model was formulated in terms of local coordinates normal to and tangential to the actual shoreline. The grain size distribution is introduced to the one-line model based on (Kumada et al. 2002). The mixing depth is based on (Kraus, 1985), and width of exchange layer is based on (Hirano, 1971)

6.5 Basic assumptions and limitations of the current study

1) The profile shape is constant, and there is a long-term trend in the shoreline evolution.

The beach profile is in equilibrium and the longshore sediment transport is the responsible of the shoreline movement. The longshore sediment transport is strongly related to the breaking wave parameters (angle, and height) and the longshore current. This assumption is not valid after strong storms however it is reasonably fair for long term analysis.

2) No cross shore sediment transport is considered

3) The shoreward and seaward limits of the profile are constant

The sediment movement is observed up to the depth of closure and beyond that depth no sediment movement is exist.

4) Small breaking wave angle with the shoreline.

No instability was considered in the analysis. If the breaking wave angle exceeds the 45^o it is considered as 45^o assuming that due to refraction the waves will refract and the breaking wave angle with the shoreline will not exceeds 45^o.

5) The nearshore circulation is ignored.

The detailed nearshore circulation is ignored except the effect of the longshore variations in the wave breaking height caused from the coastal structures.

6) No sediment supply from the River branches is considered.

7) The probability of occurrence for the wave from the NNW is 33%, 33% from both the NW, and 17% from each N and NE directions.

8) The exposure ratio of the shoreline corresponding to each grain size is equal to the content of each grain size (percentage) in the exchange layer of sand.

9) After a shoreline change, sand in the exchange layer is assumed to be mixed immediately

10) The content of each grain is constant behind the initial shoreline.

6.5.1 Governing equations

The one-line model is formulated in term of local coordinates. m is the longshore coordinate (m); n, is cross-shore shoreline position measured from baseline (m) parallel to the initial shoreline as represented in Figure 6.2

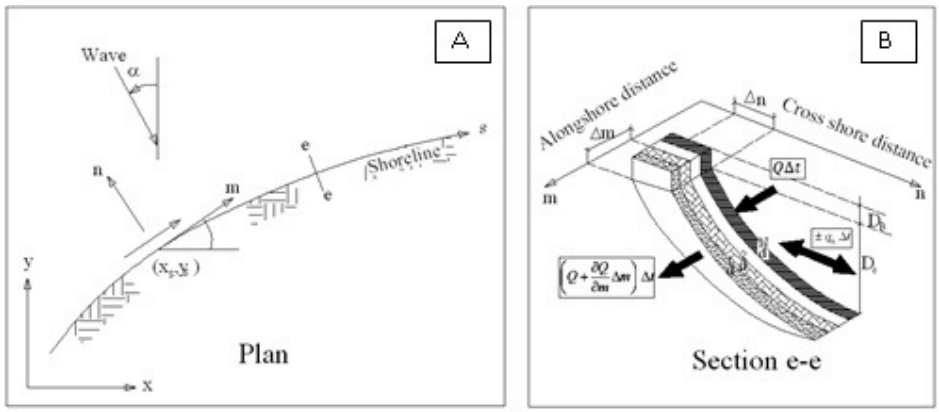

Figure 6.2. A) The shoreline and the axis considered in the current study. B) Bottom profile and change of the shoreline.

Control volume representing the shoreline change of infinitesimal element is presented in Figure 6.2.B. The volume change can be represented from the sand continuity equation,

$$\Delta V = \left\{ Q - \left(Q + \frac{\partial Q}{\partial m} \Delta m \right) \pm q_n \right\} \Delta t = \left(D_c + D_B \right).\Delta n.\Delta m \qquad \textbf{(6.1)}$$

(6.2) is the fundamental equation of the one-line theory.

$$\frac{\partial n^k}{\partial t} = -\frac{1}{D_c + D_B} \left(\frac{\partial Q^k}{\partial m} \pm q^k \right), \qquad K = 1,2,\ldots\ldots,N \qquad \textbf{(6.2)}$$

Where, t is the time (s); D_B is the average berm elevation (m); D_C is the depth of closure (m);

Q is the longshore sand transport rate (m^3/s); and q is the source or sink of sand (m^3/s). Assuming that the exposure ratio of the shoreline corresponding to each grain size is equal, the total shoreline change is the summation of the contribution of each grain size is expressed in (6.3).

$$\frac{\partial N}{\partial t} = \sum_{K=1}^{N} \frac{\partial n^k}{\partial t} \tag{6.3}$$

The longshore sand transport rate of each grain size in mixed sand is calculated based on the percentage of each grain size. Ozasa and Brompoton equation was used in this study (the details of this equation and the empirical parameters were explained in the next sections). The closure depth could be estimated by (Hallermeier and Belvoir, 1978), (6.4) or (Hallermeier, 1981), (6.6) or (Birkemeier, 1985), (6.7)

$$D_C = 2.28H_{s,12} - \frac{68.5(H_{s,12})^2}{gT^2} \tag{6.4}$$

Where, $H_{s,12}$ is the maximum wave height of non breaking waves that occur more than 12 hours per year (0.137 %). Hanson, (1987) used the H_b instead of $H_{s,12}$.

$$H_{s,12} = H_s + 5.6\delta \tag{6.5}$$

δ is the standard deviation of the annual wave height.

$$D_C = H_{sm}T\sqrt{\frac{g}{5000D_{50}}} \tag{6.6}$$

Where, H_{sm} is the mean of the annual distribution of significant wave height, Ts is the corresponding period, and D_{50} is the median grain size of the beach sand in mm

$$D_C \cong (1.5 \leftrightarrow 2.0)1.75H_s - 57.9(H_s^2 / gT_s^2) \tag{6.7}$$

Omar et al. (2005) derived several equations for the closure depth from Abu Qir up to Baltim resort based on the significant wave height and wave period and sediment size, (6.8) to (6.9).

$$D_C = 43.89H_s - 20.9 \tag{6.8}$$

$$D_C = 47.92H_s - 0.028gT_s^2 - 7.6 \tag{6.9}$$

$$D_C = 27.37H_s - 0.045gT_s^2 - 124.08D_{50} - 11.5 \quad \textbf{(6.10)}$$

Where, H_s is the mean significant wave height and T_s is the significant wave period, g is the acceleration of gravity. In the current study, D_c is taken as constant value along the NDC, 10m.

The content of each grain size in the exchange layer of sand is calculated based on the concept of the exchange layer proposed by (Hirano, 1971), (6.11) .The sand is mixed within the exchange layer due to wave action. The thickness of the exchange layer is calculated based on (Kraus, 1985), (6.12)

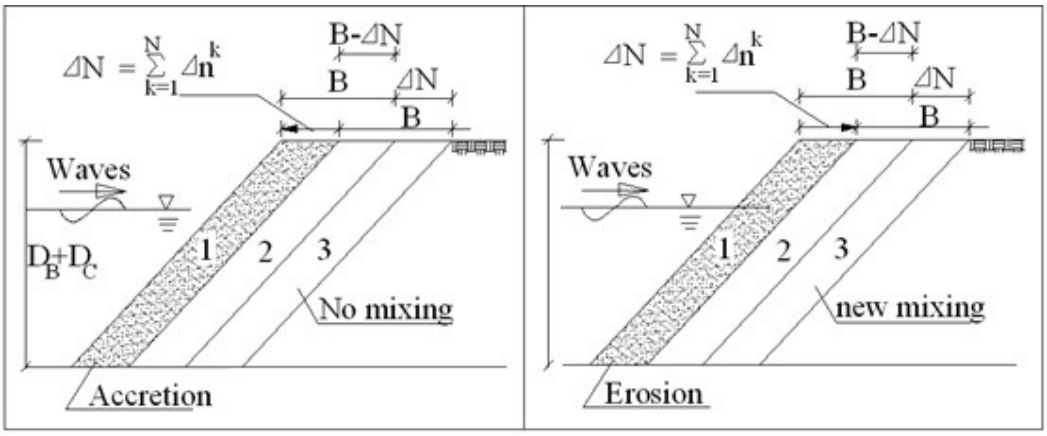

Figure 6.3. Sand mixing range after shoreline advance and recession, Kumada et al. (2002)

$$B = \Delta D_s \frac{1}{\tan\beta} \quad \textbf{(6.11)}$$

$$\Delta D_s = 0.027H_b \quad \textbf{(6.12)}$$

Where, tanβ is the beach slop. B is the mixing width, and $\triangle D_s$ is the exchange depth. The percentage of each grain size is calculated ever k time step. The state of mixing in the accretion area is different from that in the erosion area. Figure 6.3. present the state of erosion and accretion. The new percentage of each grain size is calculated based on the comparison of the volume of the exchange layer between two successive time steps. (6.14), and (6.16) used in the calculation of the new percentage of each grain size for the case of accretion and erosion respectively.

$$\frac{\partial \mu^k}{\partial t} = \frac{1}{B}\left\{\frac{\partial n^k}{\partial t} - \frac{\partial N}{\partial t}.\mu^k\right\} \quad \textbf{(6.13)}$$

$$\mu^{k^-} = \mu^k + \frac{\Delta t}{B}\left\{\frac{\partial n^k}{\partial t} - \frac{\partial N}{\partial t}.\mu^k\right\} \quad \textbf{(6.14)}$$

$$\frac{\partial \mu^k}{\partial t} = \frac{1}{B}\left\{\frac{\partial n^k}{\partial t} - \frac{\partial N}{\partial t}.\mu_B^k\right\} \quad \textbf{(6.15)}$$

$$\mu^{k^-} = \mu^k + \frac{\Delta t}{B}\left\{\frac{\partial n^k}{\partial t} - \frac{\partial N}{\partial t}.\mu_B{}^k\right\} \quad \textbf{(6.16)}$$

Where, μ is the percentage of each grain size at the current time step. μ_B is the initial percentage of each grain size. Routine was developed to determine the percentage of each grain size at different locations for the case that the same place experiencing accretion and erosion.

6.5.2 Longshore sediment transport rates.

Power models

(CERC 1984) formula

The CERC formula provides an estimate of the instantaneous (gross) sediment transport, ignoring the effects of currents and onshore-offshore processes.

$$Q = H_b^2 C_b a_1 \sin 2\alpha_b \quad \textbf{(6.17)}$$

Where, a_1 is a dimensionless coefficient

$$a_1 = \frac{K_1}{16(\rho_s/\rho - 1)(1-p)} \quad \textbf{(6.18)}$$

Where, K_1 is nominally equal to 0.39 ($H_{significant}$ base), or 0.92 (H_{rms} base) (H as presented in the shore protection manual. (Hanson, 1987) suggested the k1 value to be 0.7. Komar and Inman (1970) suggested the k_{rms} to be 0.77. Different values of k1 varying from 0.2 to 1.6 were suggested by different studies.

Ozasa and Brampton (1980) ***formula***

In this equation, alongshore wave height gradients were considered. Such situations often occur when waves diffract around a headland or a breakwater.

$$Q = \frac{H_b^2 C_{gb}}{8(\rho_s/\rho - 1)(1-\rho)w_s}\left[\frac{K_1 \sin(2\alpha_{bs})}{2} - \frac{K_2 \cos\alpha_{bs}}{\tan\beta}\frac{\partial H}{\partial x}\right]_b \qquad \textbf{(6.19)}$$

Where, H_b is breaking wave height (m); Cg_b is the breaking wave group celerity (m/s); α_{bs}, angle of breaking waves to the local shoreline; K_1 and K_2 are empirical coefficients, treated as calibration parameters; p is the porosity of sand on the bed; and β is the bottom slope from the shoreline to the depth of active longshore transport.

Kamphuis (1991) *formula*

This expression is based on an extensive series of hydraulic model tests, and depends on breaking wave height, wave period, grain size, nearshore beach slope and nearshore wave approach angle. The expression is given by:

$$Q = (6.4x10^4) H_{sb}^2 T_p^{1.5} (\tan\beta)_b^{0.75} d_{50}^{-0.25} \sin^{0.6}(2\alpha_b) \qquad (m^3/yr) \qquad \textbf{(6.20)}$$

Where, H_{sb} is the significant wave height at the breaking point, T_p is the peak wave period, m_b is the beach slope near the breaking point, d_{50} is the median grain size, α_b is the breaking wave angle.

Bayram et al. (2007) *formula*

This equation is based on the principles of sediment transport physics assuming that breaking waves mobilize the sediment, which is subsequently moved by a mean current.

$$Q = \frac{\varepsilon}{(\rho_s/\rho - 1)(1-p)gw_s} E_b C_{gb} \cos\theta_b \bar{V} \qquad \textbf{(6.21)}$$

$$\varepsilon = \left(9.0 + 4.0\frac{H_{sb}}{w_s T_p}\right)10^{-5} \qquad \textbf{(6.22)}$$

$$Q = \frac{\varepsilon}{(\rho_s/\rho - 1)(1-p)w_s} H_b^2 \; C_{gb} \cos\alpha_0 \left[K_1\left(a_1 \sin\alpha_0 + \bar{V}_{ex}\right) - K_2 a_2\right] \qquad \textbf{(6.23)}$$

$$a_1 = \frac{5\pi x}{32 C_f}\sqrt{g}A^{\frac{3}{2}} \quad ; a_2 = \frac{\pi}{C_f x^2}\sqrt{g d_b}\frac{\partial H_b}{\partial x} \quad and\ A = 2.25\left(\frac{w_s^2}{g}\right)^{\frac{1}{3}} \qquad \textbf{(6.24)}$$

Where V is the mean alongshore current velocity over the surf zone and ε is the transport coefficient. H_{sb} is the significant wave height at breaking. T_p is the peak wave period, and w_s is the particle settling velocity. V_{ex} is an external surf-zone average longshore current velocity

generated by tide or/and wind; A, shape parameter; x, breaker index; C_f = bottom friction coefficient (0.005 default value)

In the current study, since there are many structures placed along the coast, the sediment transport was calculated based on (Ozasa and Brompoton, 1980) to take the effect of varying breaking height. The empirical parameters were calibrated using the shoreline data acquired from the land-sat images.

The empirical parameters of the longshore sediment transport formulas.

The empirical parameters are a key factor in the longshore sediment transport formulas. However reference information at different sites is needed to calibrate these parameters, sometimes this information is not available. Different studies recommend guiding values for these empirical parameters. These guiding values are mainly derived from field measurements in the dynamic surf zone which is non-controllable and non-repeatable and might lead to large uncertainties. Values derived from Laboratory experiment has less uncertainties but the scale effect is one of the difficulties facing this way which might lead to unreliable values.

Various studies linked the k value with different features along the nearshore zone like the grain size characteristics (median grain size, falling velocity) or wave characteristics (breaking wave angle, orbital velocity, and surf similarity). (6.25) describe (Swart, 1976) K in terms of sediment size after (Schoonees and Theron, 1993)

$$K = 1.15\log_{10}\left(\frac{0.00148}{D_{50}}\right) \qquad 0.1x10^{-3} < D_{50} < 1.0x10^{-3}m \qquad \textbf{(6.25)}$$

Bailard, (1984) developed (6.26) which represents K as a function of the breaking wave angle and ratio of orbital velocity magnitude and the falling velocity.

$$K = 0.05 + 2.6\sin^2(2\alpha_b) + 0.007\frac{u_{mb}}{w_f} \qquad \textbf{(6.26)}$$

Where in the shallow water, $$u_{mb} = \frac{k}{2}\sqrt{gd_b} \qquad \textbf{(6.27)}$$

The data range used for the derivation of Ballard's equation is as follow.

$2.5 \le w_f\,(falling\ velocity) \le 20.5 cm/\sec;$

$0.2^o \le \alpha_b (breaking\ \ wave\ \ angle) \le 15^o; and$ (King, 2005)

$33 \le u_{mb} (orbital\ \ velocity) \le 283$

Valle et al. (1993) derived an empirical relation of K based on data from the Adra River Delta. This formula is valued for range of sediment size from 0.15 to 1.5 mm.

$$K = 1.4e^{(-2.5D_{50})} \tag{6.28}$$

Kamphuis et al. (1978) linked the empirical parameter with the surf similarity parameter.

$$K = 0.7\zeta_b \qquad where, \zeta_b = \frac{m}{\sqrt{H_{brms}/L_0}} \tag{6.29}$$

L_o is deepwater wavelength, and H_{brms} is the root mean square breaker height.

Kamphuis et al. (1986) developed a sediment transport formula (6.30), and determine the empirical parameter in term of sediment size and significant breaking wave height upon dimensional analysis.

$$\frac{Q_s}{\frac{1}{2}\rho\frac{H_{bs}^3}{T}\sin 2\alpha_{bs}} = \left(0.002\frac{H_{bs}}{D_{50}}\right)\frac{m}{(H_{bs}/L_o)^{\frac{1}{2}}} \quad where, K = \left(0.002\frac{H_{bs}}{D_{50}}\right), m = 1.8(H_b/D_{50})^{-0.5} \tag{6.30}$$

The correlation between the CERC and Kamphuis formula is expressed in (6.31).

$$Q_s = 0.018\left(\gamma\frac{H_{bs}}{D_{50}}\right)^{\frac{1}{2}} Q_{s,CERC} \tag{6.31}$$

D_{50} in meters. King (2005) pointed out that the K in CERC formula based on Kamphuis model can be calculated using the following equation.

$$K_{sig} = 0.022\sqrt{\gamma\frac{H_{bs}}{D_{50}}} \tag{6.32}$$

Comparison between different formulas of the empirical parameter in term of the grain size is presented in Figure 6.4. Also field data from different papers were add in this figure.

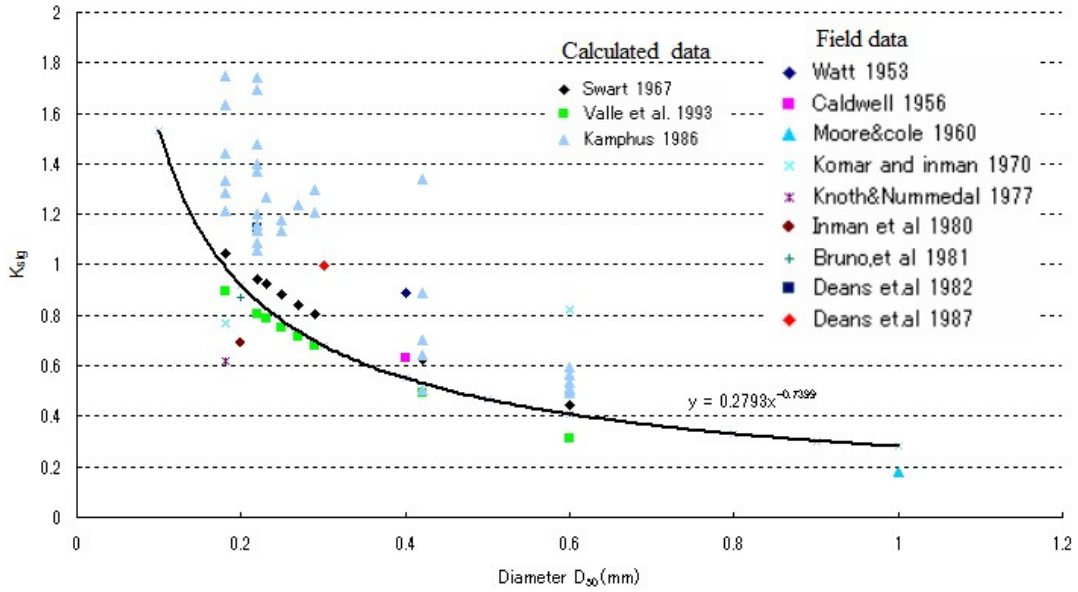

Figure 6.4. The empirical parameter (K) versus the grain size.

Power relation exists between the K and the grain size. As long as the sediment size increases the empirical parameter decrease, hence the sediment transport is decreased. In considering the grain size effect in the longshore sediment transport rates, the empirical parameters in Ozasa and Prampoton formula is calculated in term of the sediment size. The relation $K_1\alpha$ (d) $^{0.5}$ is introduced, as was given by, Kamphuis et al. (1986). $K_1=A/(d)^{0.5}$, and $K_2= 0.5\ K_1$. K_1 represent the mobility of the grains and A is calibrated using shoreline change data. If the grain size is large, *K*1 and the longshore sediment transport rate *Q* become small, because sand with a large grain size is difficult to move.

6.5.3 Boundary conditions (groins, seawalls, and breakwaters)

The boundary conditions for either n or Q at the two lateral ends of the beach, at the different coastal structures, and River mouths are essential. For the study area, the lateral boundary conditions are Dirichlet boundary condition which represents for an impermeable shore-normal barrier where sediment transport rate is equal to zero at the eastern border at Port Said breakwater and partially permeable at Idku Lake or El Burullus Lake. Details of coastal structures, function and how it included in the model are described in the below paragraphs.

Groins and jetties

The groins and jetties are narrow structures, straight and perpendicular to the shoreline used to stop the longshore sediment transport. The sediment is accumulated on its up-drift side and retreats on its down-drift side. Jetties exist around Idku inlet, El Burullus inlet, Damietta

River mouth, and El Gamil inlet. Groins exist around Rosetta River mouth, Eastward of Baltim, and Ras El-Bar. Jetties and groins start their function to interrupt the longshore sediment movement as long as they are extended inside the surf zone. The groins around Rosetta both (East and westward) were constructed on land thus; they don't have any contribution to the shoreline changes until they become into the sea. The jetties and groins might partially block or bypass the sediment depend on wave directions and structures' locations and sizes relative to the shoreline.

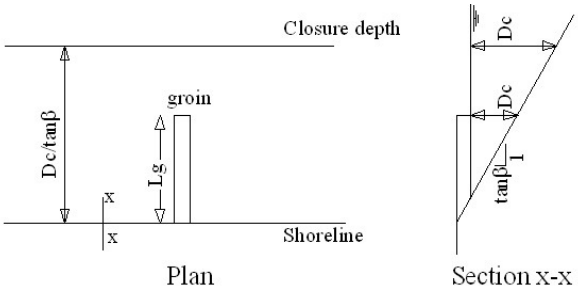

Figure 6.5. Typical layout of single groin.

Breakwaters

Offshore detached breakwaters exist at different locations along the Nile Delta Coast, i.e. Baltim resort, Ras El Bar resort on the westward of El Gamil inlet. It is a shore parallel structure. Other types of breakwaters exist at Idku fishing port, El Burullus fishing port, Damietta port, and Port Said. These breakwaters reduce the wave energy reaches the protected areas. The detached breakwaters block the offshore sediment transport and slow down the effect of the longshore current in its lee side which leads accretion within the sheltered area. The breakwater is considered as constrain for the cross shore movement as forward in case of tombolo formulation behind the detached breakwaters.

Seawalls

Artificial structures constructed on the beach to combat the shoreline movement and prevent inundation due to strong waves. Two seawalls exist around Rosetta mouth from both sides. Long seawalls exist on the eastward side of Damietta promontory however, revetment exist on the westward side. Also ling dike exist near Port Said to protect the international coastal road. Seawalls around Rosetta and on the eastward of Daimetta were constructed on land. The Seawall is considered as constrain for the cross shore movement. If the computed shoreline moves landward and crosses the boundary of the seawall, longshore sediment transport rate was reduced dependent on the relative locations of the shoreline and seawalls.

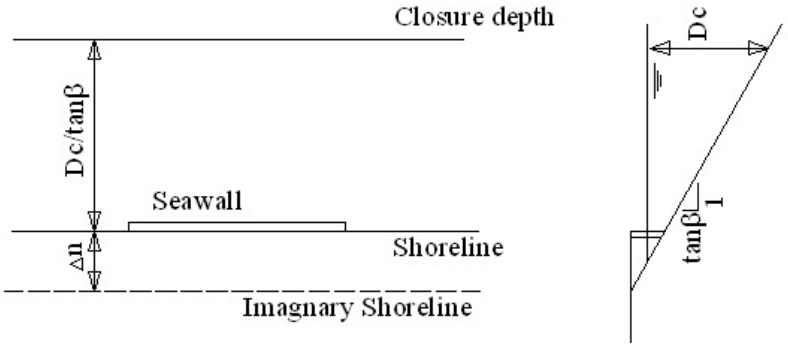

Figure 6.6. Typical layout of seawall.

River mouths

Two river mouths exist along the Nile Delta Coast i.e Rosetta, and Damietta. The sediment comes from this both branches are limited due to construction of Aswan high Dam and Aswan reservoir, in addition to several barrages along the Nile path. The sediment source from these two branches is taken as zero in the current model. The littoral drift within the width of the river is considered after multiplying it by a fraction factor.

6.5.4 Discretization scheme and stability (Numerical solution)

(6.2) will be approximated by explicit scheme finite difference. Schematic diagram of the discretaization system is presented in Figure 6.7. The time derivative of n is approximated by forward difference methodology. Sediment transport rates at the ends are defined with respect to corresponding boundary condition. If the boundary holds for no significant shoreline change with time, $\partial Q/\partial m$ is considers zero. However If a complete shore normal barrier that interrupts the longshore sediment movement, exists at one end of the shoreline, then this condition can be expressed as Q=0 (Port Said), and if shore normal barrier is partially interrupts the longshore sediment movement the Q is multiplied by a fraction factor as described in the previous section.

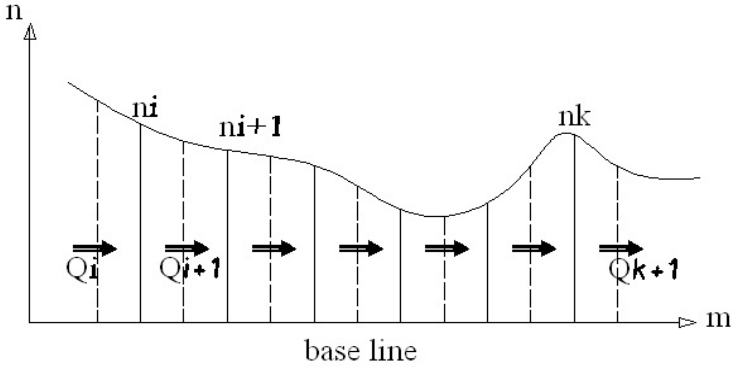

Figure 6.7. Schematic diagram for the discretaization system.

$$\left(\frac{N_i^{j+1}-N_i^j}{\Delta t}\right)=-\frac{1}{D_c+D_B}\sum_{k=1}^{k=N}\left(\frac{Q_{i+1}^j-Q_i^j}{\Delta m}\pm q\right)^k,\qquad K=1,2,.....,N \qquad \textbf{(6.33)}$$

$$N_i^{j+1}-=N_i^j-\frac{\Delta t}{D_c+D_B}\sum_{k=1}^{k=N}\left(\frac{Q_{i+1}^j-Q_i^j}{\Delta x}\pm q\right)^k,\qquad K=1,2,.....,N \qquad \textbf{(6.34)}$$

Dabees and Kamphus (2000), and Hanson, (1987) figured out that the stability is defined as;

$$\frac{Q}{\alpha_b(D_C+D_B)}\frac{\Delta t}{\Delta m^2}\le\frac{1}{2} \qquad \textbf{(6.35)}$$

In the current model the spatial resolution is taken as Δm=50m, and the temporal resolution is Δt = 0.01 day

6.6 Results and discussion

6.6.1 Straight beach bounded by groins from both sides

6.6.1.1 Single wave direction

The important contribution of the present model is that it reveals the effect of the grain size distribution on the sediment sorting along the beach. To check the effectiveness of the grain size, the model was first used on a simple case, i.e. straight beach bounded by two jetties from the east and west sides respectively (no sediment is transported outside the system). Waves are incident from N-NW; the breaking wave height and angle are about 1m and 20^o respectively. Sand with average grain size of 0.4mm was considered in the model. The shore line is assumed to be mixed of grain size of 0.1mm, and 0.7 mm, with 50 percentage of each, the average grain size is 0.4 mm. The longshore component of wave energy flux is assumed to be proportionally distributed among the different sized grains according to their percentage. Figure 6.8. A&B, shows the shoreline change for the previously mentioned case up to 8 years, and the corresponding average diameter along the shoreline for different periods, i.e., 1 week, 2 months, 6 months, 1 year, 2 years. Since the smaller grain size can move easier than the bigger ones, as predicted, the model shows that the mean grain diameter becomes larger in the erosion zones and it becomes finer in the deposition zones.

In the erosion areas the average grain size depends on the initial grain size and the initial percentage of the each grain size. The average diameter distribution reaches the equilibrium state after 1 year. In the current shoreline model, there is only one line as a solution of the

shoreline since all the assumptions like the classical one-line model. Therefore in the final state, the shoreline with different grain sizes while all other conditions are the same gives the same equilibrium shoreline. However, the rate of convergence is slightly differs from one case to the other.

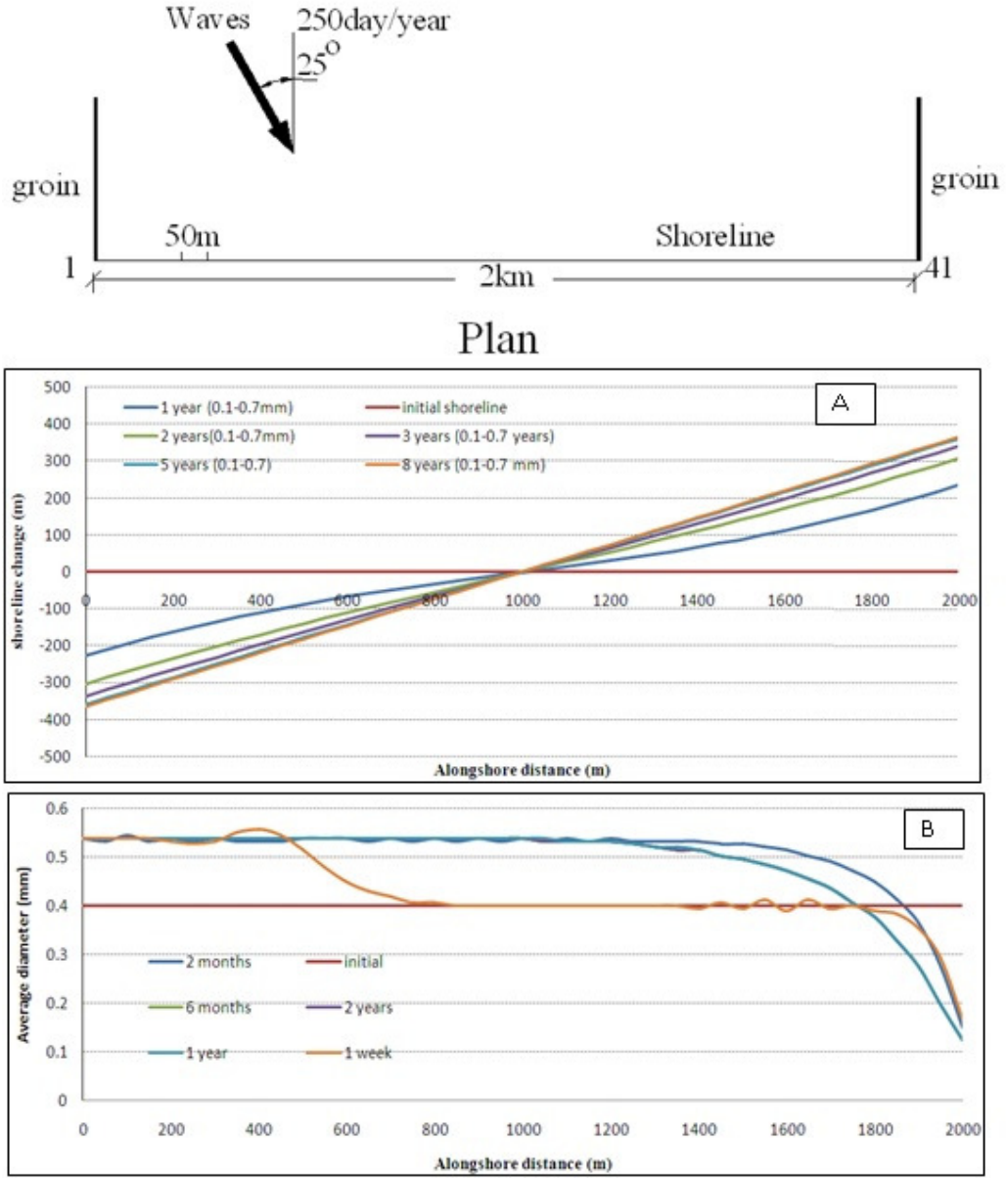

Figure 6.8. A) Schematic diagram of the straight beach with two groins, waves coming from the N-NW sector. B) Shoreline change in term of longshore distance. C) Average grain size, D_{50} along the shoreline.

Figure 6.9, shows the shoreline change and the average grain size distribution along the shore for different cases of the grain sizes (different combination of grain sizes), while the average diameter is 0.4 mm, and the standard deviation is 0, 0.1, 0.2, 0.3.

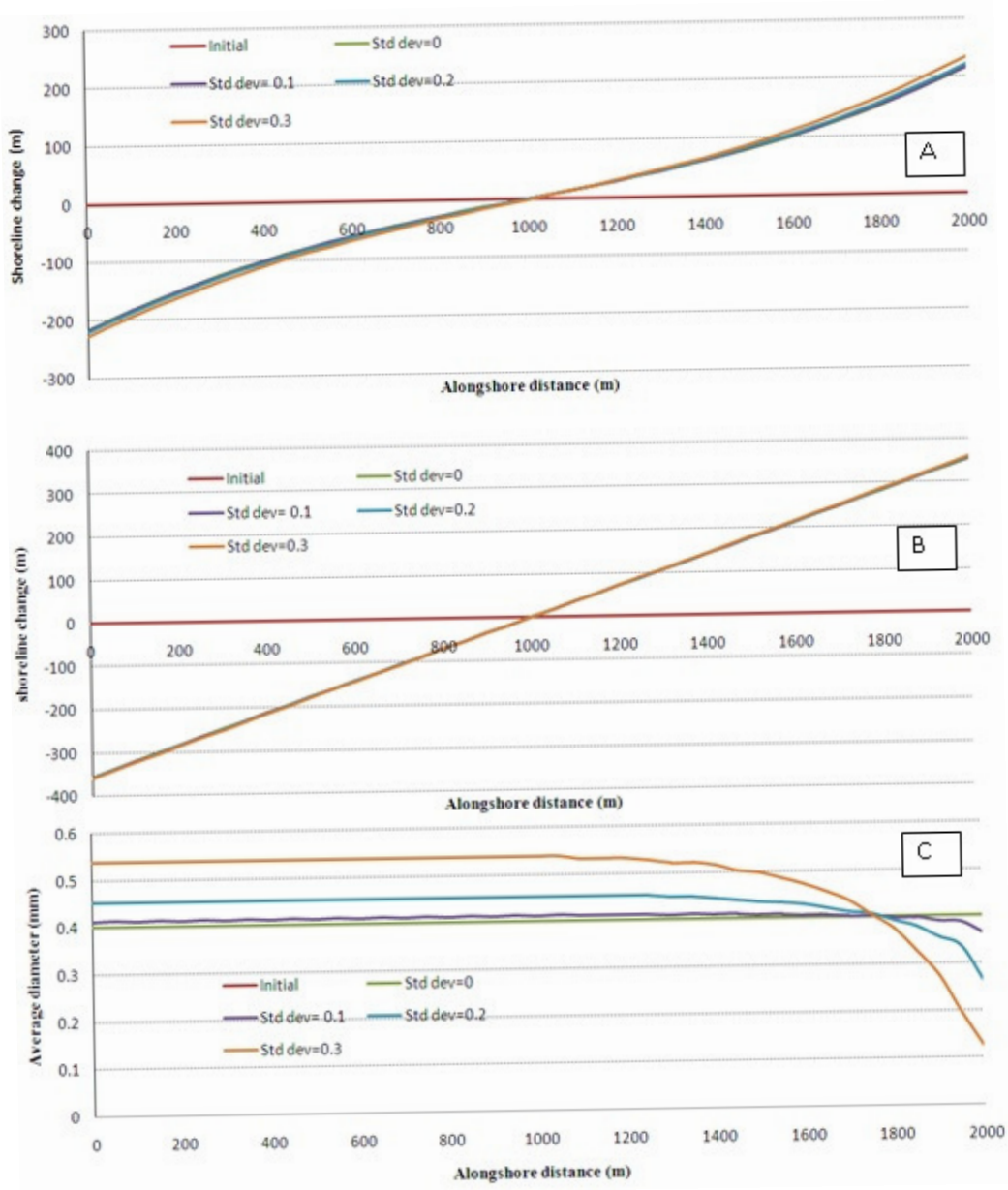

Figure 6.9. A) Comparison of the shoreline change after 1 year for different grain sizes (the average grain size is 0.4 with different standard deviation). B) Comparison of the shoreline change after 5 year. C) Average grain size, D_{50} along the shoreline after 1 year (equilibrium).

Figure 6.9 A & B shows the shore line change for different standard deviation at 1 and 5 years respectively. Difference was noticed at 1 year between the different cases. Increasing the standard deviation of the grain size distribution, increase the speed of the shoreline

change. However, after 5 years the shoreline is almost in equilibrium state so no difference between different cases.

6.6.1.2 Multiple wave direction

Kumada et al. (2002) considered the wave propagation from only one direction. In the current study, the effect of varying incoming waves is taken into account. Routine was included in the calculation to record the grain size at different locations along, and cross the shoreline. These records were used for the case of varying from accretion to erosion and vise verse. **Error! Reference source not found.** 6.10 A, shows the shoreline change along the shoreline after 1 and 2.5 years respectively due to consecutive varying waves from 20^{o} (150 days/year) and -20^{o} (100 days/year) and **Error! Reference source not found.** B, presents the corresponding average grain size distribution. In these figure comparison was made between the shoreline change and the grain distribution before and after adjustment (adjustment means considered the grain size at the cross shore direction). Difference exist between the different cases, however the difference is significant after 2.5 years.

6.6.2 Rosetta promontory

6.6.2.1 Sensitivity analysis

After trying the model for the simple pervious two cases, the model was adopted to simulate the shoreline change around Rosetta promontory. Also to figure out qualitatively the grain size distribution around Rosetta promontory. Sensitivity analysis were dedicated, i.e., sensitivity for the wave direction, for the empirical parameter in the longshore sediment transport formula (Ozasa and Prampoton), and for the pattern of the waves within the year. The sensitivity analysis was applied on the data within the period 1978 to 1990. Figure 6.1 to Figure shows the results of the shoreline change within 1978 to 1990 for different wave directions, wave patterns, and empirical parameters.

A) Wave direction

Figure 6.11 A, shows the shoreline change rates from 1978 to 1990. Comparison of the shoreline change rates during the previously mentioned period from the numerical model for different wave directions (N, NW, NNW, and NE) was illustrated. In Figure 6.11 C, the correlation between these results and the Land-sat results were shown. In this analysis the western boundary was considered as an open type boundary while the eastern boundary is

considered as closed boundary due to the existence of a groin bounded this area from the east. From Figure 6.11 B & C, the shoreline change rates are strongly dependent of the wave directions especially near the boundaries and at the River mouth. The correlation shows that the NW and NNW directions were the most nearest to the Land-sat date. In the current study, the percentage of occurrence of the waves was considered to be 100 days/year from the NW, 100 days/year from NNW, 50 days/year N, and 50 days/year from the NE. these percentage are matching with other literature studies (refer to chapter one and five).

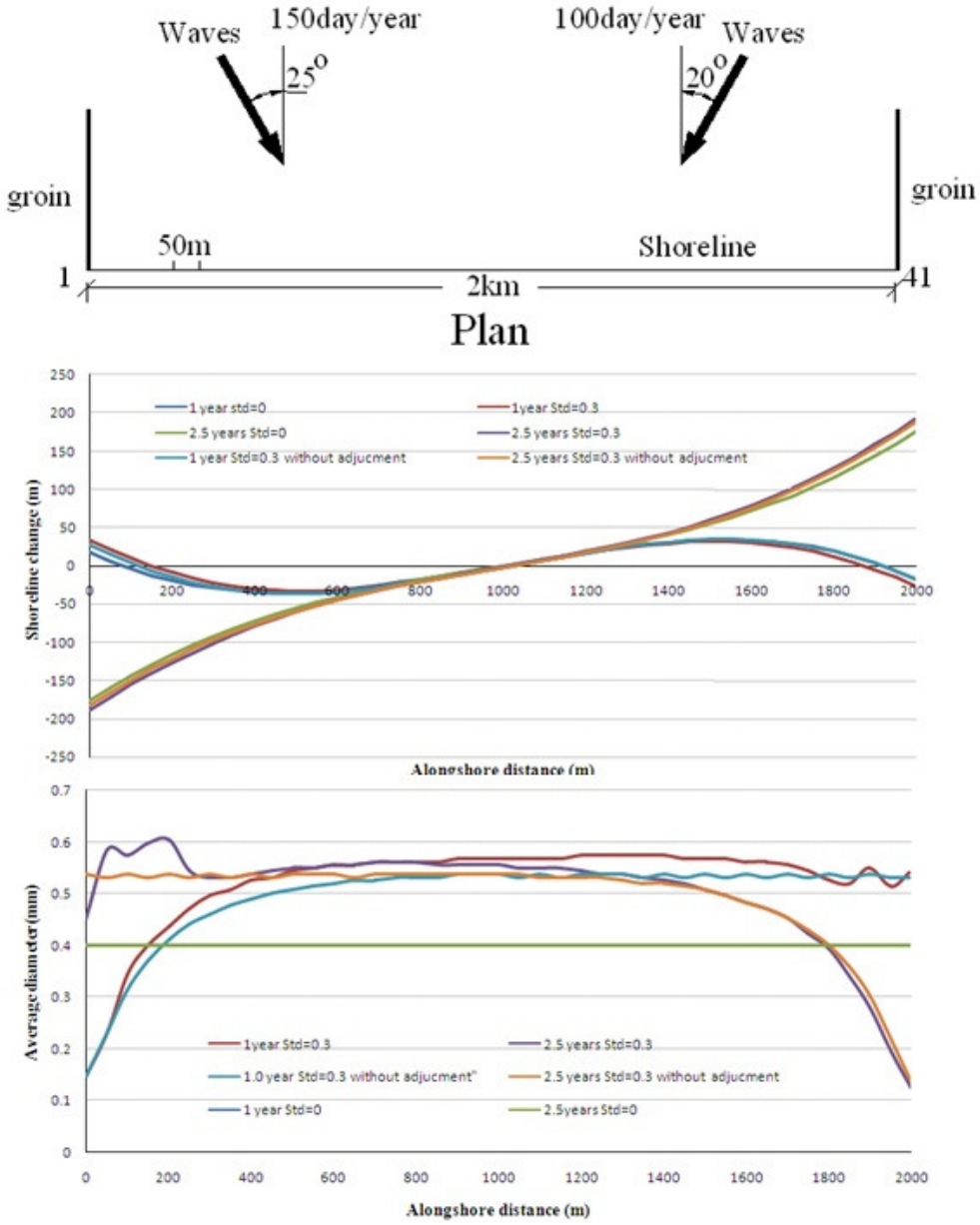

Figure 6.10. A) Schematic diagram of the straight beach with two groins, waves coming from the N- NW, and N-NE sectors. B) Shoreline change in term of longshore distance after 1 and 2.5 years. C) Average grain size, D_{50} along the shoreline.

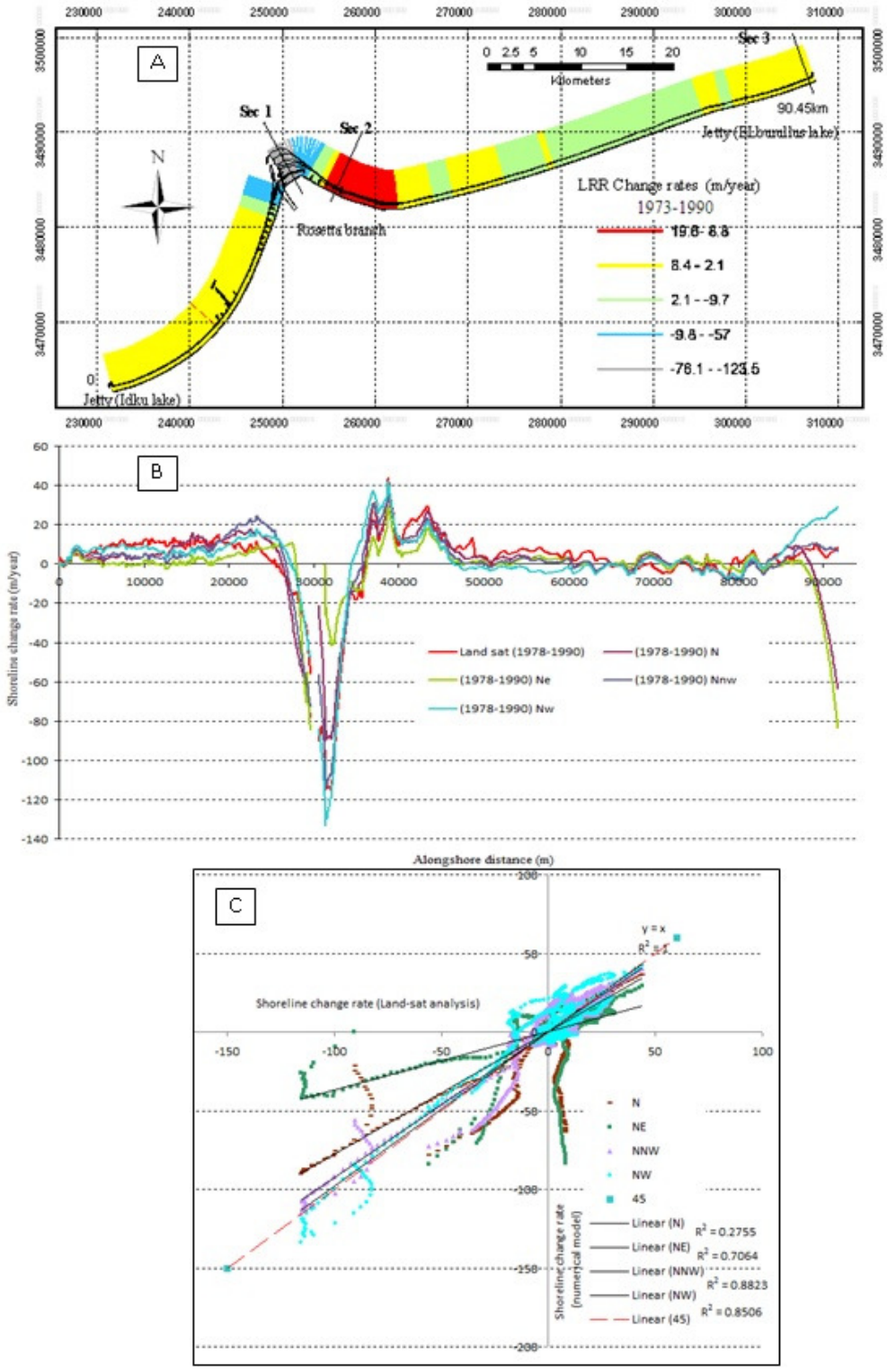

Figure 6.11. A) Shoreline change rates around Rosetta promontory from the Land-sat image analysis (1978-1990). B) Shoreline change in term of alongshore distance from different directions, NW, NWW, N, and NE. C) Correlation of the shoreline change from the land-sat analysis and the numerical model.

B) Empirical parameter (k)

Figure 6.12. A, shows the shoreline change rates for different cases of different empirical parameter (K_1) in the longshore sediment transport formula. The word mix refers to the previously mentioned combinations of waves. The correlation shown in Figure illustrate that the best value of the empirical parameter for the study site is K_1=0.3.

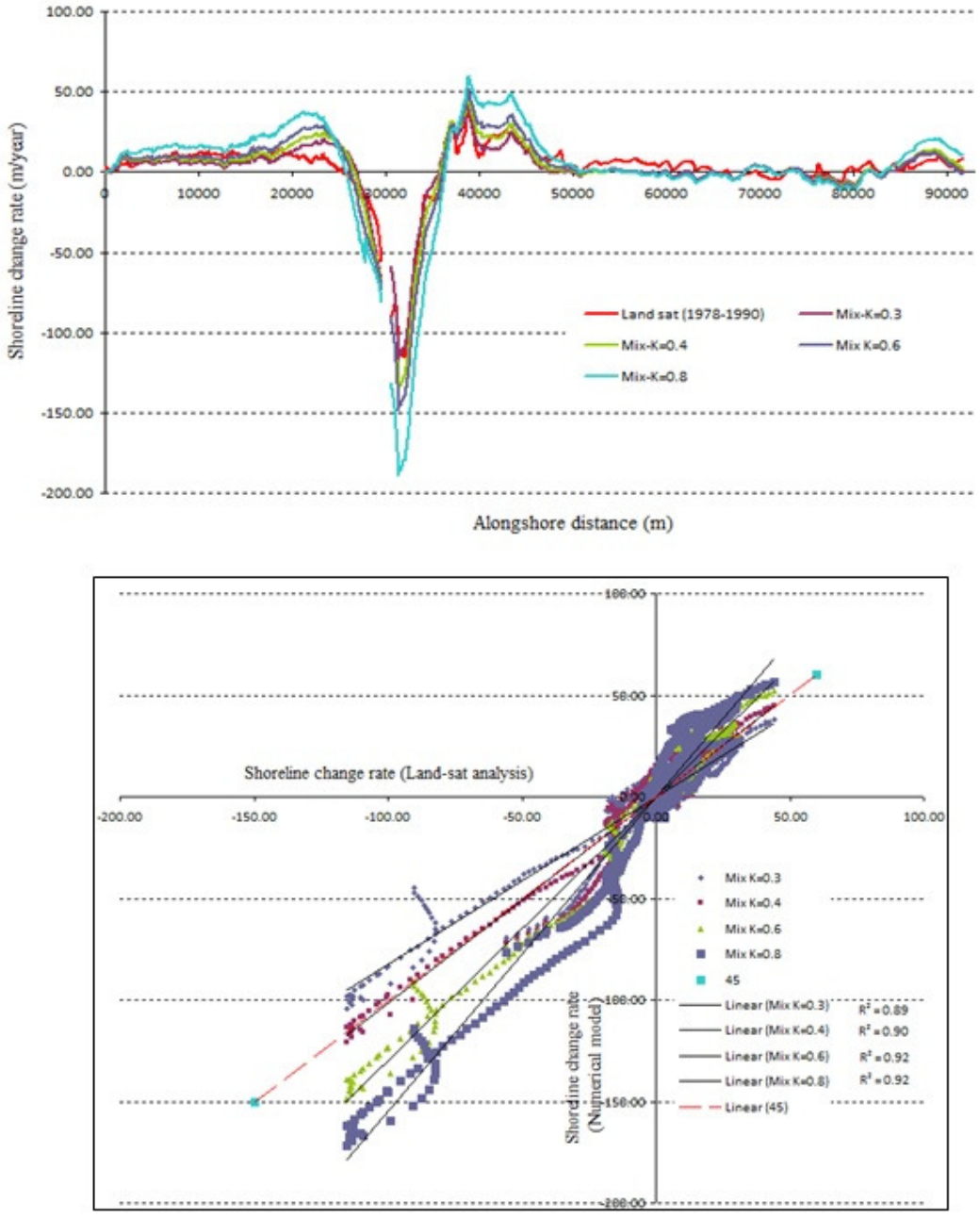

Figure 6.12. A) Shoreline change rates around Rosetta promontory in term of the empirical parameters. B) Correlation of the shoreline change from the land-sat analysis and the numerical model.

C) The wave pattern

The shoreline change rates for different patterns of waves during the year were presented in Figure 6.13 A, and the correlation between these results and the land-sat were shown in Figure 6.13 B. No significant difference between the different patterns was concluded from these two figures.

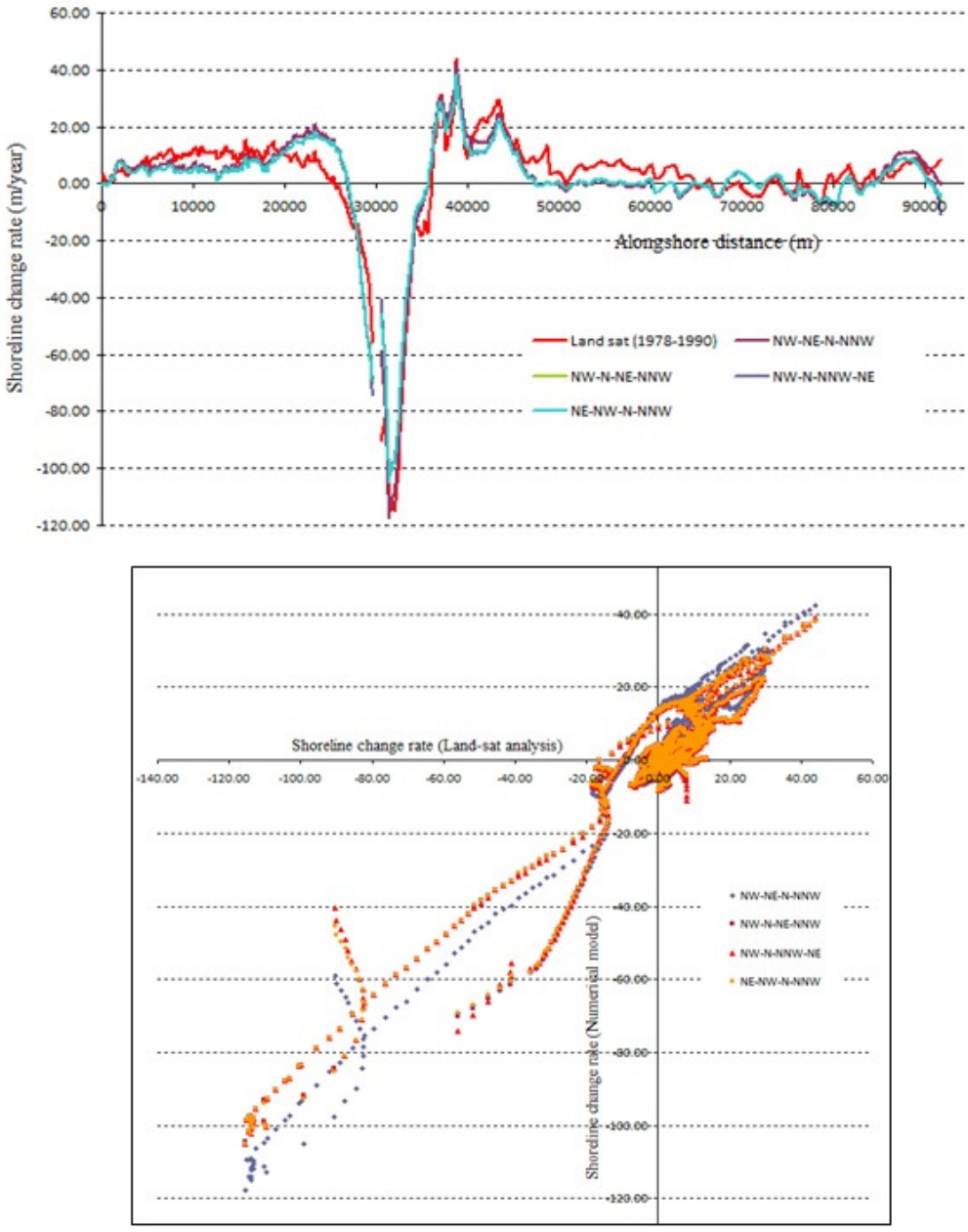

Figure 6.13. A) Shoreline change rates around Rosetta promontory in term of the different combinations of wave patterns. B) Correlation of the shoreline change from the land-sat analysis and the numerical model.

6.6.2.2 Shoreline change and alongshore sediment size distribution

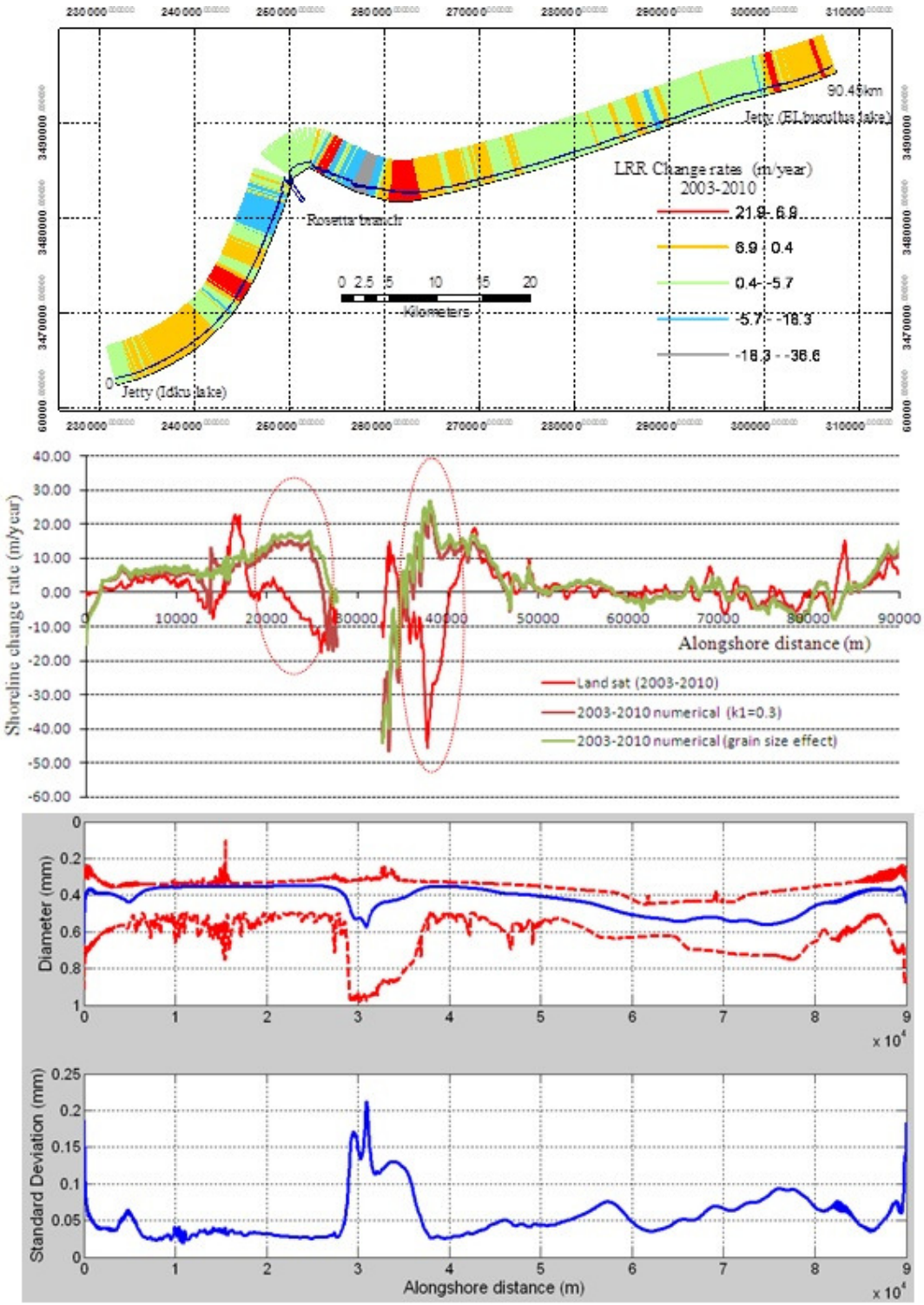

Figure 6.14. A) Shoreline change rates around Rosetta promontory from the Land-sat image analysis (2003-2010). B) Shoreline change in term of alongshore distance (land-sat analysis, numerical model k1=0.3, and numerical model taken the grain size distribution 0.15&0.6 mm). C) 1.Mean, minimum and maximum average grain size during the period of 2003 to 2010. 2. Standard deviation along the coast.

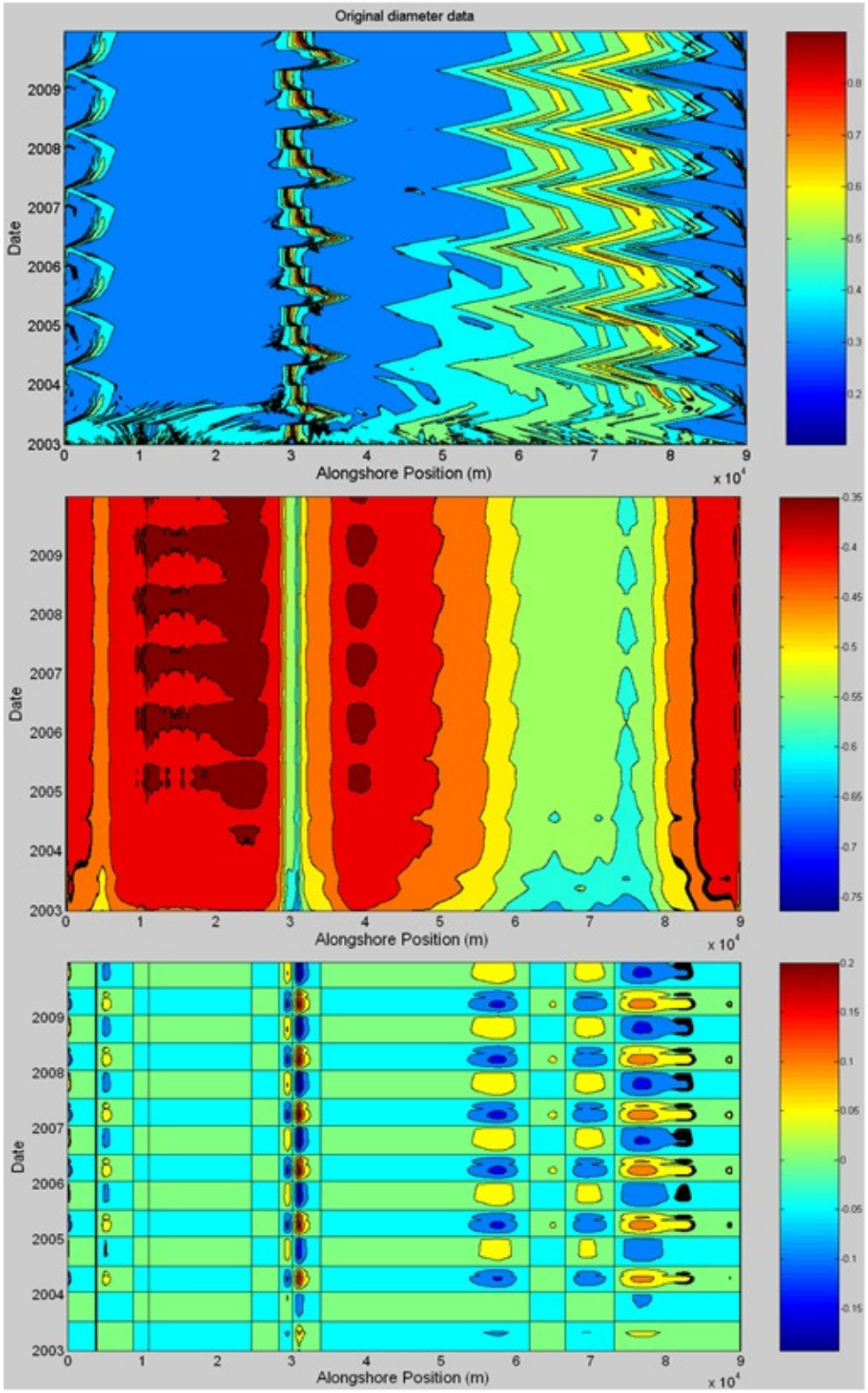

Figure 6.15. First ,and second modes contribution of the the grain size variation along Rosetta promontory,A) orginal average diameter, B) contribution from the first model, and C) contribution from the second mode.

After calibrating and validating the model using the data from 1978 to 1990, the model was used to simulate the shoreline change and the grain size distribution around Rosetta promontory within the period from 2003 to 2010 and predict the shoreline change until 2040 (the end of the design life time of the seawalls surrounding the River mouth). Figure 6.14 A, shows the shoreline change rates around Rosetta promontory during the period 2003-2010 from the Land-sat analysis. Figure 6.14 B, shows the comparison between the shoreline change rates from the Land-sat and the numerical model. Two cases were considered the first case the empirical parameter K_1 is taken as 0.3 and the second case the empirical parameter K_1 is considered as a function of the sediment size, $K1=0.2/(D_{50})^{0.5}$. From the analysis of the grain size along Rosetta promontory (refer to chapter 4), Combination of two grain sizes were considered 0.15mm with 50%, and 0.6 with 50%. Good agreement between the numerical results and the Land-sat results at different locations were recorded.

The model miss-predicate the shoreline change at the red color marked areas in Figure 6.14 B. The model could not simulate the erosion on the lee side of the last groin in the eastward of Rosetta promontory which is might be due to the ignoring of the circulation behind this groin. Another thing is that the bathymetry is developed for this period assuming that the profile is constant so it could contain difference from the actual bathymetry. In addition to that, the breaking for the considered wave condition occurs offshore the groin at this area.

Based on the shoreline changes, the grain size distribution is presented in Figure 6.14 C. the mean, maximum and minimum D_{50} are presented along Rosetta promontory. Since the grain size distribution at 2003 is not known so the analysis of the grain size is a qualitative. From the literature review, the grain size around Rosetta mouth in 2001 is characterized by 0.18 mm. Analysis of the grain size distribution around Rosetta mouth (Feb,2011) shows that the grain size has average diameter of 0.28 mm which means that the trend of the change goes toward the coarser. Figure 6.14 B, shows that the mean D_{50} is large near the river mouth (erosion area), and less near the boundaries (accretion area).

Since the grain size at any location is a function of the accretion and erosion so the grain size is changing with time. To capture the mode of the change of the grain size, analysis using the EOF (for details of the EOF refer to chapter 3) was carried out. The first two modes were considered. The first mode contributes by about 80% of the variability while the second mode is contributed by 7%. Figure 6.15, demonstrates the original average grain size and the contribution from the first and second mode respectively. Looking to the upper panel of Figure 6.15, the change of the grain size within the year is almost constant and periodic due

to the repetition of the wave pattern every year. Five locations as shown in Figure 6.15 have large variability (Around Rosetta mouth, near Idku Lake, three locations near El Burullus Lake).

6.6.2.3 The evaluation of the coastal groins around Rosetta mouth

The shore protection authority (The ministry of irrigation and water resources, Egypt) constructed two seawalls and several groins around Rosetta mouth (for more details refer to chapter 2) to combat the erosion. To check the efficiency of these groins, the model was applied ignoring the existence of the groins. Severe erosion was estimated adjacent to the lee side of the seawalls, while the maximum shoreline retreat reaches 2 km at 2040 measured from the 2010 shoreline at both sides. However, the maximum retreat in case of groins (current situation) reaches 700 m behind the last groin on the eastward side, and 400 m beside the third groin on the westward side. On the basis of the above findings, the groins plays and effective role in the protection of the surrounding area of the River. It could be wise to construct a groin or apply nourishment on the lee side of the last groin on the eastward side of Rosetta to delay the erosion took place in this area.

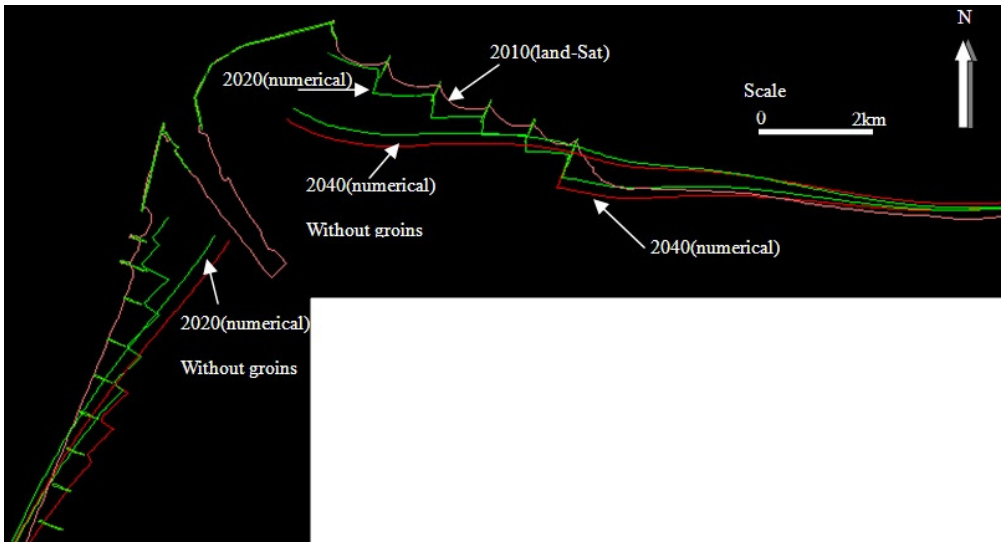

Figure 6.16. Comparsion of the shoreline change around Rosetta River mouth, in case of the groin existance,and groin ignofrance.

6.6.3 The entire Nile Delta Coast

To check the capability of the model to cover the entire Nile Delta Coast, the model was used to simulate the shoreline change in the period between 1978 and 2010. Figure 6.17, shows the calculated longshore sediment transport due to waves from the NW and NE. The shoreline

change rates were illustrated in Figure 6.18. The model could successfully simulate the general features of the erosion for the three headlands of Rosetta, El Burullus and Damietta, and the accretion for the embayment, near the structures, and sand spit.

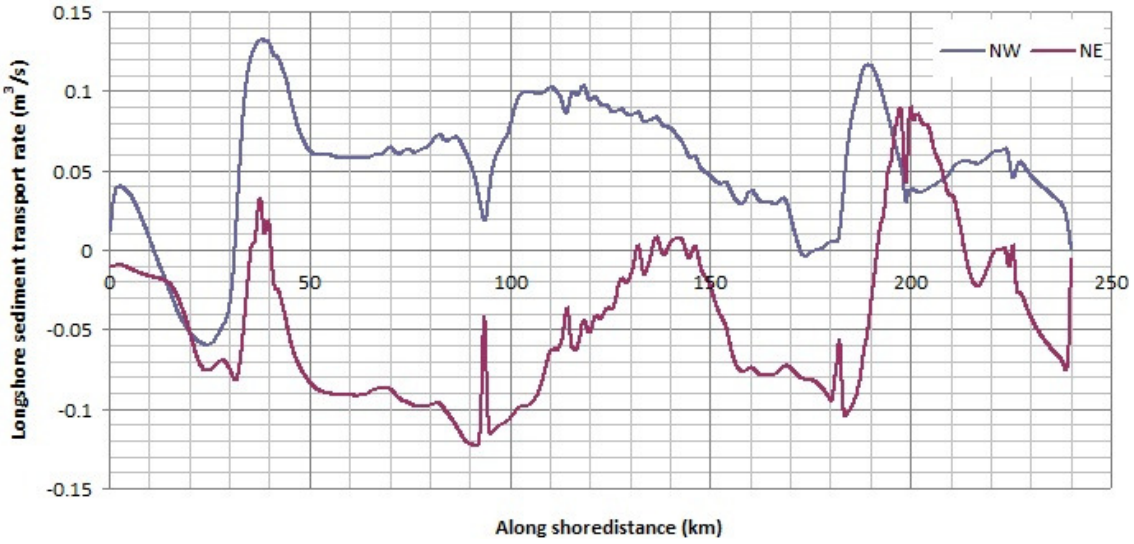

Figure 6.17. Alongshore sediment transport rates.

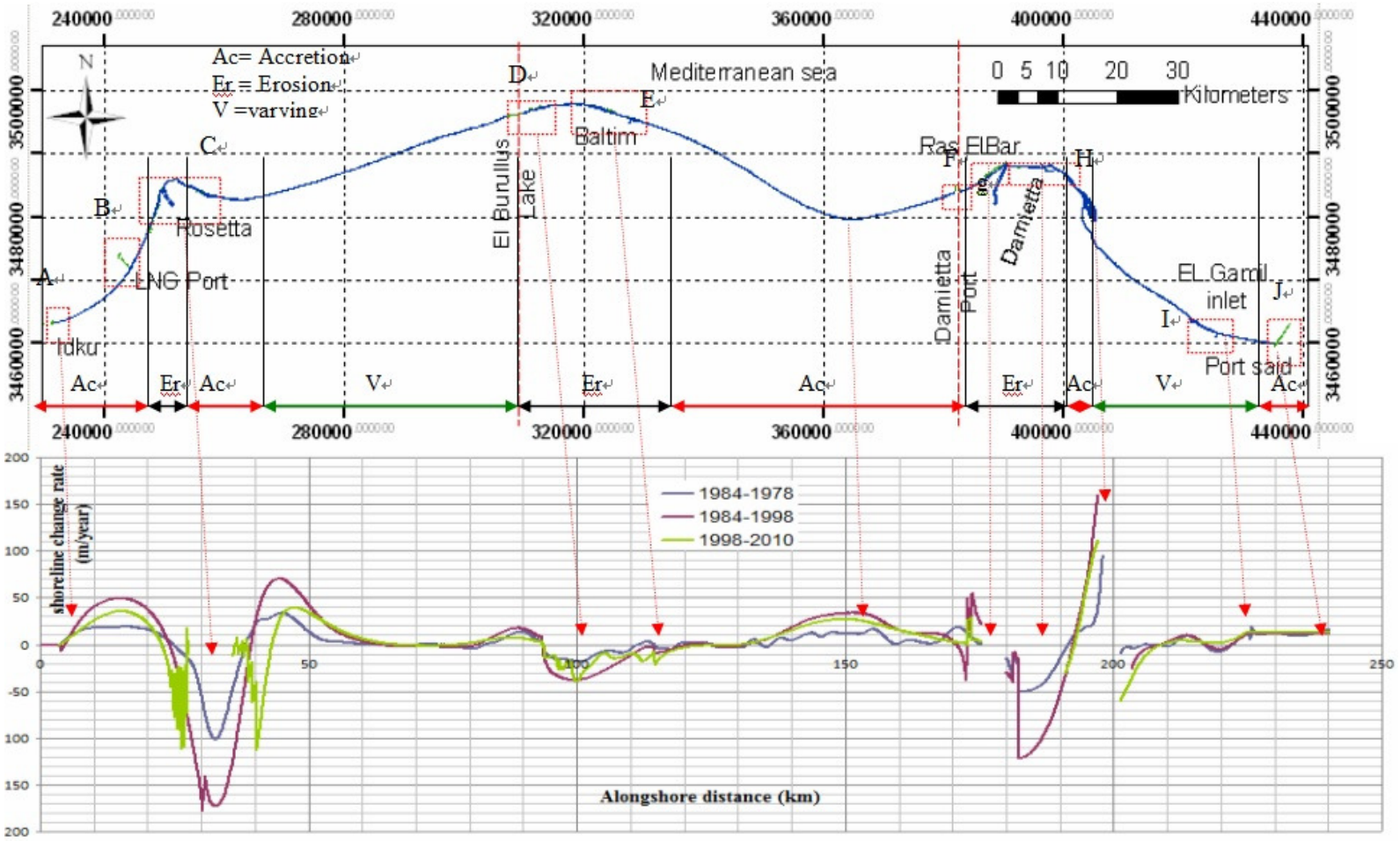

Figure 6.18. Shoreline change rates along the Nile Delta Coast, 1978-2010.

Chapter7 Conclusions.

7.1 General

The Nile Delta Coast has suffered s large scale and long term coastal erosion. This coast has different kinds of boundary conditions (coastal structures; seawalls, breakwaters, groins, and jetties), and the shape of the coast line changes very dynamically especially around the two promontories (Rosetta and Damietta).

The current study applied multiple methodologies to cover the analysis of the coastal erosion and accretion along the NDC and to improve the way of understanding of the coastal processes and to control the shoreline change. These methodologies include analysis of the land-sat images, investigations of sampled sand around the swash zone, and the numerical analysis based on the shoreline model. These three methods combined together to simulate and explain the shoreline changes and the grain size along the coast. These methods showed good consistency between each others. Some limitations of each method impede the efficiency of whole methodology. Schematic diagram showing the working pattern of the three methods are presented in Figure7.1.

The land-sat images were used to determine the shoreline changes and to estimate the eroded and accreted areas, which eventually determine alongshore sediment transport rates and directions. Sand samples were used to investigate the sediment characteristics along the coast. The Thermo-luminescence test was performed on the same samples. This test enables us to determine the sediment sources and deduce the sediment transport directions. Based on all the collected data and information, finally, a numerical model was introduced, calibrated, and applied to the prediction of the future changes. Following sections describe brief conclusions of the results of each method and possible future tasks and recommendations.

7.2 Land-sat analysis

Multi-temporal satellite images, i.e., Landsat MSS, TM, and ETM from 1973 up to 2010 were used to study the long term changes along the 250 km, along the NDC. The coastal lines were automatically extracted based on the local XY-coordinates from Land-sat satellite images over 37 years with unequal time intervals.

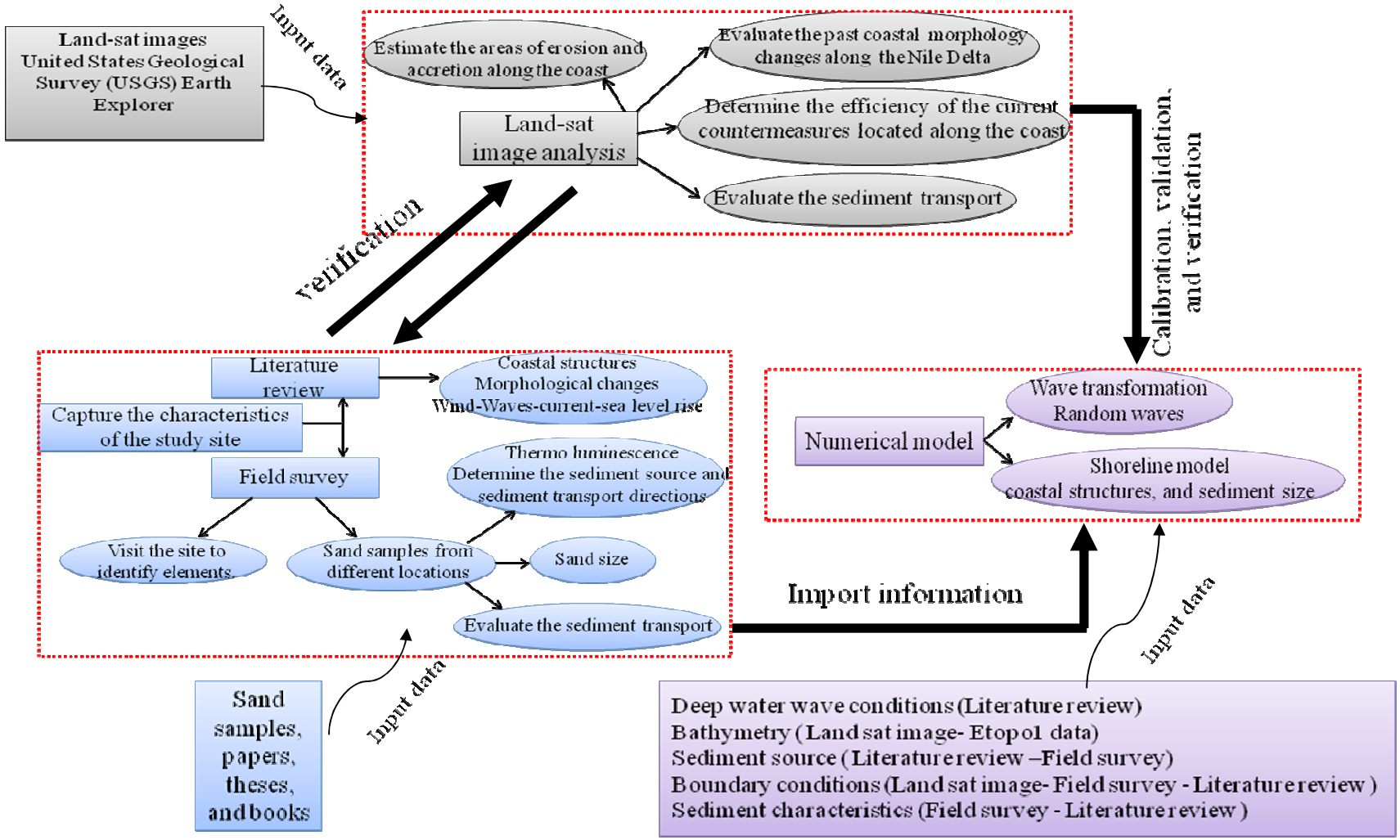

Figure 7.1. The working pattern of the three approaches.

Approximately 46% of the NDC experienced erosion while 52% undergo some accretion. The general features along the NDC are the erosion at the three headlands of Rosetta, Burullus and Damietta, and the accretion for the embayment, near the structures, and sand spit. Detailed analysis of the shoreline changes around both Rosetta and Damietta promontory were performed. This analysis is based on the linear regression technique as well as the empirical orthogonal function analysis.

Along Rosetta promontory which is 90-km-long coast, about 20-km-long coast is around the tip of Rosetta promontory and is protected by hard structures such as seawalls and groins. The erosion was the main phenomenon along the study area especially around the tip of the river mouth, where the highest rate of erosion around the river mouth of Rosetta promontory was 126m/year before protection. On the other hand, accretion was experienced beside the boundaries of the study area near the groins and the middle area had less shoreline changes relative to the other area. While the placement of the coastal countermeasures locally decreased the erosion, erosion was caused just adjacent to the protected areas. These structures appear to have caused the shoreline retreat further east side of the river mouth. The impact of these coastal structures is still extending which calls for continuous monitoring and additional counter measures.

Along the 65 km coast around Damietta promontory, the erosion was the main phenomenon around the tip of the river mouth like Rosetta mouth. The highest rate of erosion around the river mouth of Damietta promontory was 50 m/year before protection and it was terminated after constructing the seawall and the erosion shifted to adjacent area. Also the erosion along Ras El Bar resort was replaced by accretion due to the construction of eight shore parallel detached breakwaters. On the other hand, variation between accretion and erosion was observed along the eastern part (Damietta-Port Said). Within the study period accretion was experienced beside Port Said breakwater and erosion is revealed near Damietta port. The sand spit acts as a huge breakwater and is kept extended to the south-east with distance of 1.5, 1.9, 2.5, 3, and 3.8 km measured from the eastern end of the spit in 1973 to the years, 1984, 1990, 1998, 2003 and 2010, respectively. The inclination of outer line of the sand spit decreased from 2003 to 2010. The effect of seawall construction appears to have small impact on the sand spit deformation. The calculated rates of the shoreline changes from the Land-sat analysis showed good agreements with the ones of actual observed data at 30 different locations obtained through the past field survey for the period from 1972 to 1990.

EOF analysis gives indication about the mechanism of the shoreline change. The EOF revealed that the first two eigenfunctions are able to describe nearly 98% of the shoreline variability. Shoreline change due to alongshore sediment transport, which is mainly observed in the second mode, dominates the one by cross-shore movement expressed in the first mode.

The satellite imagery has many advantages. The satellite, for example, is operational all the time ove the year and it revisits the same area frequently and sattelite image covers large areas. Moreover it has less restriction, i.e. no air traffic control restrictions, no cameras or expensive equipment user. The satellie itself is very expensive,and the spatial resolution is still coarse. For the current study the resolution is varying from 15m to 80m. Since the tide is small, it was not considerd in the study (actually it is not available). Ignorance of the tidal information could put some value of uncertainty within the results.

7.3 Field survey and Thermo-luminescence test

Field survey was conducted in February 2011. Sand samples were collected at more than 60 various locations along the shoreline. TL indicates the intensity of the luminescence of certain crystalline materials such as feldspar and quartz contained in sand grains when these components are stimulated by heating. This study measured TL intensity of the feldspar extracted from the sand samples. As a result, it was found that the sand grains near the Rosetta and Damietta branches present a higher TL signal and TL intensity gradually decreases with increasing distance from the two river mouths, which indicates sediment alongshore transport features. The small difference of TL intensities between the sand grains near the river mouth and the ones on the natural coast indicates that the sediment supply from the river is limited. The estimated sediment transport directions based on the TL analysis are consistent with the interpretations based on the analysis of land-sat images around Rosetta promontory while these two estimations were contrary to each other on the west side of Damietta promontory. Observed inconsistency may be due to fluctuating errors of TL measurements since, as discussed previously, little sand supply from the river ended up to yield finite difference of TL along the coast even around the river mouth.

Sand characteristics were further investigated. The grain size distribution; the median sand size, D_{50} was measured using the laser diffraction particle size distribution measuring apparatus. The color of sand grains was also identified by naked eyes and the mineral composition based on color was interpreted using the automated analysis of images captured

by a digital microscope. Through this analysis, clear difference was noticed by the naked eyes in the sand color, and size between different areas. Around Rosetta promontory the sand color is light and average size is 0.28 mm, while in the middle part of the Delta the color is lighter and grain sizes are coarser with average size of 0.6mm, and from Damietta to Port Said the color is darker and average grain size is 0.23mm. The sediment comes from the river contains blackish sand with small size and other colors with bigger size. The dark sand is dominant in the sand dunes. The sand samples near the large traps i.e., Idku jetty, El Burullus jetty, and Damietta breakwater are characterized by dark color. This illuminates that the dark grains is smaller than other grains which moves easily and accumulated near the coastal structure.

7.4 Numerical model

The improved numerical model simulates the wave transformation, regional sediment transport, sediment size, and shoreline changes. The model is composed of two parts, Energy Balance Equation model and one-line model. For computations of the wave field, this study applied horizontal steady state conservation equations of the spectral energy of the waves and accounted for the effect of wave diffraction by introducing Mase (2001)'s dispersion-type terms. The energy dissipation was estimated by Tajima and Madsen's (2006) model and iterative procedures were applied for computations of such implicit energy dissipation term. At the offshore boundary, incident wave spectra was determined based on Bretschneider-Mitsuyasu type frequency spectrum and the Mitsuyasu type directional spreading function with specified significant wave heights, periods, mean wave directions and spreading parameters of directional spectra. The shoreline change model is based on the one-line theory, first presented by Considere (1956). No sediment discharge from the river was considered following the conclusions based on the TL analysis. Since there are many structures placed along the coast, the sediment transport was calculated based on Ozasa and Brampton's (1980) formula, which accounts for the effect of alongshore variations of the breaking wave height. The empirical parameters were calibrated using the shoreline data acquired from the land-sat images. Due to the high curvature of the shoreline along the study site, the One-line model was formulated in terms of local coordinates normal to and tangential to the actual shoreline. The introduction of the grain size distribution is introduced to the One-line model based on Kumada et al. (2002). The mixing depth is based on (Kraus, 1985), and width of exchange layer based on (Hirano, 1971).

The improved model was calibrated and validated against the data from Land-Sat images along the Nile Delta Coast in Egypt. The model successfully simulates the general features of the erosion for the three headlands of Rosetta, Burullus and Damietta, and the accretion for the embayment, near the structures, and sand spit. The model exhibits its ability in the prediction of the shoreline around Rosetta promontory before and after placing the countermeasure structures. The correlation between the numerical model simulation and the Land-Sat image data was more than 90%. The model was used to check the importance of placing the current coastal structures around Rosetta mouth by simulating the shoreline changes with and without structures. Severe erosion was estimated in the case if there are no structures around the Rosetta mouth. By comparing the grain size distribution around Rosetta mouth in 1988 with the size in 2012, it is noted that the grain size become coarser due to the erosion. The model succeeded to qualitatively simulate such change of the grain size around the Rosetta mouth.

The one-line model is one of most practical methods that provide reasonably accurate shoreline changes with relatively less effort of calibration and with less input data. However it doesn't consider the tides and rip currents. Also it doesn't consider the cross shore movement and assuming the profile is constant all the time. These assumptions increase the uncertainty and the source of error. In the current study the bathymetry is developed from different sources of data. This bathymetry affects the wave transformation which is an important factor for the one-line model.

Finally the shoreline change and the grain size analysis along the coast were investigated. The developed methodology was successful and could be applied for local areas along the NDC or extended to other study areas. Data base related to the shoreline, bathymetry, wave, tide, grain size distribution, sediment sources, sediment paths and coastal structures were updated along the NDC during the study. This data base is useful for the coastal management along the NDC. It is recommended to carry out more studies for investigation of the detailed problems at local areas, for proposing alternative counter measures against the problems of erosion and accretion, and for investigations of the influence of wave overtopping on coastal erosion in wider areas. The wave data (Height, direction) needs to be investigated much and extended to cover the study period. Sensitivity analysis indicates that coastline changes respond strongly to wave data especially near the structures and at the River mouth. In the current study wave date analyzed for one year is repeated along the study time interval. Since

the wave information is only available at three locations along the NDC for different periods and it doesn't cover all the time, analysis of the wind data using WAM or other model could be useful.

7.5 Recommendations

- The methodology of the present study could successfully describe the shoreline changes and the variation of the sediment characteristics along the Nile Delta coast and could be applied to other locations. The three different methods: land sat analysis; sediment characteristics analyses; and the numerical model, are compatible with each other and thus integration of these three methods strengthens the validity of the analysis. So the present methodology should be applied with more detailed data in the future to sustain the coastal management along the Nile Delta Coast.
- The analysis of Land-sat images is very useful to study the shoreline changes along the Nile delta coast. The present method for shoreline-extraction has sufficient accuracy, i.e., the correlation of estimated shoreline change rates between the present method and past field survey exceeded 90%. The sea level rise and tide should be included in the future to have better results.
- The TL technique shows capability in predicting the sediment transport direction, and sediment sources. It indicated that the sediment from the River Nile is very limited. For better analysis of the sediment characteristics, it would be useful to resample the entire length of the Nile Delta Coast using a small interval between samples. Sampling should not be conducted during the winter season as the strong water waves overtopped the shore which makes it very difficult to perform the sampling. Samples should be extracted from the shore as well as from the seabed to check the effect of the water depth on the TL. Samples from the onshore (in the land) direction is valuable to determine the source of the sediment at the surf zone (Does the sediment comes from other locations or it is located originally in its place?)
- The TL technique is very sensitive and it depends on different factors. It would be useful to study the effect of these parameters on the TL in the future. Quantitatively study to link the sediment transport rates with the TL intensities could be an important study in the future.
- The improved Shoreline model could successfully describe the shoreline changes and qualitatively estimate the variation of the sediment characteristics. The correlation

between the results of the numerical model and the land sat is more than 90%. For the future improvement of the numerical model to include the sand spit deformation is recommended. The current circulation and cross shore sediment transport could be good enhancement in the future especially to study local areas on short term bases.

- It is recommended to carry out more studies for investigation of the detailed problems at local areas, for proposing alternative counter measures against the problems of erosion and accretion, and for investigations of the influence of wave overtopping on coastal erosion in wider areas.
- The wave data (Height, direction) needs to be investigated much and extended to cover the study period. Sensitivity analysis indicates that coastline changes respond strongly to wave data especially near the structures and at the River mouth. In the current study wave date analyzed for one year is repeated along the study time interval. Since the wave information is only available at three locations along the NDC for different periods and it doesn't cover all the time, analysis of the wind data using WAM or other model could be useful.

Bibliography

Abd El-Kawy, O. R., Rod, J. K., Ismail, H. a., and Suliman, A. S. (2011). "Land Use and Land Cover Change Detection in the Western Nile Delta of Egypt Using Remote Sensing Data." *Applied Geography*, Elsevier Ltd, 31(2), 483-494.

Abo-Zed, A. I., and Shereet, S. M. (2005). "Dynamics of Nearshore Sediments and Coastal Changes." *Emirates Journal of Engineering research*, 10(2), 51-61.

Aitken, M.J. (1998). An Introduction to Optical Dating, the Dating of Quaternary Sediments by the Use of Photon-Stimulated Luminescence. Oxford university press inc.,New York, 279.

Alesheikh, A., Ghorbanali, A., and Nouri, N. (2007). "Coastline Change Detection Using Remote Sensing." *International journal for Environmental science and Technology*, 4(1), 61-66.

Bailard, J. A. (1984). "A Simplified Model for Longshore Sediment Transport." *19th International Conference on Coastal Engineering,ASCE*, Houston, Texas, 1454-1470.

Bakker, W. T. (1968). "The Dynamics of a Coast with a Groyne System." *11th international conference on Coastal Engineering*, London, United Kingdom, 492-517.

Banna, M. M. E., and Frihy, Omran E. (2009). "Geomorphology Human-induced changes in the geomorphology of the northeastern coast of the Nile delta, Egypt." *Geomorphology*, Elsevier B.V., 107(1-2), 72-78.

Barbaro, G., Malara, G., Martino, M. C., and Arena, F. (2010). "Analytical Development of a One-Line Model for the Analysis of Shoreline Change by Wind Generated Waves." *Ocean Engineering*, 39(0), 108-115.

Bayram, A., Larson, M., and Hanson, Hans. (2007). "A New Formula for the Total Longshore Sediment Transport Rate." *Coastal Engineering*, 54(9), 700-710.

Bin, Z., Haiqiang, G., Yaner, Y., Qing, W., and Bo, L. (2008). "A simple Waterline Approach for Tidelands using Multi-Temporal Satellite Images: A Case Study in the Yangtze Delta." *Estuarine, Coastal and Shelf Science*, 77(1), 134-142.

Blodget, H.W, Taylor, P.T, and J. H. R. (1991). "Shoreline Changes Along the Rosetta-Nile Promontory: Monitoring With Satellite Observations." Marine Geology, 99, 67-77.

CORI. (2010). *Proposal for Egypt*, *Review Literature And Arts Of The Americas*.

Chen, L. C., and Rau, J. Y. (1998). "Detection of Shoreline Changes for Tideland Areas Using Multi-Temporal Satellite Images." *International Journal of Remote Sensing*, 19(17), 3383-3397.

Dabees, M. A., and Kamphus, J. W. (2000). "NLINE;Efficient Modeling of 3-D Beach Change." *25th international Conference on Coastal Engineering*, Sydeny-Australia, 2700-2713.

Dabees, M., Kamphuis, J William, and Asce, M. (1998). "ONELINE , A Numerical Model for Shoreline Change." *Coastal Engineering*, 2668-2681.

Dally, W. R., and Dean, R. G. (1985). "Wave Height Variation Across Beaches of Arbitrary Profile." *Journal of Geophysical Research*, 90(C6), 917-927.

David B. King, J. (2005). *Influence of Grain Size on Sediment Transport Rates with Emphasis on the Total Longshore Rate*.

Dewidar, K., and Frihy, O. (2008). "Pre- and Post-Beach Response to Engineering Hard Structures Using Landsat Time-Series at the Northwestern Part of the Nile Delta , Egypt." *journal of coast conservation*, 11(2007), 133-142.

Dewidar, Khalid M, and Frihy, Omran E. (2010). "Automated Techniques for Quantification of Beach Change Rates Using Landsat Series Along the North-Eastern Nile Delta, Egypt." *Journal of Oceanography and Marine Science*, 1(February), 28-39.

Duller, G. A. T., and Augustinus, P. (1997). "Luminescence Studies of Dunes from North-Eastern Tasmania." *Quaternary Science Reviews*, 16(96), 357-365.

ERDAS, I. (1997). *ERDAS Field Guide*. *Imagine*, Atlanta,Georgia-USA, 645.

Edward N. Lorenz. (1956). *Empirical Orthogonal Functions and Statistical Weather Prediction*. Cambridge,Massachusetts, 49.

El Banna, M. M. (2004). "Nature and Human Impact on Nile Delta Coastal Sand Dunes, Egypt." *Environmental Geology*, 45(5), 690-695.

El-Gamal, A. a. (2012). "New Approach for Erosion and Accretion Coasts Discrimination." *Journal of Coastal Research*, 280(2), 389-398.

El Raey, M. (2010). Impacts and Implications of Climate Change for the Coastal Zones of Egypt.

Fanos, A. M. (1995). "The Impact of Human Activities on the Erosion and Accretion of the Nile Delta." *Journal of Coastal Research*, 11(3), 821-833.

Forrest, B. M. (2003). "Application of Luminescence Techniques to Coastal Studies at the St . Joseph Peninsula , Gulf County , Florida." *Access*, MCMaster University.

Frihy, O. E, and Komar, P .D. (1993). "Long-Term Shoreline Changes and the Concentration of Heavy Minerals in Beach Sands of the Nile Delta , Egypt." *Marine Gelogy*, 115, 253-261.

Frihy, O. E. (1992). "Sea-Level Rise and Shoreline Retreat of the Nile Delta Promontories , Egypt." *Natural Hazards*, 65-81.

Frihy, O. E. (2003). "The Nile Delta-Alexandria Coast□: Vulnerability to Sea Level Rise , Consequenses and Adaptation." *Mitigation and Adaptation Strategies for Global Change*, 8(2), 115-138.

Frihy, O. E., and Lawrence, A. D. (2004). "Evolution of the Modern Nile Delta Promontories□: Development of Accretional Features During Shoreline Retreat." *Environmental Geology*, 914-931.

Frihy, O. E, and Dewidar, K.M. (2003). "Patterns of Erosion / Sedimentation , Heavy Mineral Concentration and Grain Size to Interpret Boundaries of Littoral Sub-Cells of the Nile Delta , Egypt." *Marine Geology*, 199, 27-43.

Frihy, O. E, Deabes, E. A., Gindy, A. A. E., and Shallalat, E. (2010). "Wave Climate and Nearshore Processes on the Mediterranean Coast of Egypt." 103-112.

Frihy, O. E, Fanos, Ally M, Khafagy, A. A., and Paul, D. K. (1991). "Patterns of Nearshore Sediment Transport Along the Nile Delta , Egypt." *Coastal Engineering*, 15(2), 409-429.

Frihy, O.E, Nasr, S.M, El Hattab, M.M., M. E. R. (1994). "Remote Sensing of Beach Erosion Along the Rosetta Promontory, Northwestern Nile Delta , Egypt." International Journal of Remote Sensing, 15, 1649-1660.

Goda, Y., Takayama, T., and Suzuki, and Y. (1978). "Diffraction Diagrams for Directional Random Waves." *Coastal Engineering*, 628-650.

Haslam, D. W. (1984). Admiralty Tide Tables. European Waters (including the Mediterranean Sea). 434.

Hallermeier, R. J., and Belvoir, F. (1978). "Uses for a Calclated Limit Depth to Beach Erosion." *Coastal Engineering*, 1493-1512.

Hallermeier, R. J. (1981). "A Profile Zonation for Seasonal Sand Beaches From Wave Climate." *Coastal Engineering*, 4, 253-277.

Hanson, H. (1987). "GENESIS - A Generalized Shoreline Change Numerical Model for Engineering Use." Lund Inst. of Tech./Univ.

Hanson, Hans, and Kraus, N. C. (2011). "Long-Term Evolution of a Long-Term Evolution Model." *Journal of Coastal Research*, 59(1989), 118-129.

Hinrichsen, D. (1999). *The Coastal Population Explosion*. 31-34.

Hirano, M. (1971). "River Bed Degradation with Armouring." *Japan Socity of Civil Engineering*, 3(2), 194-195.

Horikawa, K., and Kuo, C.-T. (1966). "A Study on Wave Transformation Inside Surf Zone." *Coastal Engineering*, New York, 217-233.

Kamphuis, J W, Readshaw, J. S., Canada, W., and Laboratories, H. (1978). "A Model Study of Along Shore Sediment Transport Rate." *21st International Conference on Coastal Engineering, ASCE*, Malaga, 1253-1264.

Kamphuis, J W, Davies, M. H., Nairn, R. B., and Sayao, O. J. (1986). "Calculations of Littoral Sand Transport Rate." *Coastal Engineering*, 10, 1-21.

Kamphuis, J. W. (1991). "Alongshore Sediment Transport Rate." *Journal of Waterway, Port, Coastal and Ocean Engineering,ASCE*, 117(6), 624-641.

Keizars, Z. K., Forrest, B. M., and Rink, W. J. (2008). "Natural Residual Thermoluminescence as a Method of Analysis of Sand Transport along the Coast of the St . Joseph Peninsula , Florida K . Zen K." *Journal of Coastal Research*, 24(2), 500-507.

Khafagy, A. A. and Manohar, M. (1979). "Coastal Protection of the Nile Delta." *Natural Resources*, 15, 7-13.

Komar, Paul D, and Inman, D. L. (1970). "Longshore Sand Transport on Beaches in and near and compute and spectra." *Journal of Geophysical Research*, 75(30), 5914-5927.

Kraus, N. (1985). "Field Experiments on Vertical Mixing of Sea of Japan." *Journal of Sedimentary Petrology*, 55, 0003-0014.

Kumada, T., Kobayashi, A., T. Uda, M. S., Hoshigami, Y., and Masuda, K. (2002). "Development of a Model for Predicting Beach Changes Considering Sorting of Sand of Mixed Grain Size." *Annual Journal of Coastal Engineering, JSCE*, (48), 561-565.

Liu, H., Ogawa, Y., Takagawa, T., and Sato, and S. (2009). "Longshore Sediment Movement along the Enshunada CoastInferred from Feldspar Thermoluminescence." *Coastal Dynamics*, 12.

Liu, H., Tajima, Y., and Sato, S. (2010). "Long-Term Monitoring on the Sand Spit Morphodynamics at the Tenryu River Mouth." *32nd International conference on Coastal Engineering*, Shanghai, China, 15.

Liu, H., Hamamoto, A., and Sato, S. (2011). "Monitoring the Nourished Sand Longshore Movement Based on Feldspar Luminescence Measurement." *Coastal Sediments*, Miami,Florida, 57-70.

Madsen, P. a., Fuhrman, D. R., and Wang, B. (2006). "A Boussinesq-Type Method for Fully Nonlinear Waves Interacting with a Rapidly Varying Bathymetry." *Coastal Engineering*, 53(5-6), 487-504.

Manohar, M. (1981). "Coastal processes at the Nile Delta coast." *Shore Beach*, 49, 8-15.

Mase, H. (2001). "Multi-Directional Random Wave Transformation Model Based on Energy Balance Equation." *Coastal Engineering Journal*, 43(04), 317-337.

Mase, H., Oki, K., Hedges, T. S., and Li, H. J. (2005). "Extended energy-balance-equation wave model for multidirectional random wave transformation." *Ocean Engineering*, 32(8-9), 961-985.

Mckeever, S.W.S. (1983). Thermoluminescence of solids. Oklahama state, 376.

Miller, J. K., and Dean, R. G. (2007). "Shoreline Variability via Empirical Orthogonal Function Analysis: Part I Temporal and Spatial Characteristics." *Coastal Engineering*, 54(2), 111-131.

NASA. "NASA image." *geology.com*, <http://geology.com/articles/satellite-photo-earth-at-night.shtml>.

Omar, W. M., El-mooty, M. M. A., and Nagy, H. M. (2005). "Evaluation of Closure Depth Along the Northern Nile Delta Coast , Egypt." *Alexandria Engineering Journal*, 44, 623-635.

Ozasa, H, and Brampton, A.H. (1980). "Mathematical Modelling of Beaches Backed by Seawalls." Coastal Engineering,, 4, 47-63.

Pelnard-Considere, R. (1956). "Essai de Theorie de l'Evolution des Formes de Rivage en Plages de Sable et de Galets." *4th Joumees de l'Hydraulique, Les Energies de la Mar, Question HI, Repport No.1*, 289-298.

Peregrine, D. H. (1966). "Long waves on a beach." *Journal of Fluid Mechanics*, 27(4), 815-827.

Perlin, M. and Dean, R. (1983). *A Numerical Model to Simulate Sediment Transport in the Vicinity o/Coastal Structures.* vicksburg mississippi.

Rink, W.J. and Pieper, K. D. (2001). "Quartz Thermoluminescence in a Storm Deposit and a Welded Beach Ridge." *Quaternary Science Reviews*, 20, 815-820.

Schoonees, J. S., and Theron, A. K. (1993). "Review of the Feld-Database for Longshore Sediment Transport." *Coastal Engineering,*, 19, 1-25.

Shibutani, Y., Kuroiwa, M., Kim, Y. M. M., and Abualtaef, M. (2009). "Development of N-Line Numerical Model Considering the Effects of Beach Nourishments." 2009(56), 554-558.

Shirai, M., and Omura, A. (2007). "Sand Grains Transport From River to Deep Marine Revealed by OSL Measurement Technique." *Quaternary International*, 167/168, 381.

Stanley, D. J. (1990). "Recent Subsidence and Northeast Tilting of the Nile Delta , Egypt." *Marine Geology*, 94, 147-154.

Swart, D. H. (1976). "Predictive Equations Regarding Coastal Transports." *15th International Conference on Coastal Engineering,ASCE*, Honolulu, Hawaii,, 1113-1132.

Tajima, Y., Mochizuki, S., Funatake, S., Bandula, W., Samalakoon, Shin-ichi, s., and Sato. S. (2011). "Investigation of Nearshore Sedimentary Characteristics along the West Coast of Sri Lanka Based on the Analysis of Satellite Images and Feldspar Thermoluminescence." *Journal of Japan Society of Civil Engineers*, 67(2), I-631-I-633.

Tajima, Y., and Madsen, O. S. (2006). "Modeling Near-Shore Waves, Surface Rollers, and Undertow Velocity Profiles." *Journal of Waterway, Port, Coastal, and Ocean Engineering*, (December), 429-438.

UNDP, and U. (1975). *Proceedings of seminar on Nile Delta sedimentology*. Academy of Scentific Research and Technology,Egypt.

USGS-EROS. "Earth Resources Observation and Science Center." <http://eros.usgs.gov/>.

Uda, T., Serizawa, M., Kumada, T., and Sakai, and K. (2010). "A New Model for Predicting Three-Dimensional Beach Changes by Expanding Hsu and Evans." *Coastal Engineering*, 2(57), 194-202.

Uda, T., Yamagata, H., Katoh, K.-ichi, and Akamatsu, N. (1998). "Predictive Model of Three-Dimensional Development and Deformation of a River Mouth Delta by Applying Contour Line Change Model." *16th international conference on Coastal Engineering*, 3138-3150.

Usama M. Saied. (2004). "Integrated Coastal Engineering Modeling." *Coastal Engineering*, McMaster University.

Valle, R. del, Medina, R., and Losada, and M. A. (1993). "Dependence of Coefficient K on Grain Size." *Journal of Waterway, Port, Coastal and Ocean Engineering*, 119(5), 568-574.

White, K., and Asmar, H. M. E. (1999). "Monitoring Changing Position of Coastlines Using Thematic Mapper Imagery, an Example From the Nile Delta." *Geomorphology*, 29, 93-105.

William A. Birkemeier. (1985). "Field Data on Seaward Limit of Profile Change." *Journal of Waterway, Port, Coastal and Ocean Engineering*, 111(3), 598-602.

Winant, C. D., Inman, D. L., and Nordstrom, C. E. (1975). "Description of Seasonal Beach Changes Using Empirical Eigenfunctions." *Journal of Geophysical Research*, 80(15), 1979-1986.

Rink W.J. (1999). "Quartz Luminescence as a light-Sensitive Indicator of Sediment Transport in Coastal Processes." *Journal of Coastal Research*, 15(1), 148-154.

Rink.W.J. (2003). "Thermoluminescence of Quartz and Feldspar Sand Grains as a Tracer of Nearshore Environmental Processes in the Southeastern Mediterranean Sea." *Journal of Coastal Research*, 19(3), 723-730.

Appendix A

A-1

Sand samples characteristics.

Table.1. Sand samples locations and acquisition date and time.

Sample no	Gps no	Acquisition date	Acquisition Time	Latitude	longitude
1	116	2011/2/17	12:26:26	N31 16.384	E30 11.134
2	118	2011/2/17	13:45:03	N31 17.537	E30 14.253
3	120	2011/2/17	14:08:38	N31 18.654	E30 16.166
4	125	2011/2/17	14:30:05	N31 19.136	E30 16.814
5	126	2011/2/17	14:42:03	N31 20.115	E30 17.910
6	131	2011/2/17	16:11:08	N31 24.358	E30 20.509
7	133	2011/2/17	16:30:36	N31 27.005	E30 22.445
8	134	2011/2/17	16:43:06	N31 27.793	E30 21.888
9	136	2011/2/18	7:14:04	N31 18.601	E30 31.010
10	139	2011/2/18	7:33:17	N31 18.079	E30 30.986
11	140	2011/2/18	8:54:35	N31 27.917	E30 25.866
12	143	2011/2/18	9:04:59	N31 27.903	E30 26.113
13	146	2011/2/18	9:08:32	N31 27.882	E30 26.143
14	147	2011/2/18	9:20:08	N31 27.565	E30 26.424
15	150	2011/2/18	9:27:34	N31 27.495	E30 26.962
16	151	2011/2/18	10:25:30	N31 27.341	E30 36.682
17	154	2011/2/18	11:45:17	N31 32.101	E30 48.284
18	155	2011/2/18	12:12:37	N31 34.898	E30 57.815
19	156	2011/2/18	13:42:50	N31 35.109	E30 59.675
20	157	2011/2/18	13:46:31	N31 35.190	E30 59.683
21	158	2011/2/18	13:51:16	N31 35.291	E30 59.941
22	159	2011/2/18	13:55:18	N31 35.319	E31 00.048
23	160	2011/2/18	13:57:01	N31 35.293	E31 00.068
24	161	2011/2/18	14:02:46	N31 35.535	E31 00.570
25	162	2011/2/18	14:22:58	N31 36.067	E31 05.863
26	163	2011/2/18	14:27:54	N31 36.072	E31 06.077
27	164	2011/2/18	14:30:29	N31 36.039	E31 06.145
28	165	2011/2/18	14:34:38	N31 36.044	E31 06.307
29	166	2011/2/18	14:43:37	N31 35.866	E31 07.624
30	167	2011/2/18	14:46:37	N31 35.829	E31 07.703
31	168	2011/2/18	15:28:03	N31 34.291	E31 13.727
32	169	2011/2/18	15:59:14	N31 29.941	E31 24.766
33	170	2011/2/18	16:26:17	N31 26.771	E31 32.934
34	171	2011/2/19	5:10:47	N31 27.869	E31 41.253
35	173	2011/2/19	5:33:35	N31 28.762	E31 44.411
36	174	2011/2/19	6:12:32	N31 30.466	E31 48.874
37	175	2011/2/19	6:25:44	N31 30.060	E31 48.215
38	176	2011/2/19	7:01:43	N31 30.508	E31 50.070
39	177	2011/2/19	7:38:01	N31 24.380	E31 46.997
40	178	2011/2/19	8:00:45	N31 24.777	E31 47.594

Sample no	Gps no	Acquisition date	Acquisition Time	Latitude	longitude
41	179	2011/2/19	8:06:12	N31 24.833	E31 47.726
42	180	2011/2/19	8:24:47	N31 26.676	E31 47.956
43	181	2011/2/19	10:22:20	N31 31.016	E31 54.837
44	182	2011/2/19	11:11:44	N31 29.894	E31 57.475
45	184	2011/2/19	6:18:46	N31 30.035	E31 57.682
46	185	2011/2/19	11:54:45	N31 26.837	E31 58.691
47	186	2011/2/19	12:00:59	N31 26.262	E31 58.992
48	187	2011/2/19	12:15:55	N31 25.753	E31 59.504
49	188	2011/2/19	12:19:14	N31 25.872	E31 59.389
50	189	2011/2/19	14:45:44	N31 21.571	E32 04.447
51	190	2011/2/19	14:48:37	N31 21.811	E32 03.934
52	191	2011/2/19	14:51:35	N31 22.394	E32 02.988
53	192	2011/2/19	14:57:07	N31 21.113	E32 05.299
54	193	2011/2/19	15:01:18	N31 20.412	E32 06.698
55	194	2011/2/19	15:03:56	N31 20.202	E32 07.157
56	195	2011/2/19	15:08:20	N31 19.421	E32 08.686
57	196	2011/2/19	15:13:19	N31 18.648	E32 09.986
58	197	2011/2/19	15:24:52	N31 18.181	E32 10.180
59	198	2011/2/19	15:27:19	N31 17.485	E32 12.275
60	199	2011/2/19	10:28:43	N31 17.460	E32 12.301
61	200	2011/2/19	15:30:15	N31 17.442	E32 12.352
62	201	2011/2/19	15:32:35	N31 17.366	E32 12.509
63	202	2011/2/19	15:36:10	N31 17.249	E32 12.790
64	203	2011/2/19	15:48:25	N31 16.755	E32 15.430

Table .2.Sand samples, grains size distribution (μm)

Sample Gps no	trial	D_{25}	D_{50}	D_{75}	$D_{meadian}$	D_{mode}	D_{avg}	std deviation	ϕ avg
116	1	172.5	273.5	655.5	273.5	191.7	319.2	0.35	1.67
	2	161.1	201.9	284.5	201.9	191.7	217.0	0.19	2.25
	3	167.2	247.1	589.6	247.1	153.8	303.8	0.33	1.79
	4	172.8	243.0	464.5	243.0	191.7	278.9	0.29	1.89
	5	167.2	225.8	409.4	225.8	191.7	273.8	0.30	2.01
	6	168.2	236.6	536.0	236.6	191.7	290.8	0.31	1.85
120	1	193.1	243.4	307.9	243.4	238.9	245.5	0.16	2.04
	2	200.4	253.5	316.5	253.5	297.7	250.4	0.15	1.99
	3	207.7	266.6	335.0	266.6	297.7	261.8	0.16	1.92
	4	193.6	245.8	312.9	245.8	238.9	249.1	0.17	2.02
	5	192.3	243.1	307.6	243.2	238.9	242.2	0.15	2.04
	6	194.3	224.4	305.3	244.4	297.7	241.6	0.15	2.08
125	1	224.5	277.9	347.4	277.9	297.7	289.1	0.19	1.84
	2	226.7	282.8	349.0	282.8	297.7	278.0	0.15	1.83
	3	221.6	277.3	345.1	277.3	297.7	273.7	0.15	1.85
	4	220.8	277.5	346.5	277.5	297.7	274.2	0.15	1.85
	5	223.7	280.0	347.4	280.0	297.7	275.9	0.15	1.84
	6	220.8	275.6	344.8	275.6	297.7	276.8	0.16	1.86
126	1	194.4	233.3	279.2	233.3	238.9	232.5	0.12	2.10
	2	198.0	240.6	291.8	240.6	238.9	239.7	0.13	2.06
	3	196.9	239.2	290.1	239.2	238.9	238.2	0.13	2.06
	4	199.2	246.8	306.6	246.8	238.9	248.8	0.21	2.02
	5	196.7	240.0	293.6	240.0	238.9	245.8	0.16	2.06
	6	193.1	235.7	288.1	235.7	238.9	235.0	0.13	2.08
131	1	260.6	334.5	390.8	334.5	297.7	363.9	0.59	1.17
	2	249.4	301.2	364.9	301.2	297.7	305.7	0.15	1.73
	3	251.2	300.2	358.6	300.7	297.7	299.2	0.12	1.74
	4	244.9	296.4	359.0	296.4	297.7	299.1	0.14	1.75
	5	253.9	309.9	379.2	309.9	297.7	319.1	0.16	1.69
	6	248.7	297.3	354.0	297.3	297.7	295.5	0.12	1.75
133	1	255.4	304.5	362.2	304.5	297.7	303.9	0.12	1.72
	2	249.4	301.2	364.9	301.2	297.7	305.7	0.15	1.73
	3	256.4	304.6	361.4	304.6	297.7	304.1	0.12	1.72
	4	251.5	302.3	362.9	302.3	297.7	301.7	0.13	1.73
	5	252.5	299.8	354.8	299.8	297.7	298.1	0.11	1.74
	6	251.9	302.9	362.8	302.9	297.7	295.9	0.20	1.72

Sample Gps no	trial	D_{25}	D_{50}	D_{75}	$D_{meadian}$	D_{mode}	D_{avg}	std deviation	ϕ avg
134	1	220.4	263.2	314.5	263.2	238.9	262.3	0.12	1.93
	2	225.1	267.2	314.1	267.2	297.7	263.8	0.11	1.91
	3	228.4	278.7	340.5	278.7	297.7	290.1	0.18	1.84
	4	223.7	269.0	321.3	269.0	297.7	268.1	0.13	1.90
	5	224.2	270.0	323.8	270.0	297.7	268.2	0.12	1.89
	6	229.5	277.9	333.5	277.9	297.7	281.9	0.15	1.85
140	1	223.1	263.0	309.5	263.0	297.7	263.2	0.10	1.93
	2	176.9	218.6	288.6	218.6	191.7	202.2	0.40	2.16
	3	219.0	261.8	311.1	261.8	297.7	260.0	0.11	1.94
	4	214.7	261.0	318.7	261.0	238.9	271.8	0.17	1.94
	5	203.1	242.6	290.8	242.6	238.9	243.8	0.12	2.04
	6	219.0	262.8	314.3	262.8	297.7	270.8	0.15	1.93
143	1	238.4	284.9	336.1	284.9	297.7	280.2	0.12	1.82
	2	234.6	282.3	336.2	282.3	297.7	278.7	0.12	1.83
	3	242.6	293.4	352.1	293.4	297.7	289.9	0.13	1.77
	4	240.3	289.3	345.0	289.3	297.7	285.1	0.12	1.79
	5	237.6	287.0	342.8	287.0	297.7	282.0	0.12	1.81
	6	241.0	292.0	350.9	292.0	297.7	288.2	0.13	1.78
146	1	234.3	277.0	323.3	277.0	297.7	273.9	0.10	1.86
	2	241.1	285.6	333.1	285.6	297.7	281.5	0.10	1.82
	3	237.7	282.8	333.7	282.8	297.7	281.6	0.11	1.83
	4	232.3	279.8	334.1	279.8	297.7	254.5	0.33	1.84
	5	234.3	278.1	326.2	278.1	297.7	274.9	0.10	1.85
	6	238.2	280.7	326.1	280.7	297.7	276.9	0.10	1.84
147	1	221.0	259.1	304.6	259.1	238.9	259.4	0.11	1.95
	2	220.6	260.9	308.2	260.9	297.7	260.3	0.11	1.94
	3	220.7	259.0	304.9	259.0	238.9	259.6	0.11	1.95
	4	223.7	263.7	309.9	263.7	297.7	263.1	0.11	1.92
	5	222.3	258.4	302.3	258.4	238.9	260.3	0.10	1.95
	6	221.7	260.4	306.2	260.4	238.9	261.0	0.10	1.94
150	1	219.1	258.1	304.8	258.1	238.9	258.5	0.11	1.95
	2	220.2	258.9	305.3	258.9	238.9	260.4	0.11	1.95
	3	219.9	257.1	302.1	257.1	238.9	258.2	0.10	1.96
	4	219.7	258.9	306.5	258.9	238.9	259.8	0.11	1.95
	5	223.9	262.5	309.4	262.5	238.9	280.3	0.20	1.93
	6	221.1	258.6	303.7	258.6	238.8	259.8	0.10	1.95
151	1	170.7	208.2	256.5	208.2	191.7	210.9	0.14	2.26
	2	147.3	178.5	219.6	178.5	153.8	182.3	0.19	2.48
	3	170.8	204.6	247.7	204.6	191.7	207.1	0.13	2.28
	4	158.3	189.9	234.9	189.9	191.7	198.3	0.15	2.38
	5	162.2	194.6	236.5	194.6	191.7	198.1	0.14	2.36
	6	172.1	201.9	241.1	201.9	191.7	178.7	0.37	2.30

Sample Gps no	trial	D_{25}	D_{50}	D_{75}	$D_{meadian}$	D_{mode}	D_{avg}	std deviation	ϕ avg
153	1	224.5	278.8	345.5	278.8	297.7	282.3	0.2	1.84
	2	227.6	281.5	345.1	281.5	297.7	277.7	0.1	1.83
	3	223.8	274.7	333.1	274.7	297.7	270.0	0.1	1.87
	4	222.9	271.8	328.0	271.8	297.7	266.8	0.1	1.88
	5	222.8	274.8	334.6	274.8	297.7	269.1	0.1	1.87
	6	223.4	273.4	331.2	273.4	297.7	268.8	0.1	1.88
155	1	230.3	329.7	413.7	329.7	370.9	310.9	0.20	1.66
	2	237.0	352.6	517.2	352.6	370.9	352.1	0.25	1.51
	3	251.6	379.6	516.9	379.6	370.9	373.9	0.26	1.45
	4	227.4	346.7	455.5	346.7	370.9	325.9	0.23	1.60
	5	222.9	337.2	438.3	337.2	370.9	317.5	0.22	1.64
	6	230.5	370.1	541.4	370.1	370.9	357.5	0.26	1.48
156	1	241.9	288.6	339.0	288.6	297.7	282.4	0.11	1.80
	2	256.1	301.3	353.5	301.3	297.7	298.3	0.10	1.73
	3	244.4	287.1	331.4	287.1	297.7	282.8	0.10	1.81
	4	245.1	291.6	344.3	291.6	297.7	288.0	0.12	1.78
	5	253.9	298.8	351.7	298.8	297.7	300.8	0.12	1.74
	6	242.9	288.1	336.1	288.1	297.7	282.3	0.11	1.80
157	1	187.6	232.1	295.4	232.1	191.7	237.4	0.15	2.09
	2	192.9	249.1	390.8	249.1	191.7	286.3	0.25	1.91
	3	193.2	244.1	354.1	244.1	161.7	265.7	0.20	1.97
	4	193.3	246.5	341.4	246.5	238.9	267.6	0.21	1.98
	5	194.2	251.0	361.5	251.0	238.9	283.0	0.26	1.94
	6	187.6	236.2	315.7	236.2	191.7	252.3	0.20	2.05
158	1	186.2	235.7	303.2	235.7	191.7	237.4	0.16	2.08
	2	169.4	213.5	381.4	213.5	191.7	256.3	0.26	2.06
	3	187.0	244.2	328.8	244.2	191.7	246.0	0.19	2.02
	4	202.5	256.6	395.8	256.6	238.9	288.7	0.23	1.87
	5	181.4	233.7	314.9	233.7	191.7	238.1	0.30	2.08
	6	193.5	272.1	411.0	272.1	191.7	285.2	0.24	1.84
159	1	240.7	346.2	473.9	346.2	462.2	339.9	0.22	1.55
	2	240.0	365.6	492.1	365.6	462.2	306.6	0.40	1.51
	3	191.2	232.8	284.3	232.8	238.9	233.1	0.13	2.10
	4	212.3	304.2	630.8	304.2	238.9	383.8	0.36	1.54
	5	222.4	298.2	390.2	298.2	297.7	295.7	0.19	1.76
	6	227.2	311.8	421.7	311.8	297.7	317.6	0.21	1.69
160	1	226.9	259.3	299.4	259.3	238.9	260.6	0.10	1.94
	2	234.8	274.2	317.4	274.2	297.7	272.0	0.10	1.87
	3	235.6	274.1	316.3	274.1	297.1	272.2	0.10	1.87
	4	224.7	263.5	307.5	263.5	297.7	203.8	0.45	1.93
	5	225.9	265.4	309.3	265.4	297.7	198.8	0.49	1.92
	6	230.3	267.1	309.5	267.1	297.7	266.9	0.10	1.91

Sample Gps no	trial	D_{25}	D_{50}	D_{75}	$D_{meadian}$	D_{mode}	D_{avg}	std deviation	ϕ avg
161	1	230.5	338.1	444.3	338.1	370.9	321.7	0.22	1.62
	2	244.1	352.3	474.0	352.3	370.9	356.4	0.26	1.54
	3	230.6	344.7	458.0	344.7	370.9	338.2	0.29	1.59
	4	236.7	346.4	484.5	346.4	370.9	339.9	0.25	1.55
	5	245.6	348.2	444.0	348.2	370.9	332.9	0.21	1.57
	6	237.5	346.3	456.2	346.3	370.9	338.8	0.24	1.58
162	1	270.6	315.1	369.4	315.1	297.7	316.7	0.10	1.66
	2	272.5	315.9	368.0	315.9	297.7	313.2	0.13	1.66
	3	270.6	315.1	369.4	315.1	297.7	316.7	0.10	1.66
	4	271.6	320.0	379.3	320.0	297.7	326.2	0.13	1.64
	5	274.0	318.1	371.1	318.1	297.7	319.2	0.10	1.65
	6	273.9	319.1	373.2	319.1	297.7	320.8	0.11	1.65
166	1	234.3	276.1	322.0	276.1	297.7	283.2	0.15	1.86
	2	227.3	267.3	313.7	267.3	297.7	273.3	0.14	1.90
	3	240.4	280.7	323.6	280.7	297.7	277.4	0.10	1.84
	4	244.8	287.3	331.3	287.3	297.7	283.1	0.10	1.81
	5	245.2	289.8	339.9	289.8	297.7	287.3	0.11	1.79
	6	243.9	286.9	333.8	286.9	297.7	284.9	0.10	1.81
167	1	160.0	194.7	250.5	194.7	191.7	221.5	0.23	2.33
	2	150.2	182.0	229.1	182.0	191.7	195.3	0.18	2.44
	3	179.0	221.7	389.3	221.7	191.7	257.2	0.34	2.01
	4	154.7	192.0	251.2	192.0	191.7	187.7	0.33	2.36
	5	150.7	181.5	329.4	181.5	153.8	248.0	0.34	2.26
	6	155.1	197.3	264.9	197.3	191.7	158.6	0.52	2.32
168	1	610.3	698.9	787.3	698.9	717.7	698.1	0.07	0.52
	2	567.1	661.1	748.7	661.1	717.7	649.8	0.10	0.61
	3	549.1	645.8	738.0	645.8	717.7	628.5	0.11	0.64
	4	518.5	609.2	713.6	609.2	717.7	597.2	0.12	0.72
	5	562.5	661.6	749.8	661.6	717.7	642.0	0.11	0.61
	6	514.7	612.2	717.8	612.2	717.7	589.9	0.13	0.71
169	1	361.3	451.8	579.4	451.8	462.2	453.1	0.17	1.13
	2	306.4	422.4	527.8	422.4	462.2	274.2	0.58	1.29
	3	362.0	460.0	646.5	460.0	462.2	517.0	0.25	1.07
	4	289.6	427.6	569.2	427.6	462.2	266.8	0.61	1.28
	5	272.5	398.8	530.4	398.8	370.9	246.5	0.62	1.37
	6	358.3	450.1	682.3	450.1	462.2	493.7	0.22	1.06
170	1	570.6	631.8	720.2	631.8	576.0	647.5	0.07	0.65
	2	531.1	571.7	615.4	571.7	576.0	571.1	0.07	0.81
	3	541.9	586.7	635.2	586.7	576.0	585.4	0.07	0.77
	4	579.2	663.7	748.6	663.7	717.7	662.6	0.09	0.60
	5	562.6	616.2	699.3	616.2	576.0	631.4	0.07	0.68
	6	504.7	556.6	605.7	556.6	576.0	553.6	0.07	0.85

Sample Gps no	trial	D_{25}	D_{50}	D_{75}	$D_{meadian}$	D_{mode}	D_{avg}	std deviation	ϕ avg
171	1	275.8	561.4	690.8	561.4	717.7	442.4	0.26	1.07
	2	301.5	569.7	699.3	569.7	714.7	459.0	0.25	1.02
	3	450.0	597.9	707.3	597.9	717.7	509.7	0.23	0.80
	4	291.8	551.4	685.5	551.4	717.7	444.5	0.26	1.06
	5	366.3	564.3	679.5	564.3	576.0	473.4	0.23	0.94
	6	540.5	653.7	745.6	653.7	717.7	576.2	0.20	0.64
173	1	146.4	177.2	217.7	177.2	153.8	181.4	0.15	2.49
	2	145.1	175.6	215.7	175.6	153.8	178.6	0.16	2.50
	3	137.9	169.5	208.7	169.5	153.8	155.7	0.32	2.56
	4	130.1	168.0	213.4	168.0	153.8	143.2	0.42	2.58
	5	145.0	181.2	246.6	181.2	153.8	192.0	0.33	2.42
	6	127.8	163.0	201.5	163.0	153.8	152.2	0.23	2.63
174	1	158.1	196.1	253.2	196.1	153.8	214.7	0.22	2.33
	2	150.7	183.0	226.8	183.0	153.8	186.9	0.15	2.44
	3	148.7	180.4	224.1	180.4	153.8	189.5	0.18	2.46
	4	149.7	184.4	242.2	184.4	153.8	202.2	0.22	2.41
	5	144.0	173.4	210.9	173.4	153.8	175.5	0.14	2.52
	6	142.8	171.5	209.5	171.5	153.8	172.8	0.14	2.54
175	1	430.8	513.6	626.9	513.6	462.2	518.2	0.13	0.95
	2	447.5	562.5	660.9	562.5	576.0	562.8	0.11	0.86
	3	454.5	559.7	699.0	559.7	462.2	562.6	0.14	0.83
	4	446.3	517.6	597.0	517.6	576.0	515.9	0.11	0.95
	5	439.6	511.9	600.1	511.9	462.2	513.7	0.11	0.96
	6	448.3	533.7	631.6	533.7	576.0	530.4	0.12	0.91
181	1	168.8	231.3	409.8	231.3	191.7	264.9	0.27	1.99
	2	163.0	220.7	342.7	220.7	191.7	234.4	0.32	2.11
	3	165.8	210.2	295.4	210.2	191.7	225.3	0.20	2.20
	4	165.1	217.2	327.0	217.2	191.7	232.7	0.21	2.14
	5	165.1	231.6	351.2	231.6	191.7	245.6	0.27	2.07
	6	168.0	230.8	387.6	230.8	191.7	282.1	0.34	2.02
184	1	187.6	218.7	255.9	218.7	191.7	225.9	0.14	2.19
	2	190.4	224.9	266.2	224.9	191.7	226.2	0.12	2.15
	3	191.0	225.4	266.0	225.4	238.9	235.1	0.16	2.15
	4	198.8	235.2	309.9	235.2	191.7	268.3	0.23	2.04
	5	190.4	219.6	251.1	219.6	238.9	218.5	0.10	2.19
	6	186.3	217.6	250.2	217.6	238.9	215.5	0.10	2.21
185	1	205.5	245.2	294.3	245.2	238.9	247.1	0.12	2.03
	2	210.1	250.0	299.2	250.0	238.9	255.4	0.14	2.00
	3	209.8	251.1	303.5	251.1	238.9	263.9	0.16	1.99
	4	206.0	246.5	295.8	246.5	238.9	247.5	0.12	2.02
	5	207.0	269.8	468.5	269.8	191.7	318.0	0.24	1.75
	6	209.1	249.1	299.6	249.1	238.9	260.6	0.16	2.00

Sample Gps no	trial	D_{25}	D_{50}	D_{75}	$D_{meadian}$	D_{mode}	D_{avg}	std deviation	ϕ avg
191	1	171.9	207.7	252.5	207.7	191.7	208.5	0.13	2.26
	2	174.8	216.2	272.0	216.2	191.7	227.1	0.19	2.20
	3	169.6	206.3	254.8	206.3	191.7	214.0	0.16	2.27
	4	166.4	202.6	248.2	202.6	191.7	204.9	0.14	2.30
	5	166.3	203.6	252.0	203.6	191.7	208.5	0.15	2.29
	6	165.8	201.6	246.8	201.6	191.7	204.1	0.14	2.31
195	1	180.5	209.8	244.0	209.8	191.7	207.8	0.14	2.25
	2	185.1	199.5	217.1	199.5	191.6	201.6	0.06	2.32
	3	181.6	210.4	244.0	210.4	191.7	210.5	0.10	2.25
	4	181.1	210.5	244.3	210.5	238.9	200.7	0.22	2.25
	5	186.4	219.7	252.7	219.7	238.9	216.4	0.10	2.20
	6	184.5	218.4	259.6	218.4	191.7	220.2	0.12	2.19
196	1	186.2	224.3	275.6	224.3	191.7	241.7	0.20	2.15
	2	185.6	221.2	262.7	221.2	238.9	221.5	0.12	2.18
	3	186.4	223.2	266.9	223.2	238.9	237.2	0.18	2.16
	4	183.5	218.8	260.1	218.8	238.9	218.8	0.12	2.19
	5	187.8	226.9	274.2	226.9	238.9	227.1	0.12	2.14
	6	187.2	226.4	275.5	226.4	238.9	227.6	0.13	2.14
199	1	162.4	196.2	244.6	196.2	191.7	217.9	0.21	2.33
	2	174.4	206.9	249.8	206.9	191.7	212.0	0.12	2.26
	3	179.5	218.9	273.9	218.9	191.7	239.9	0.20	2.18
	4	175.2	209.5	255.9	209.5	191.7	215.7	0.13	2.24
	5	168.0	200.5	243.1	200.5	191.7	213.7	0.17	2.31
	6	169.5	200.7	239.9	200.7	191.7	202.8	0.12	2.31
203	1	185.9	223.7	276.0	223.7	191.7	240.1	0.19	2.15
	2	189.2	228.5	283.2	228.5	191.7	242.6	0.18	2.12
	3	188.6	225.9	272.5	225.9	191.7	227.1	0.12	2.14
	4	197.4	246.1	352.1	246.1	191.7	281.1	0.23	1.96
	5	203.1	257.4	393.0	257.4	191.7	301.2	0.25	1.87
	6	191.9	234.2	305.5	234.2	198.2	254.9	0.20	2.06

Table .3.Sand samples TL detailed information.

GPs sample no	TL intensity first integration	TL intensity second integration
116	0.52	0.70
	0.70	0.67
	0.66	0.57
	0.74	0.69
118	0.65	0.64
	0.48	0.50
	1.65	1.76
	0.60	0.71
120	0.76	0.68
	0.47	0.33
	0.58	0.53
	0.63	0.92
126	0.50	0.46
	0.61	0.58
	1.02	0.93
	0.87	0.97
131	0.98	0.84
	1.28	1.63
	0.66	0.82
	0.75	0.85
133	0.90	0.86
	0.89	0.87
	1.30	1.29
	0.79	0.89
134	0.80	0.90
	0.72	0.70
	0.61	0.55
	1.31	1.60
136	1.07	0.76
	2.13	1.76
	1.55	1.65
	1.37	1.49
139	2.14	1.42
	1.14	0.99
	2.43	1.78
	2.35	1.50
140	2.02	1.69
	1.24	0.97
	1.94	1.36
	25.83	26.38

GPs sample no	TL intensity first integration	TL intensity second integration
143	1.18	1.21
	0.79	0.70
	1.02	0.99
	1.16	1.19
146	2.16	3.25
	0.83	1.05
	0.97	1.12
	0.94	1.21
147	0.87	1.08
	0.59	0.71
	0.54	0.70
	0.59	0.75
150	0.67	0.92
	0.85	1.02
	0.57	0.73
	0.53	0.59
154	0.36	0.37
	0.64	0.53
	0.86	1.02
	0.60	0.74
155	0.56	0.65
	0.43	0.49
	0.89	0.77
	0.54	0.45
156	0.40	0.39
	0.35	0.35
	0.32	0.30
	0.25	0.24
157	1.17	1.31
	4.51	1.24
	0.62	0.70
	0.28	0.28
158	0.87	0.78
	0.55	0.52
	0.48	0.48
	0.65	0.62
159	0.70	0.61
	0.48	0.39
	0.60	0.46
	0.58	0.54

GPs sample no	TL intensity first integration	TL intensity second integration
160	0.38	0.50
	1.12	1.07
	0.36	0.61
	0.39	0.46
162	0.75	0.83
	0.45	0.60
	0.59	0.56
	0.73	0.86
163	0.44	0.41
	0.61	0.53
	0.53	0.42
	0.43	0.34
164	0.41	0.42
	0.69	0.69
	0.57	0.57
	0.49	0.53
165	0.58	0.58
	0.66	0.59
	0.57	0.51
	0.57	0.48
166	0.60	0.58
	0.67	0.69
	0.67	0.79
	0.53	0.50
167	0.56	0.51
	0.46	0.36
	0.68	0.65
	-0.73	0.11
168	0.82	0.75
	0.55	0.44
	0.47	0.55
	0.46	0.61
169	0.35	0.38
	0.39	0.37
	0.40	0.35
	0.44	0.45
170	0.61	0.70
	0.77	1.14
	0.49	0.61
	0.43	0.48

GPs sample no	TL intensity first integration	TL intensity second integration
171	0.69	0.81
	1.05	1.32
	1.14	1.31
	0.66	0.77
173	0.92	0.83
	0.98	0.88
	1.28	1.09
	0.81	0.83
174	1.12	1.09
	0.84	0.74
	0.69	0.64
	0.78	0.69
175	0.63	0.98
	0.29	0.34
	0.70	0.96
	0.42	0.85
177	1.88	2.13
	2.79	4.70
	7.92	8.00
	4.07	4.58
178	1.98	4.32
	1.39	1.33
	1.84	2.80
	0.52	0.57
180	0.58	0.55
	4.08	4.25
	0.60	0.58
	0.99	1.00
181	0.46	0.48
	0.87	0.86
	0.65	0.50
	0.69	0.58
182	1.02	1.22
	1.02	0.99
	0.47	0.59
	0.91	0.81
183	1.47	1.81
	1.10	1.23
	0.79	0.91
	0.85	1.03

GPs sample no	TL intensity first integration	TL intensity second integration
184	0.79	0.90
	1.04	1.28
	0.66	0.66
	1.02	1.11
185	0.39	0.39
	0.47	0.45
	0.60	0.48
	0.49	0.40
186	0.56	0.52
	0.78	0.69
	0.75	0.67
	0.53	0.37
187	0.71	0.84
	0.72	1.04
	0.90	0.95
	0.40	0.43
188	0.56	0.51
	0.88	0.97
	0.60	0.64
	0.48	0.50
189	0.62	0.52
	0.82	0.74
	0.69	0.62
	0.64	0.70
190	0.81	0.95
	0.64	0.60
	0.65	0.63
	0.77	0.70
191	0.81	0.91
	0.70	0.76
	0.50	0.50
	0.84	0.85
192	0.92	1.00
	0.62	0.63
	0.64	0.88
	0.52	0.49
193	0.39	0.44
	0.46	0.46
	0.55	0.48
	0.48	0.39

GPs sample no	TL intensity first integration	TL intensity second integration
194	0.71	0.82
	0.73	0.74
	0.48	0.50
	0.79	0.66
195	0.60	0.55
	0.64	0.66
	0.68	0.58
	0.36	0.42
196	0.54	0.49
	0.45	0.43
	0.55	0.50
	0.61	0.58
198	0.78	0.72
	0.52	0.58
	0.42	0.50
	0.63	0.68
200	0.60	0.48
	0.45	0.39
	0.45	0.40
	0.45	0.45
201	0.57	0.51
	0.64	0.52
	0.61	0.53
	0.66	0.60
202	0.72	0.65
	0.53	0.41
	0.49	0.41
	0.57	0.47
203	0.53	0.53
	0.45	0.43
	0.51	0.62
	0.55	0.58

A-2

Sand samples locations on Google Earth images.

Figure 1. Sand samples locations, from Idku lake to Rosetta promontory.

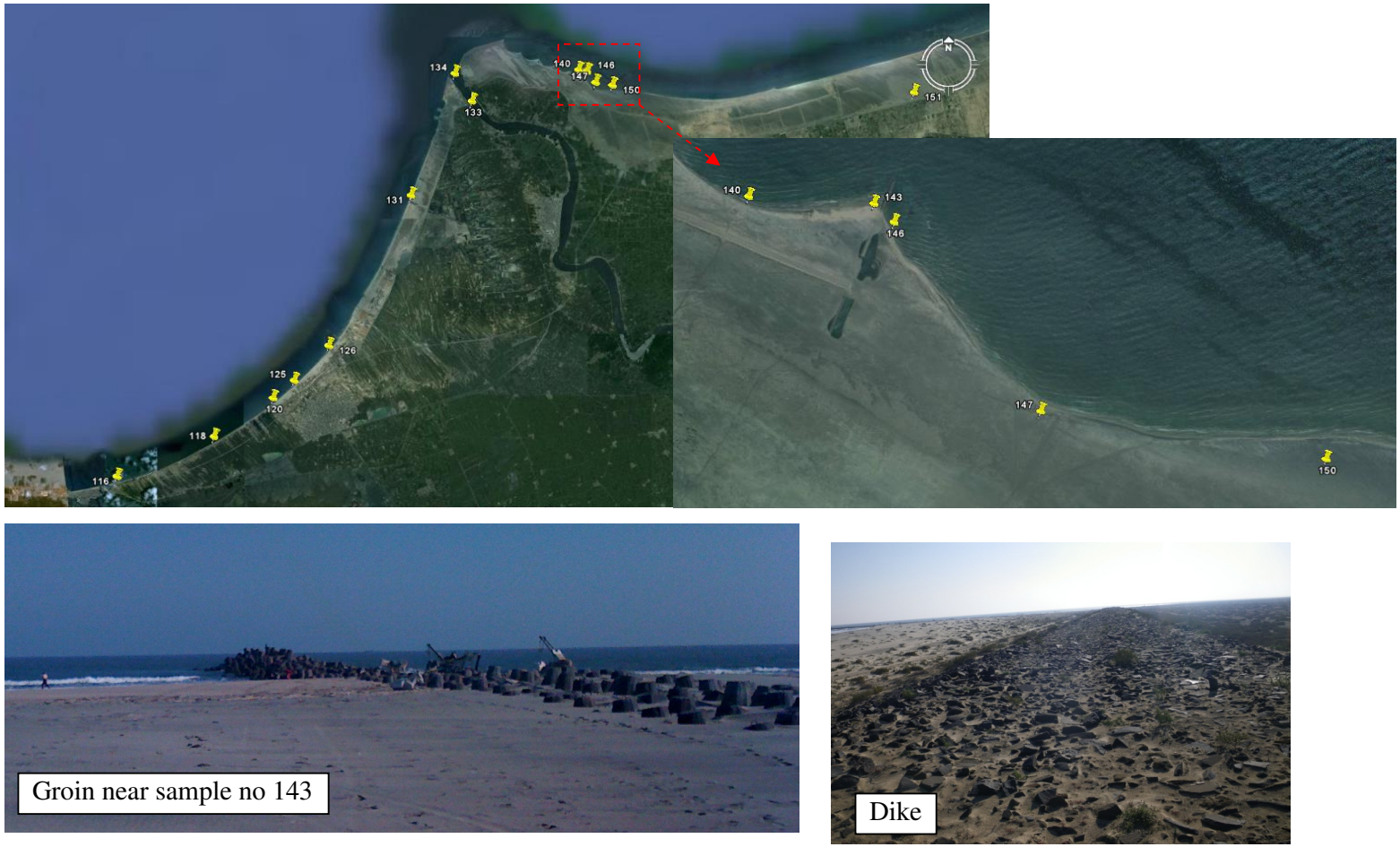

Figure 2. Sand samples locations, the eastward of Rosetta mouth.

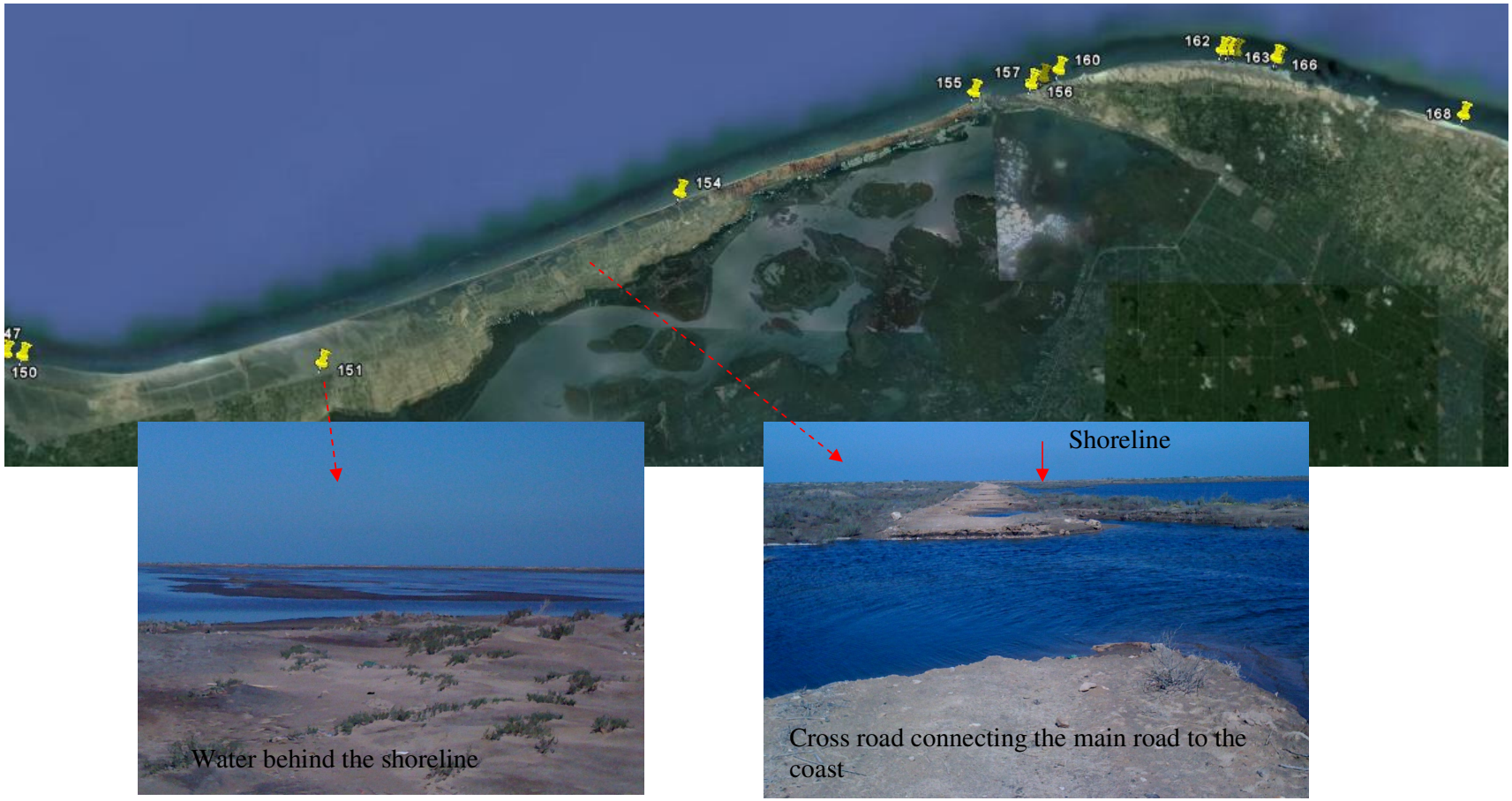

Figure 3. Sand samples locations, the westward part of El Burullus Lake.

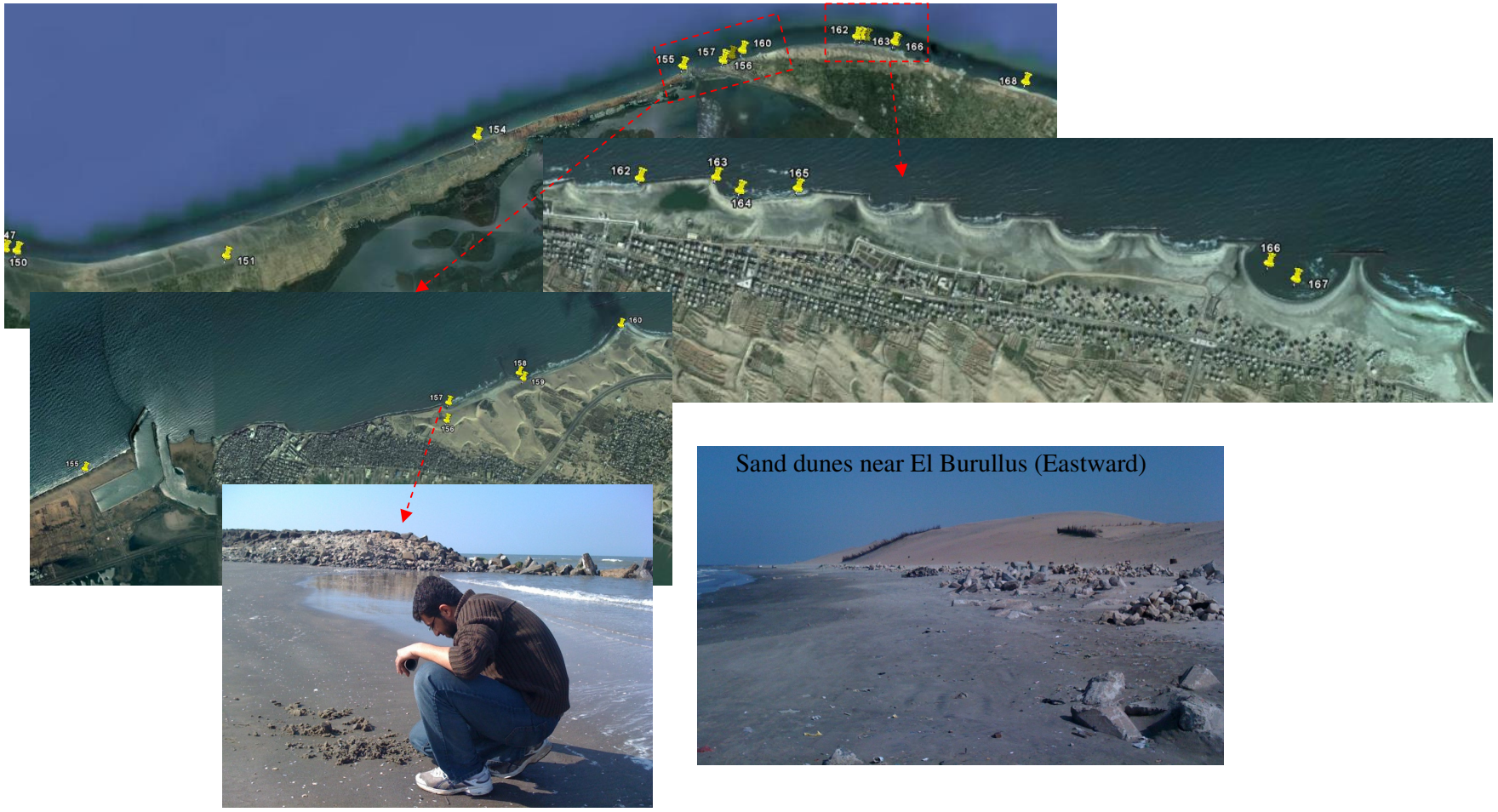

Figure 4. Sand samples locations, the westward part of El Burullus Lake.

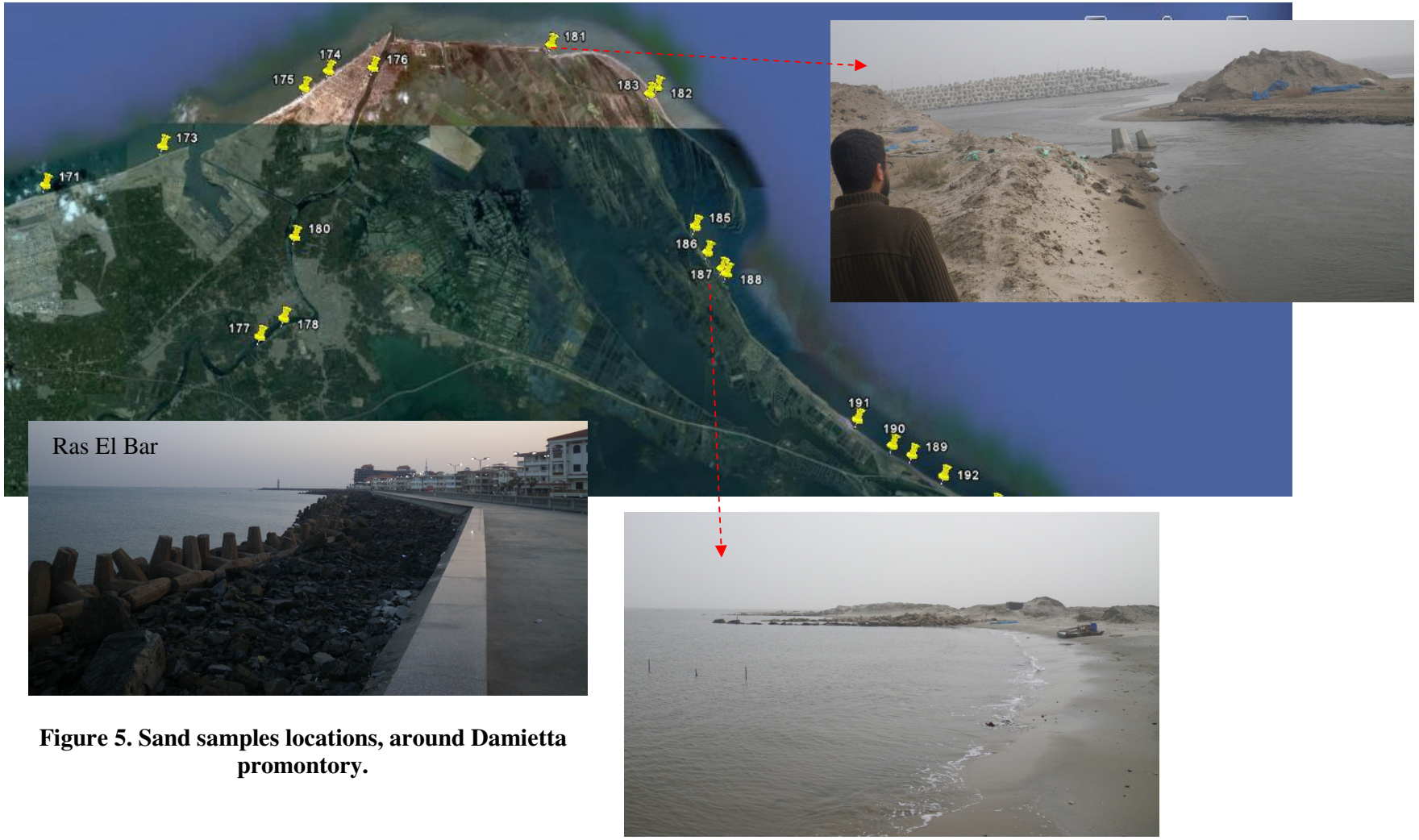

Figure 5. Sand samples locations, around Damietta promontory.

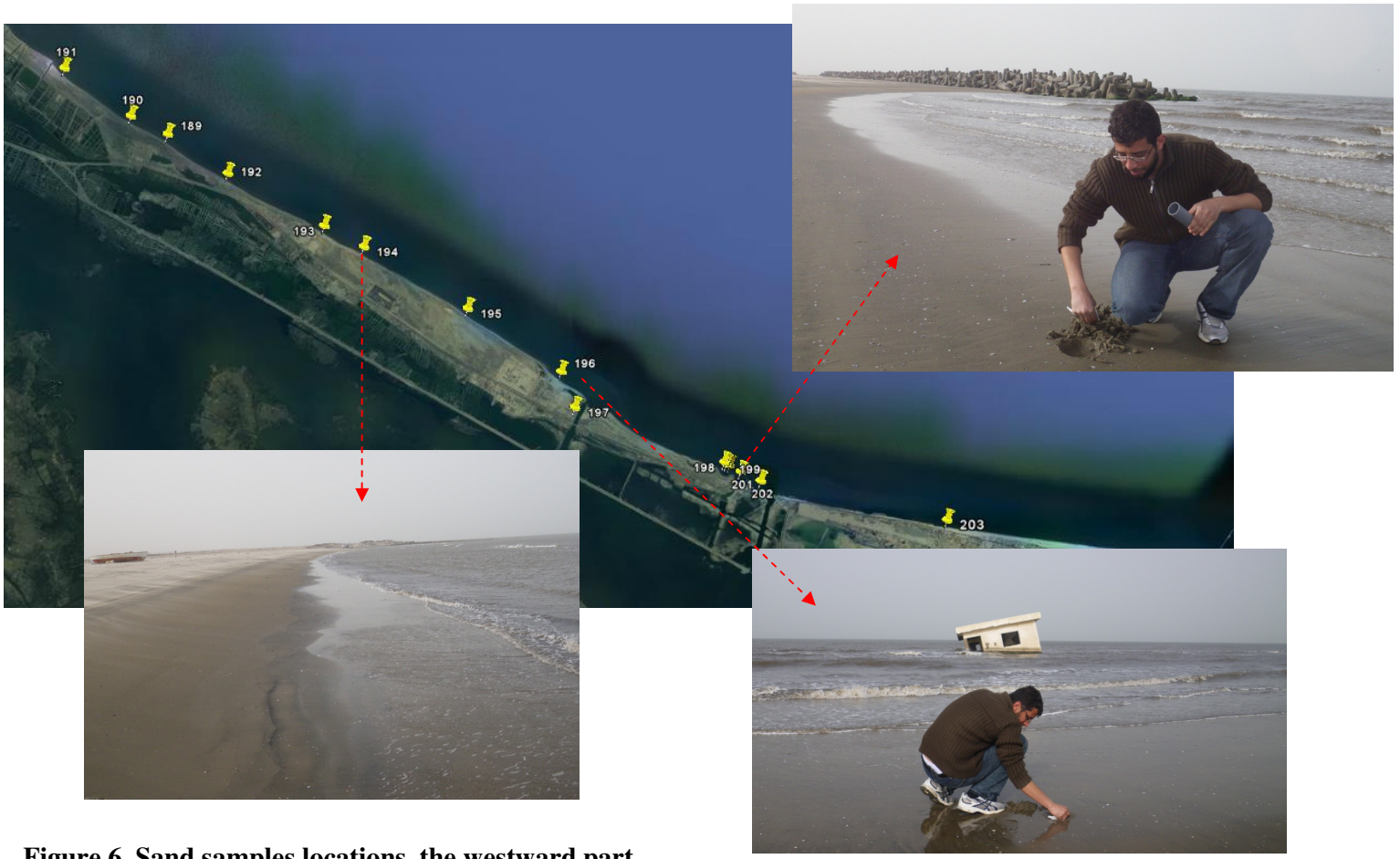

Figure 6. Sand samples locations, the westward part of Port Said.

A-3

Schematic for the TL reader, the Laser diffraction measuring apparatus, and the microscope.

Figure 1. schematic diagram for the Risϕ–48 TL/OSL reader

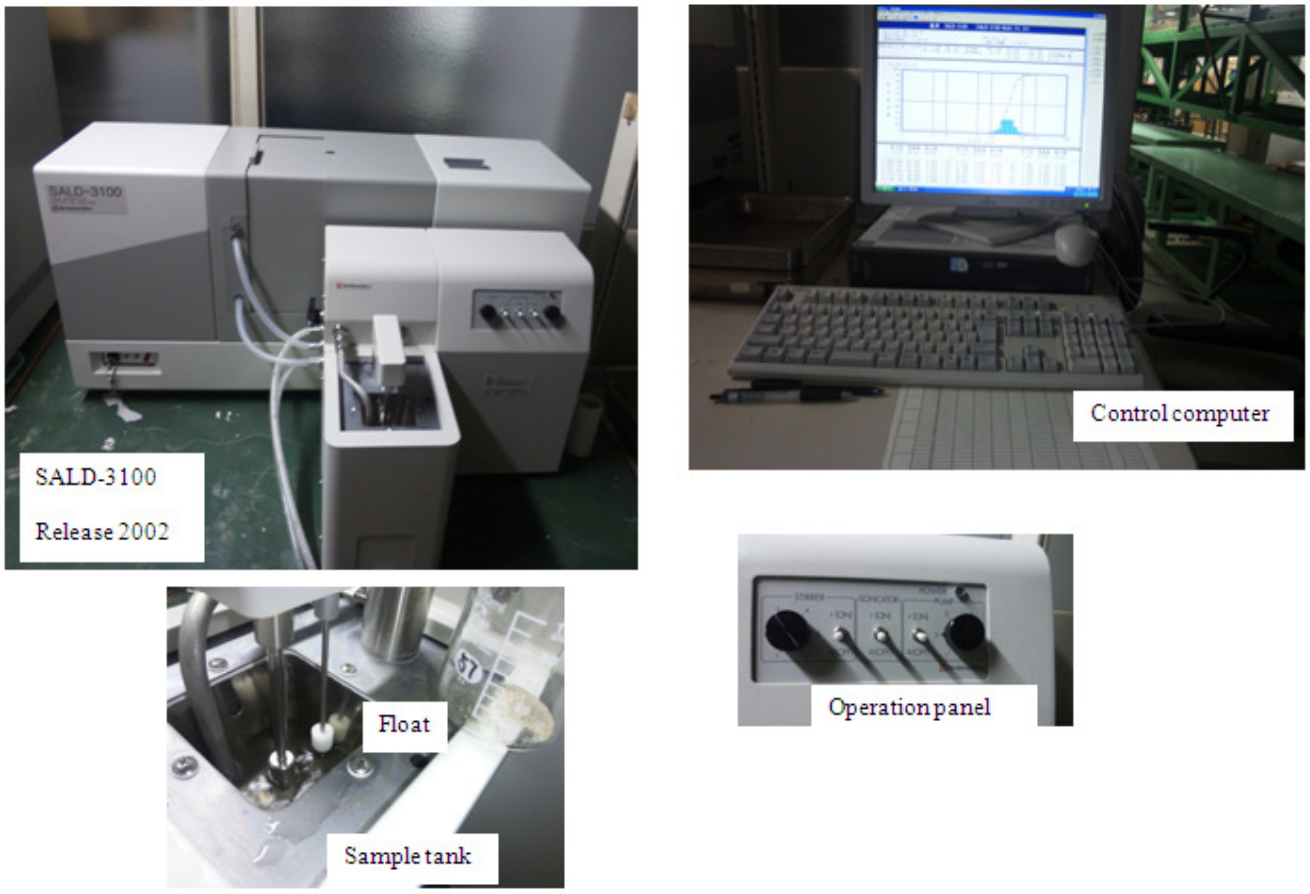

Figure 2. Laser diffraction measuring apparatus (SALD-3100).

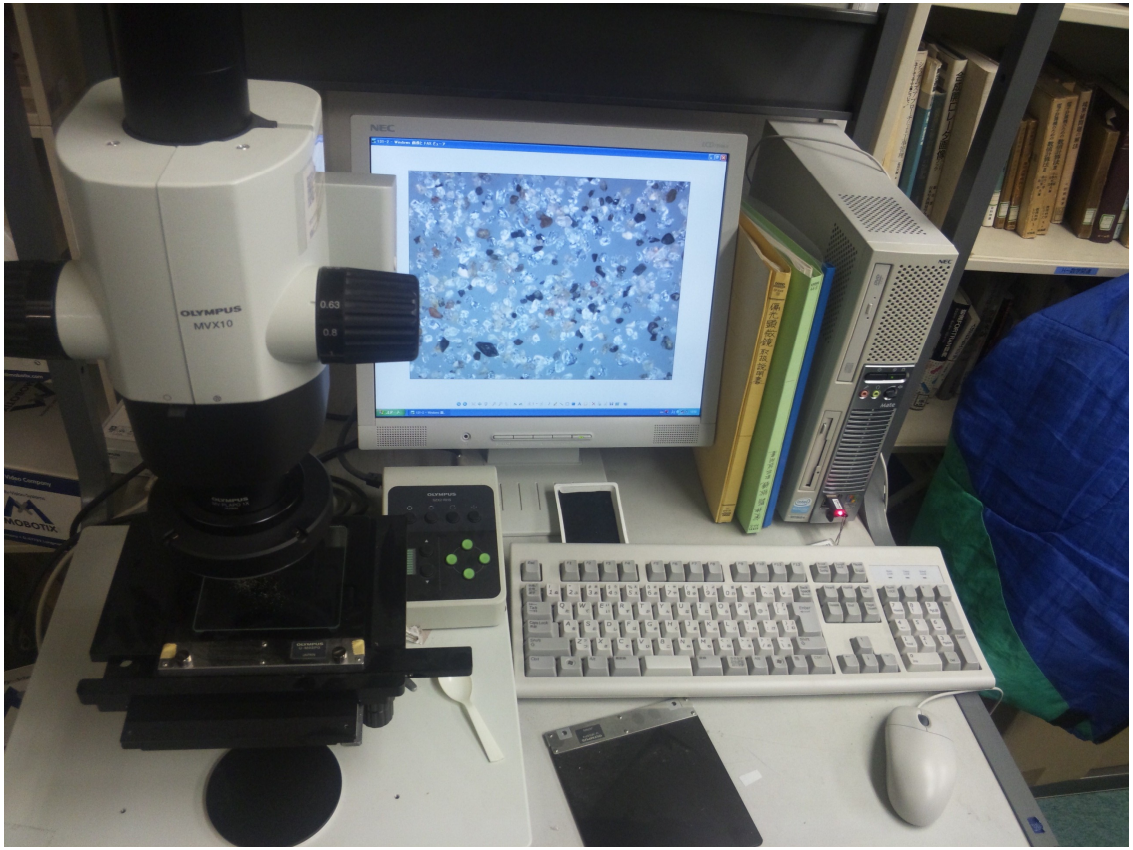

Figure 3. MACROVIEW (Olympus MVX10).

A-4

Scanned sand samples (direct and under microscope images).

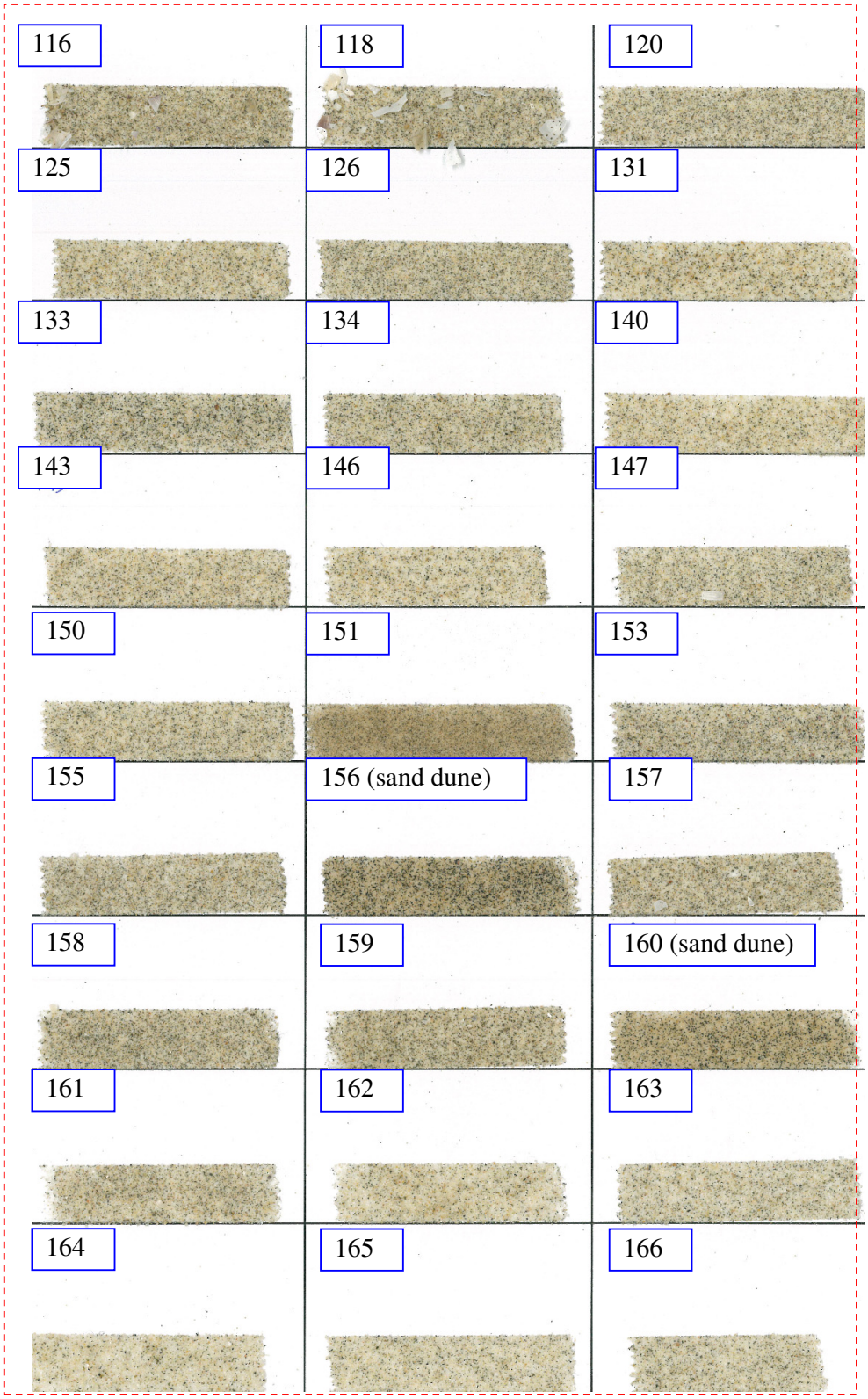

Figure 1. Scanned sand samples1.

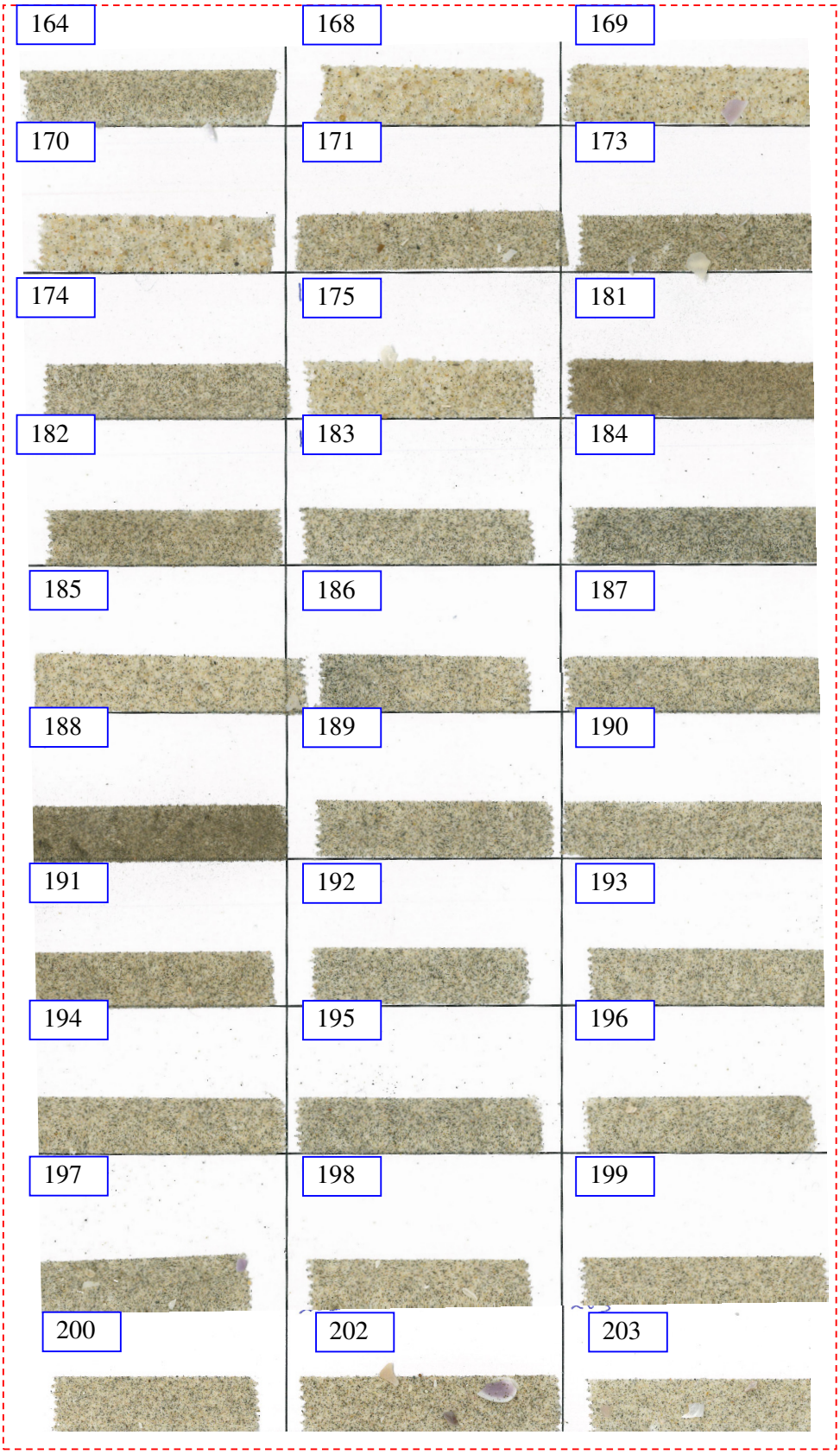

Figure 2. Scanned sand samples2

116

120

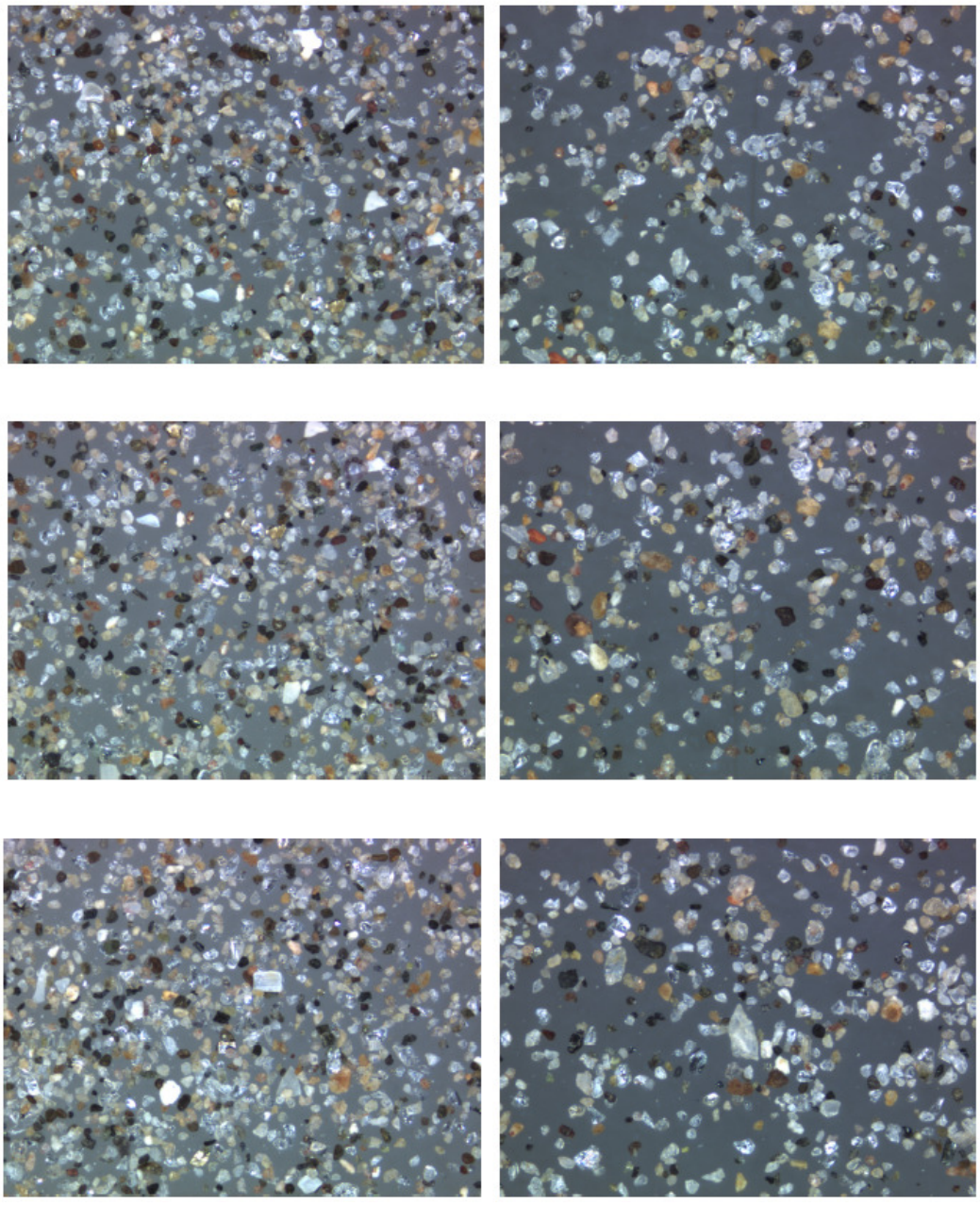

126

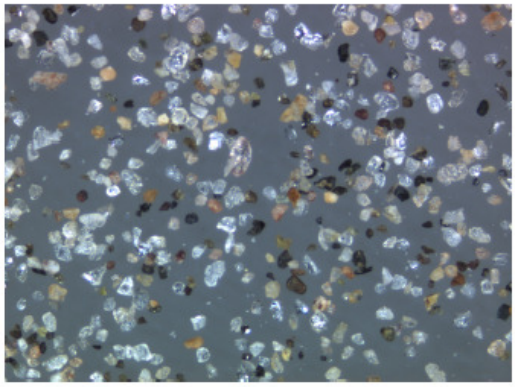

131

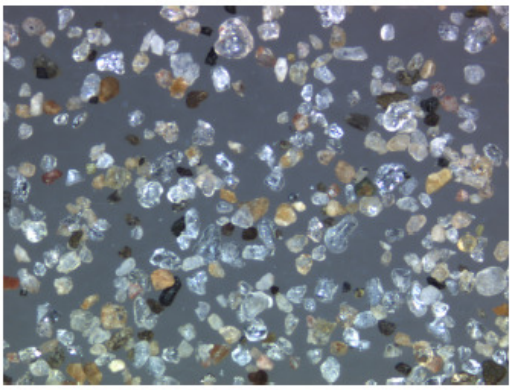

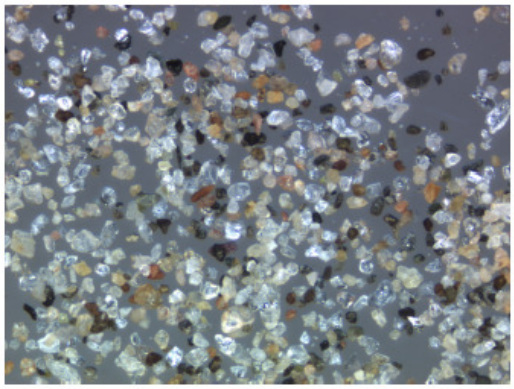

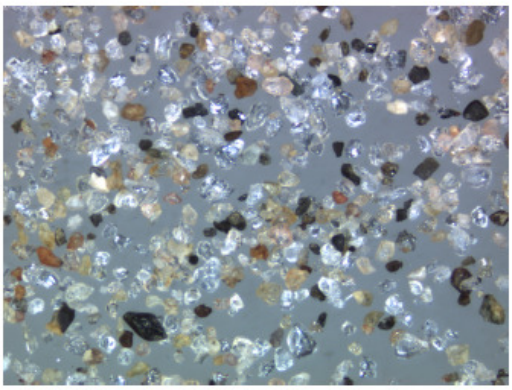

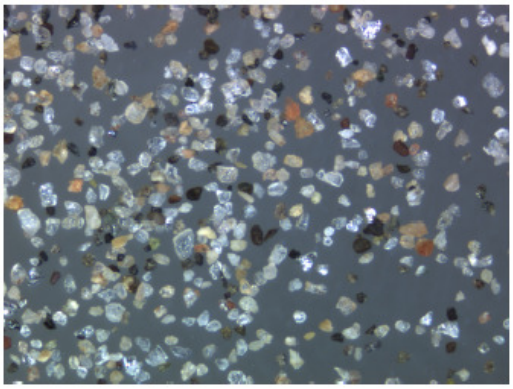

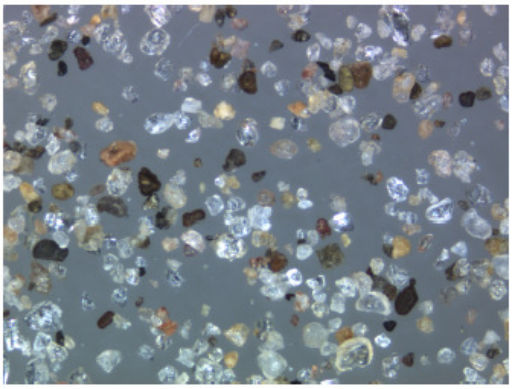

133

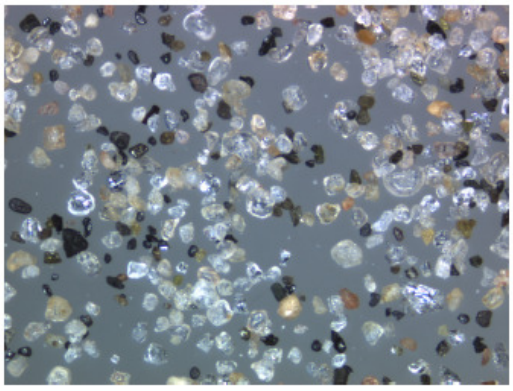

143

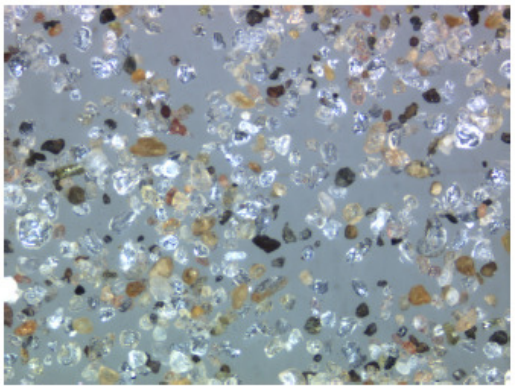

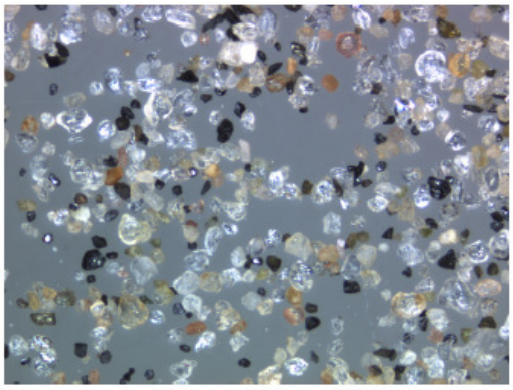

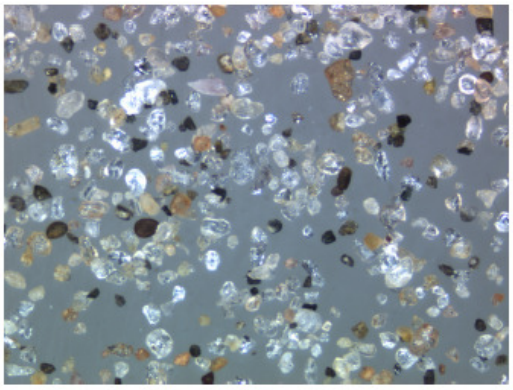

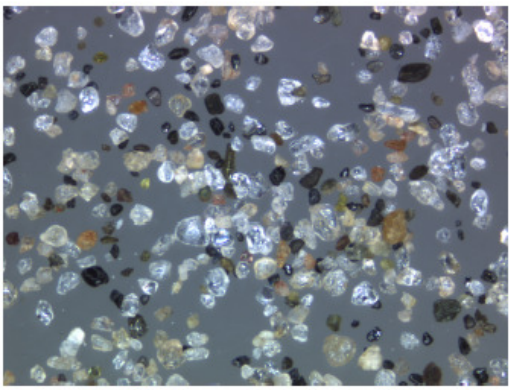

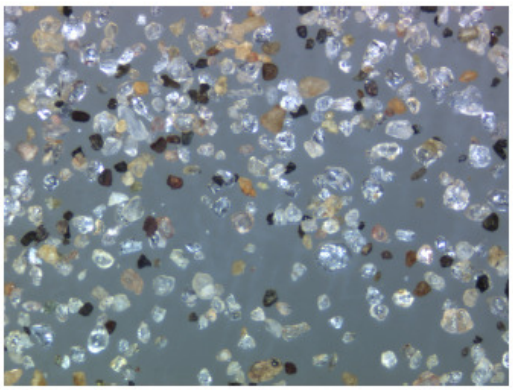

153

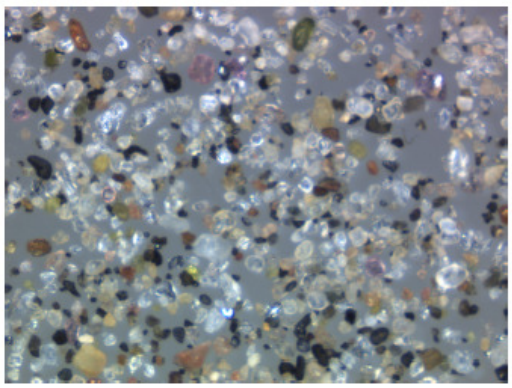

155

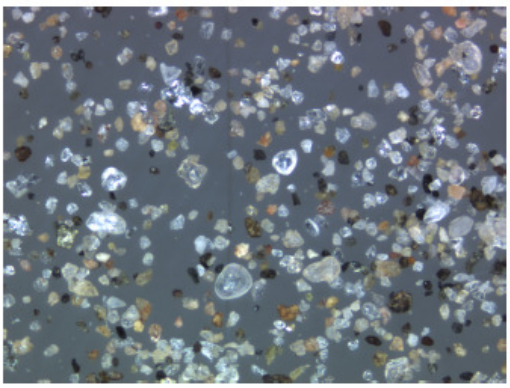

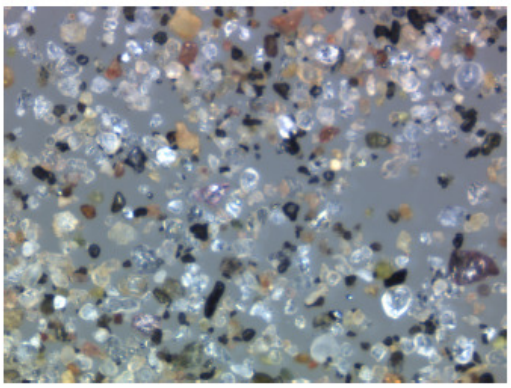

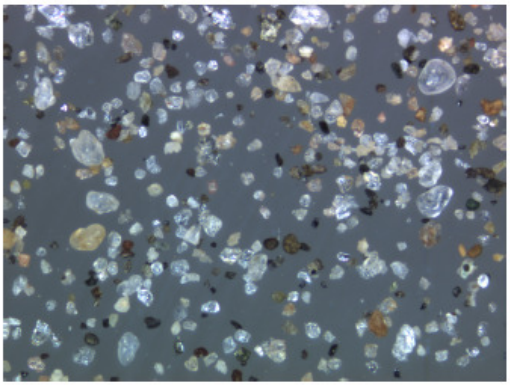

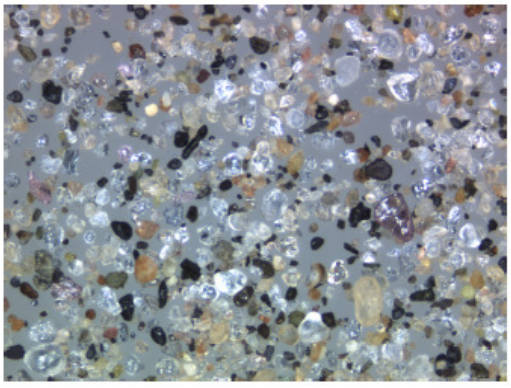

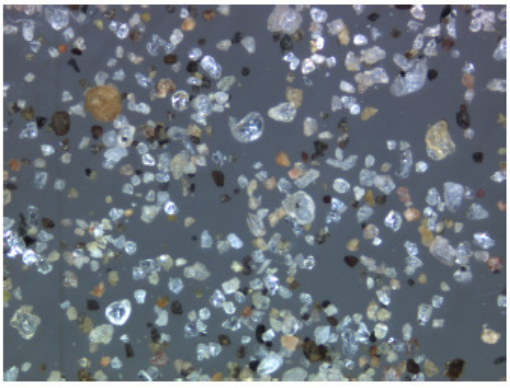

156

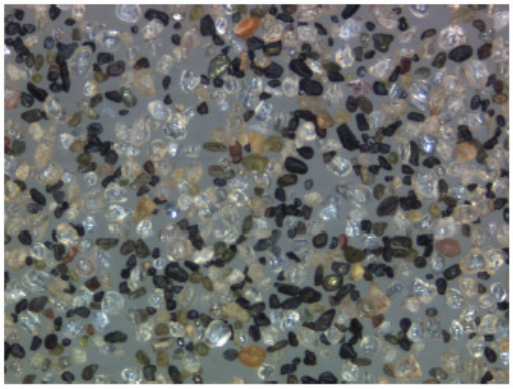

158

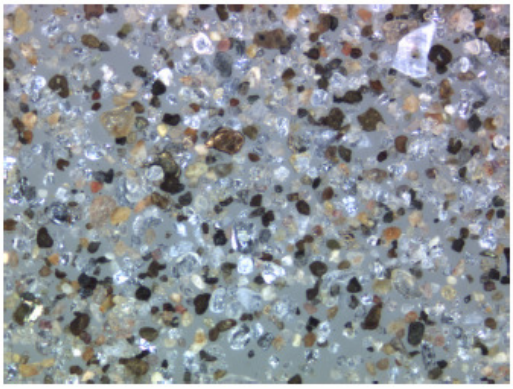

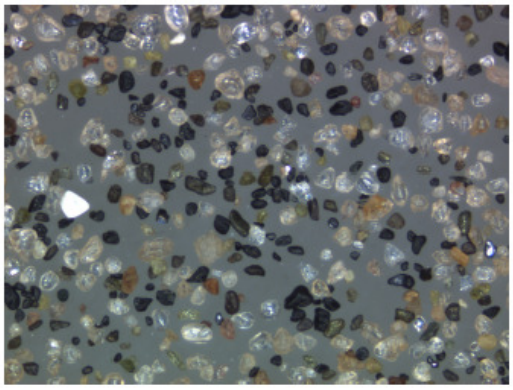

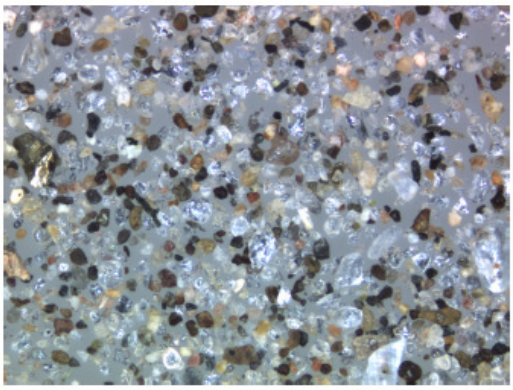

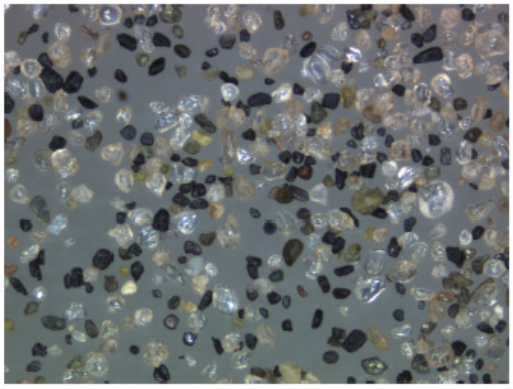

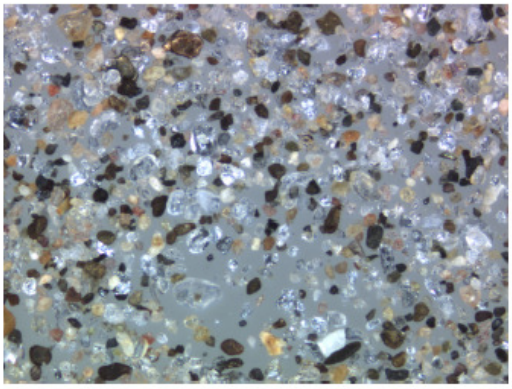

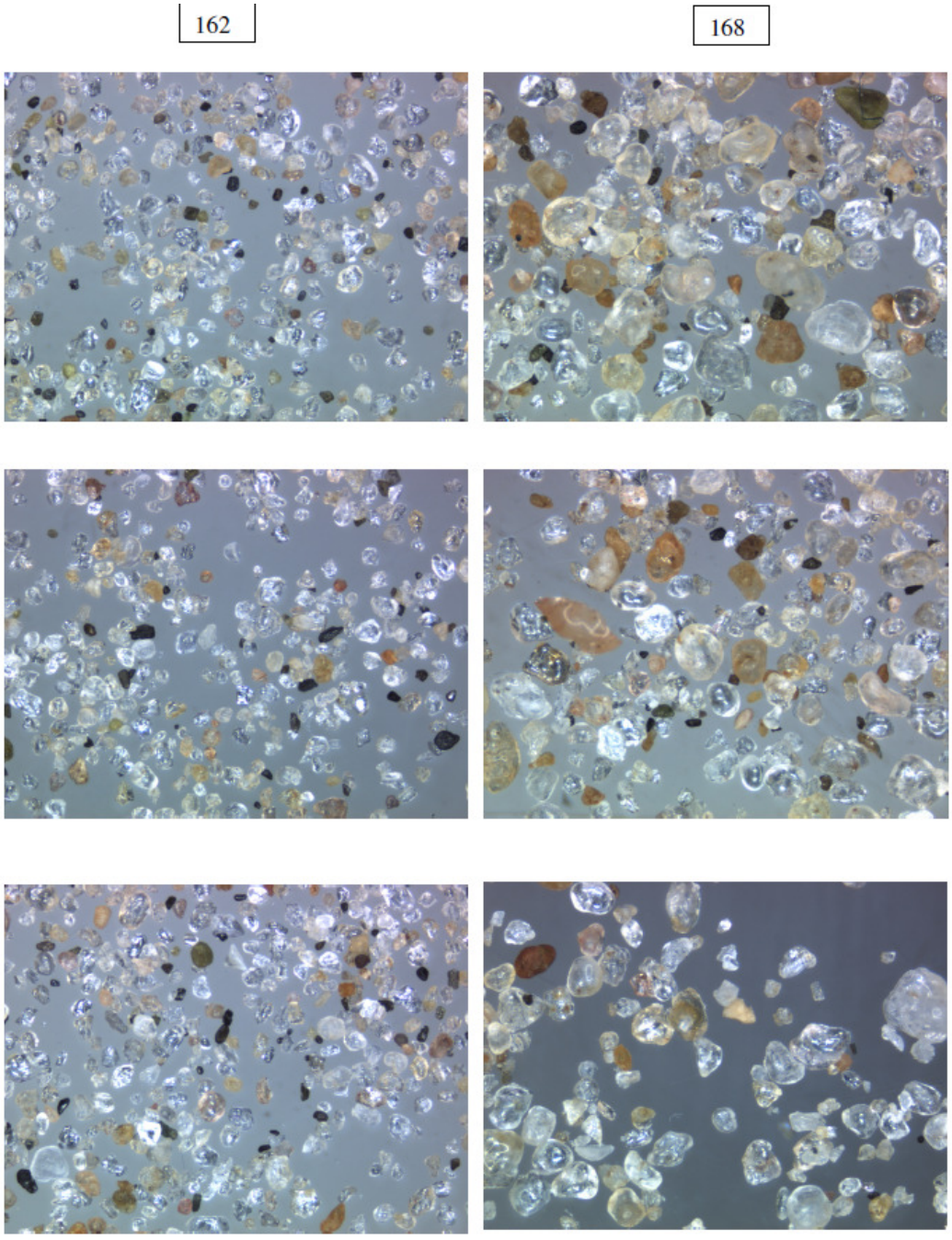
162
168

169

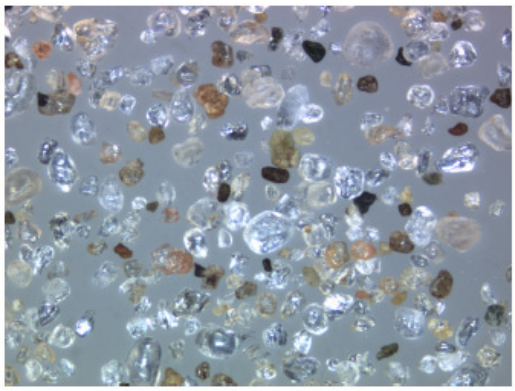

170

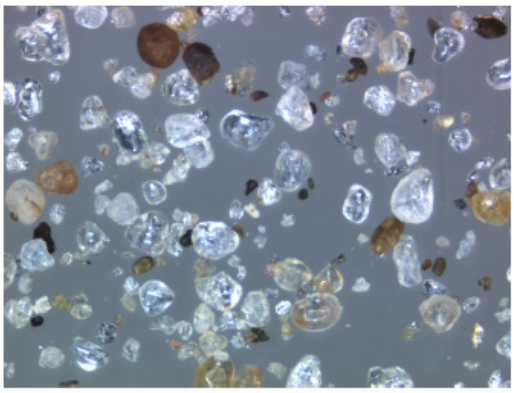

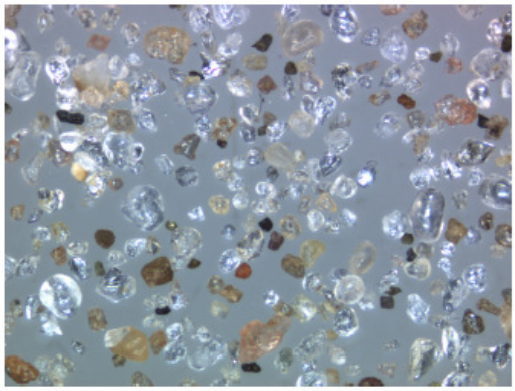

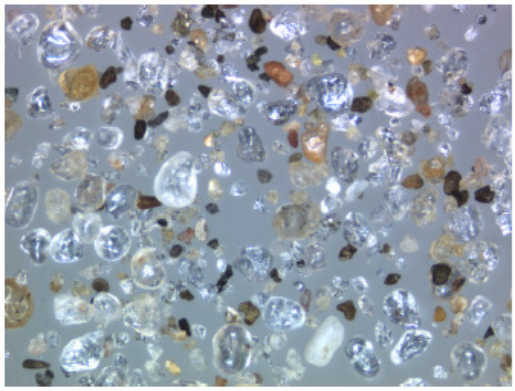

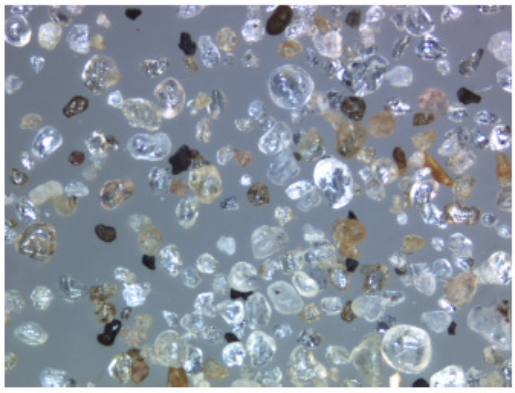

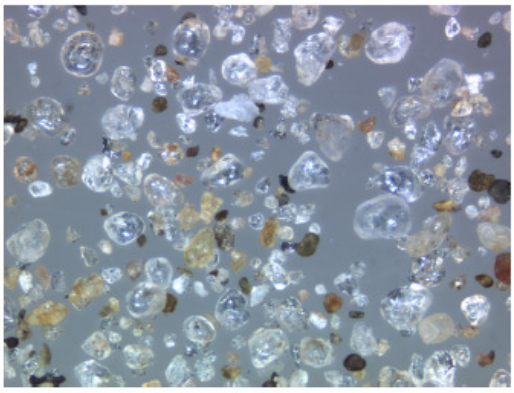

171

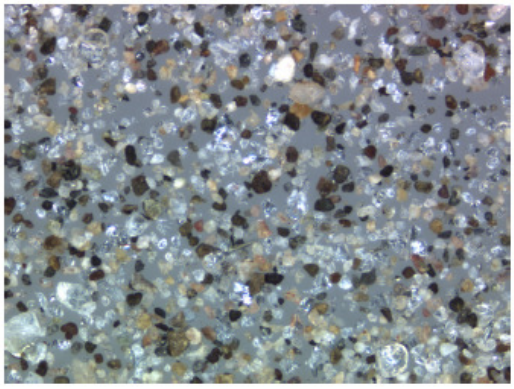

174

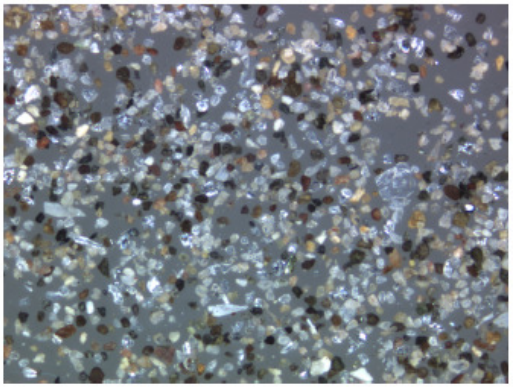

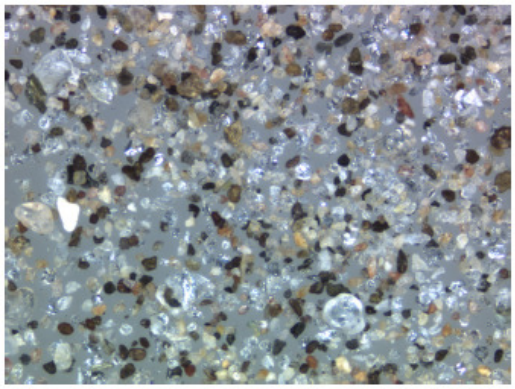

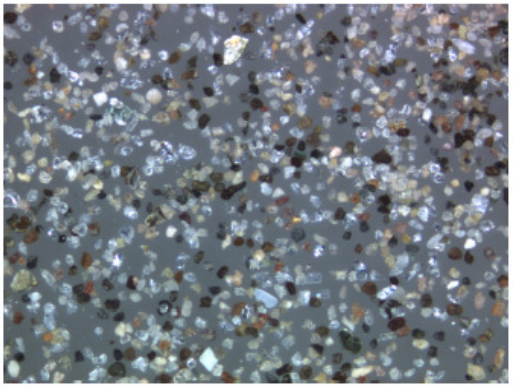

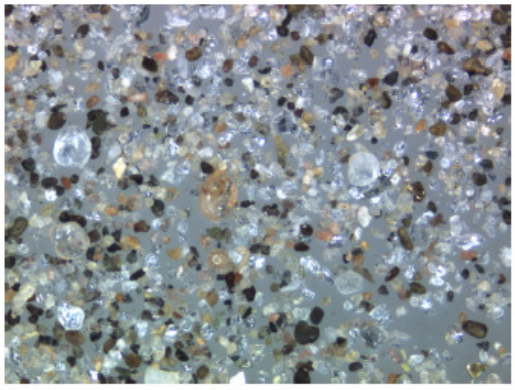

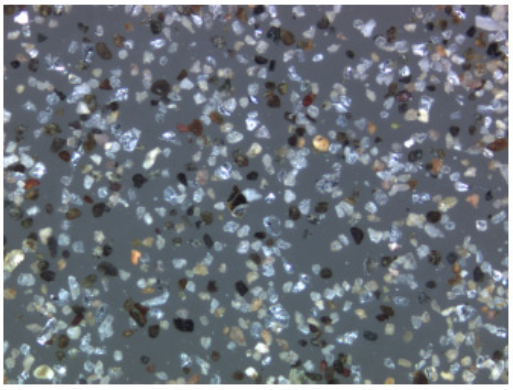

175

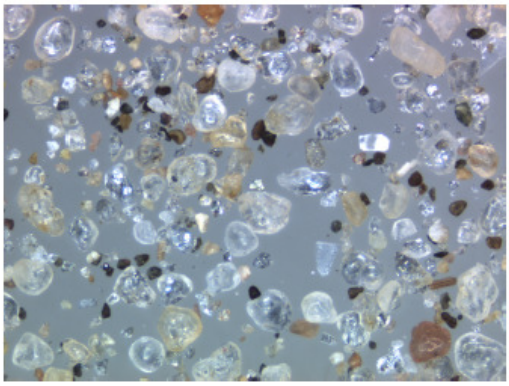

184

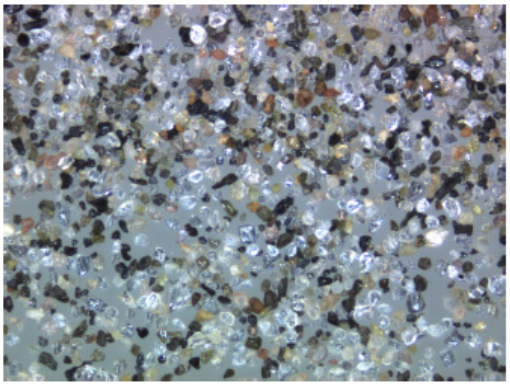

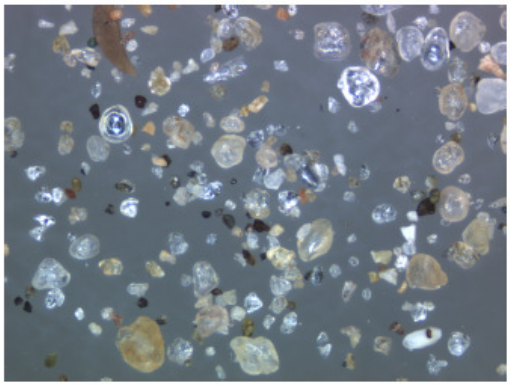

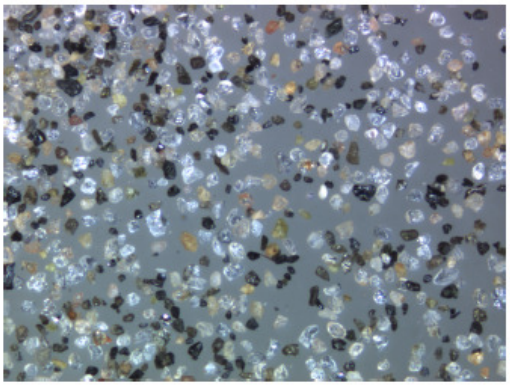

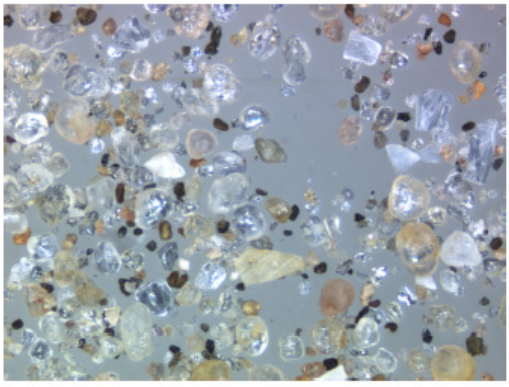

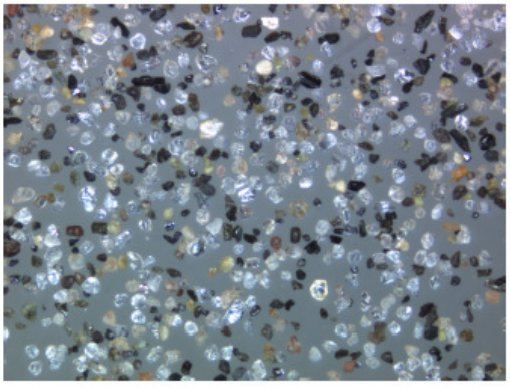

189

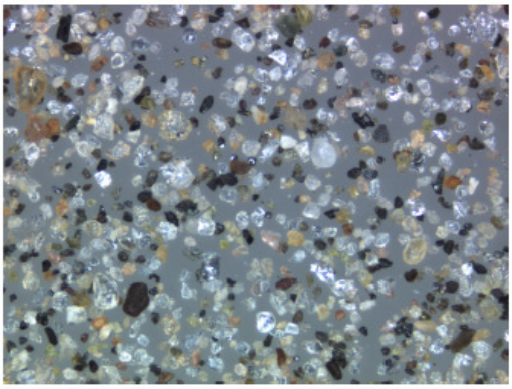

194

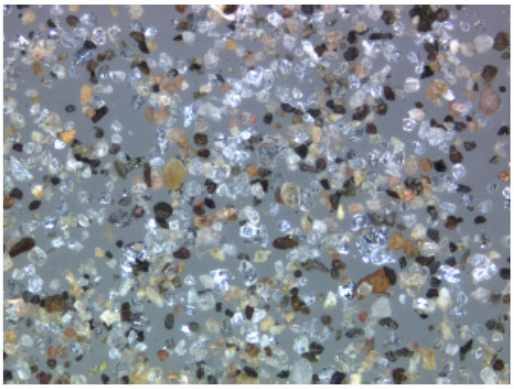

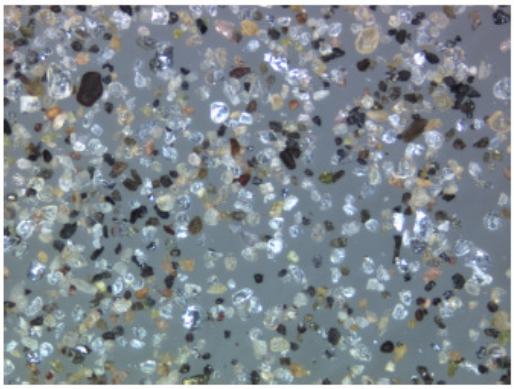

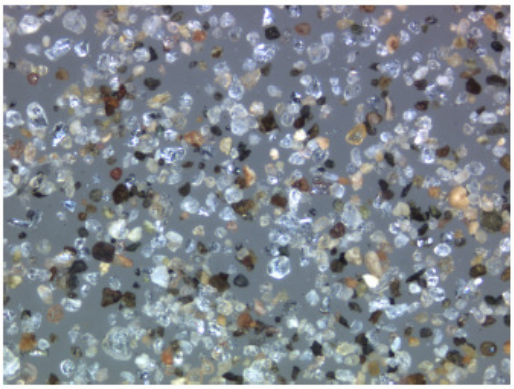

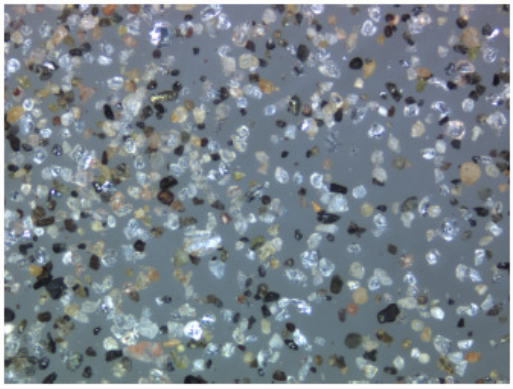

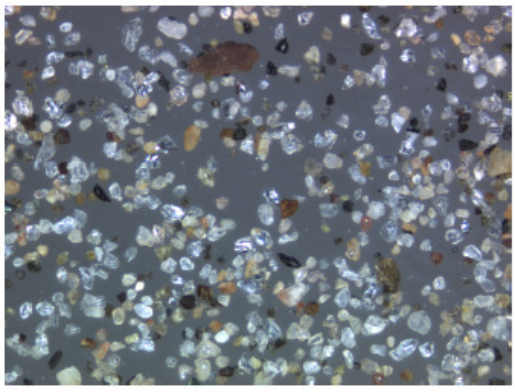

196

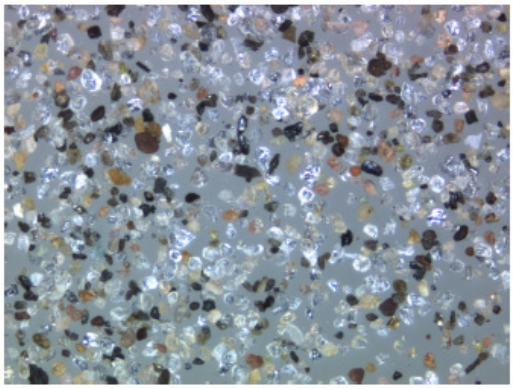

200

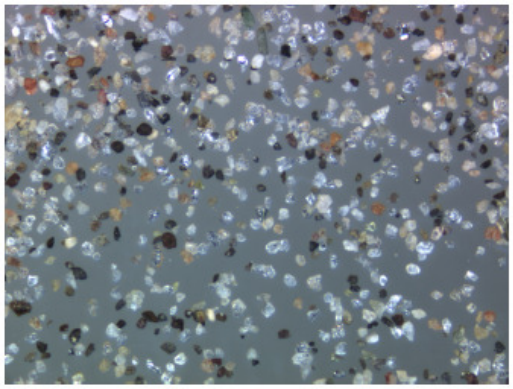

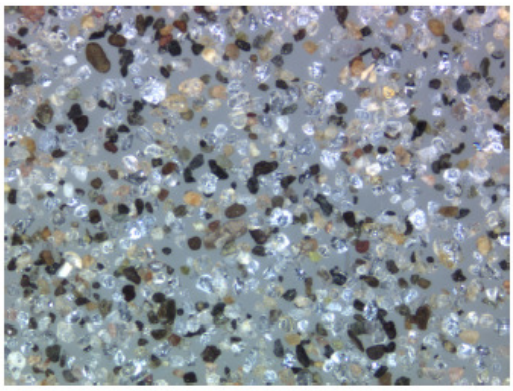

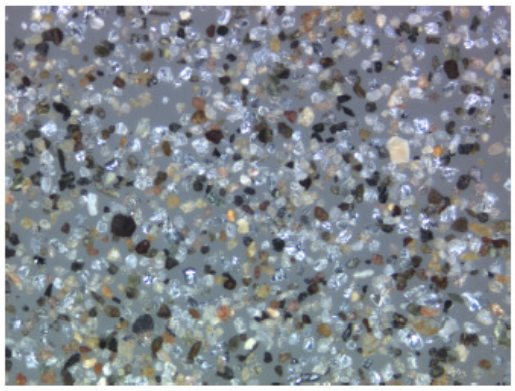

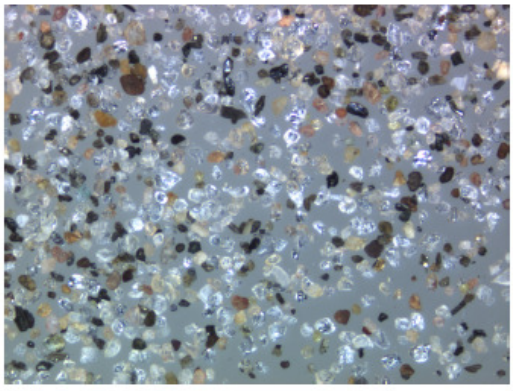

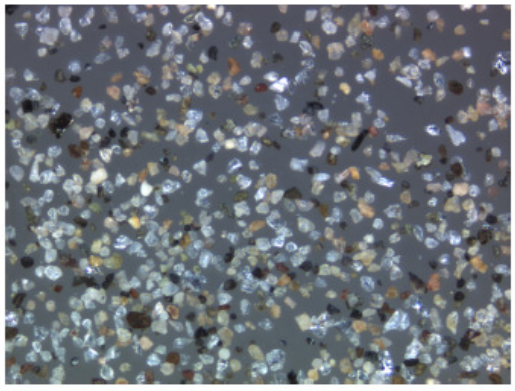

203